Durham University

Durham E-Theses

Characterization of FER1L5, a novel dysferlin myoferlin related protein

Usha Kalyani Ramachandran

How to cite:

Ramachandran, Usha Kalyani (2009) Characterization of FER1L5, a novel dysferlin myoferlin related protein. Doctoral thesis, Durham University.

Use policy

The full-text may be used and/or reproduced, and given to third parties in any format or medium, without prior permission or charge, for personal research or study, educational, or not-for-profit purposes provided that:

- a full bibliographic reference is made to the original source
- a https://etheses.durham.ac.uk/id/eprint/2046/ is made to the metadata record in Durham E-Theses
- the full-text is not changed in any way

The full-text must not be sold in any format or medium without the formal permission of the copyright holders.

Please consult the full Durham E-Theses policy for further details.

Academic Support Office, The Palatine Centre, Durham University, Stockton Road, Durham, DH1 3LE
e-mail: e-theses.admin@durham.ac.uk Tel: +44 0191 334 6107
https://etheses.durham.ac.uk

CHARACTERIZATION OF FER1L5, A NOVEL DYSFERLIN AND MYOFERLIN RELATED PROTEIN

by

Usha Kalyani Ramachandran

The copyright of this thesis rests with the author or the university to which it was submitted. No quotation from it, or information derived from it may be published without the prior written consent of the author or university, and any information derived from it should be acknowledged.

A thesis submitted to the University of Durham for the degree of Doctor of Philosophy

School of Biological and Biomedical Sciences

University of Durham

September 2009

1 0 FEB 2010

DECLARATIONS

I declare that the experiments described in this thesis were carried out by myself in the School of Biological and Biomedical Sciences, University of Durham, under the supervision of Dr. Rumaisa Bashir. This thesis has been composed by myself and is a record of work that has not been submitted previously for a higher degree in this or any other University. All references have been consulted by myself unless stated otherwise.

Usha Kalyani Ramachandran

I certify that the work reported in this thesis has been performed by Usha Kalyani Ramachandran, who, during the period of study, has fulfilled the conditions of the Ordinance and Regulations governing the Degree of Doctor of Philosophy.

Rumaisa Bashir

The copyright of this thesis rests with the author. No quotation from it should be published in any format, including electronics and the internet, without the author's prior written consent. All information derived from this thesis must be acknowledged appropriately.

PRESENTATIONS AND PUBLICATIONS

Poster presentations

Evidence of ferlin mediated membrane shedding in muscle cells highlights the existence of muscle cell exosomes, myosomes. (2008) *Neuromuscular Disorders*, Volume 18, Issue 9, Pages 793-793. U. Ramachandran, K. Saleki, G. Marlow, R. Bashir.

3rd International Congress of Myology (2008), Marseille, France. Overlapping properties of dysferlin, myoferlin and FER1L5 vesicles in muscle cells. U. Ramachandran, K. Saleki, G. Marlow, R. Bashir.

MRC Inaugural International Neuromuscular Conference (2008), London. Characterisation of the dysferlin related proteins, myoferlin and FER1L5, potential compensatory proteins of dysferlin. U. Ramachandran, K. Saleki, G. Marlow, R. Bashir.

Papers (s) for Publication:

Under preparation

U. Ramachandran, K. Saleki, W. Lostal, G. Marlow, J. Jimenez, H. Haase, L. Anderson, I. Richard and R. Bashir (2009) "FER1L5 is implicated in muscle membrane fusion".

J. Reimann, U. Ramachandran, K. Saleki, K. Kesper, L. Anderson, R. Schroder and R. Bashir (2009) FER1L5 expression in dysferlinopathy to be submitted to Neuromusc. Disord.).

ACKNOWLEDGEMENTS

I would like to take this opportunity to thank a number of people whose help was invaluable to me:

I specially thank my parents Mr. Ramachandran and Kasthuri, my sisters Thilagavathy, Brinda, Varalakshmi and my brother JothiRam for all their immeasurable love, affection, constant support and boundless encouragement all through my life.

I express my deep sense of gratitude to my supervisor Dr.Rumaisa Bashir, without whose support, inspiration, patience and guidance throughout the research, this thesis would not have been possible. Many thanks to Prof Roy Quinlan, whose advice and extended support during the early meetings got me going and who challenged me to think outside the box. Their wisdom, knowledge and commitment to the highest standards inspired and motivated me.

I thank my collegues Dr. Gareth Marlow for helpful suggestions and Dr. Khalil Saleki who taught me everything I needed to know about the western blot. I would like to thank Dr. Paul Hunt, who taught me all about immunohistochemistry. A big thanks to all my friends especially to Eulalia Banguera for her wonderful and timely help.

With great pleasure I like to thank Dr. Jahoda's entire group, who kindly shared tissue culture and microscope facilities. Thanks to Ming, Eva and Vanja for making me feel welcome whenever I approach their for antibodies and everyone within the ICBL for their support while I used their facilities.

I am also grateful to Mrs. Christine Richardson and Georgia for help with confocal imaging and live cell imaging respectively. Thanks to Dr. Stephen for his timely help to learn adobe photoshop. Also special thanks to Andrew for providing end-note software.

Finally, I would like to thank my Tamil Nadu Government and Muscular Dystrophy Campaign for funding me during my doctoral study.

ABSTRACT

The ferlins are mammalian homologues of the *C-elegans* sperm vesicle fusion protein FER-1 characterised by multiple C2 domains and a C-terminal anchor. To date three human ferlin proteins, dysferlin, myoferlin and otoferlin have been characterized. Dysferlin and myoferlin have a role in muscle membrane fusion. Dysferlin mutations cause muscular dystrophy and are associated with defective sarcolemmal repair. Myoferlin has a role in myogenesis. Through bioinformatic analysis our group identified a novel ferlin, FER1L5, which by homology modelling and sequence analysis showed highest similarity with dysferlin and myoferlin. Previously, FER1L5 gene expression was shown to be elevated during C2C12 myoblast fusion. This led to the hypothesis that FER1L5 may have a role in muscle membrane fusion. In this study this was investigated in the C2C12 cell line using a specific polyclonal antibody to FER1L5. FER1L5 was shown to be present in vesicles. By biochemical fractionation FER1L5 was detected in low density vesicles the membranes of which were non-resistant to non-ionic detergent. The fractionation data showed that FER1L5, dysferlin and myoferlin vesicles have similar properties. By immunolabelling FER1L5 was shown to be present in distinct vesicles in myotubes compared to dysferlin and myoferlin respectively. During myoblast fusion FER1L5 expression was detected at all stages and high expression was observed at membrane fusion sites of fusing myoblasts. FER1L5 (but also dysferlin and myoferlin) showed a nuclear distribution during myoblast fusion. In myotube nuclei FER1L5 was localized to subnuclear bodies sensitive to actinomycin D. Using the C3H-ER-MyoD cell line, I have shown that FER1L5 is not an early marker of muscle differentiation. The role of FER1L5 in muscle membrane fusion was investigated by examining the fusion index and membrane repair ability of C2C12 cells following FER1L5 inhibition. FER1L5 was shown to be required for myoblast fusion and membrane repair.

In this study, I have also shown that C2C12 myotubes are active in membrane shedding. Using live cell imaging and confocal analysis, MVB like structures containing ferlin vesicles were shown to be released extracellularly from C2C12 myotubes. EM studies confirmed these findings.

Overall my data shows that FER1L5 has a role in muscle membrane fusion. My work highlights that further studies on FER1L5 are required for example to determine if FER1L5 a therapeutic target in dysferlinopathy and to identify the mechanisms involved in FER1L5 mediated membrane fusion.

TABLE OF CONTENTS

LIST OF FIGURES

LIST OF TABLES

ABBREVIATIONS

APS	Ammonium persulphate
Act D	Actinomycin D
AP	Affinity Purified
BSA	Bovine serum albumin
cDNA	Complementary DNA
CNS	Central nervous system
C-terminal	Carboxy terminal
CO_2	Carbon dioxide
DAPI	4',6-diamidine-2-phenylindole dihydrochloride
dH_2O	Distilled water
DMEM	Dulbeccos modified eagles medium
DMSO	Dimethyl sulphoxide
DM	Differentiation media
DNA	Deoxyribonucleic acid
DysF	Dysferlin domain
EDTA	Ethylenediaminetetra acetic acid
EGTA	Ethylene glycol tetraacetic acid
EM	Electron microscopy
ER	Endoplasmic reticulum
FCS	Foetal calf serum
FB	Final Bleed
FER-1	Fertilization factor 1
FER1L5	Fertilization factor 1-like 5
FITC	Fluorescein isothiocyanate
Gal-1	Galetin-1
GFP	Green fluorescent protein
GLUT4	Glucose transporter 4
G3PDH	Glyceraldehyde 3 phosphate dehydrogenase
GM	Growth media
HBSS	Hank's balanced salt solution
HCL	Hydrochloric acid
HDM	High density microsomes
HEPES	N-2-Hydroxyethylpiperazine-N'-2-ethanesulphonic acid
HRP	Horse radish peroxidise
Ig	Immunoglobulin
IHC	Immunohistochemistry
kDa	Kilo dalton
L	Loop
LDM	Low density microsomes
M	Molar
mAb	monoclonal antibody
MB	Myoblast
MCD	Methyl cyclodextrin
MES	2-(N-morpholino) ethanesulfonic acid
mRNA	Messenger RNA
Mg	Microgram
$MgSO_4$	Magnesium sulphate

$MgCl_4$	Magnesium chloride
ml	Milli-litre
mM	Milli-molar
MVB	Multivesicular body
MyoD	Myoblast determination protein 1
NaCl	Sodium chloride
NaOH	Sodium Hydroxide
NMDAR1	N-methyl-D-aspartate receptor subunit 1
nM	Nano Molar
ng	Nano gram
NRK	Normal rat kidney cells
N-terminal	Amino terminal
O.D.	Optical density
°C	Degrees centigrade
P/S	Penicillin and Streptomycin
PAGE	Polyacrylamide gel electrophoresis
pAb	polyclonal antibody
PBS	Phosphate buffered saline
PCR	Polymerase chain reaction
PFA	Paraformaldehyde
pH	Potential of Hydrogen
PM	Plasma membrane
RIPA	Radioimmunoprecipitation assay
RNA	Ribonucleic acid
RNAi	RNA intereference
RT	Room temperature
RT-PCR	Reverse transcription Polymerase chain reaction
S.D.	Standard deviation
SDS	Sodium dodecyl sulphate
SDS-PAGE	SDS-Polyacrylamide gel electrophoresis
TBS	Tris-buffered saline
TE buffer	Tris-HCL, EDTA buffer
TEMED	NNN'N'- Tetramethylenediamine
TGN	Trans Golgi
Tris	Tris(hydroxymethyl)methylamine
TRITC	Tetramethyl rhodamine isothiocyanate
TX-100	TritonX-100
µg	Microgram
µl	Microlitre
µm	Micron (micrometre)
µM	Micromolar

CHAPTER I: GENERAL INTRODUCTION

1.1 Introduction

The cloning of the dysferlin gene has led to the identification of a novel mammalian protein family called the 'ferlins'. The dysferlin gene was identified by positional cloning and shown to be mutated in several types of inherited muscular dystrophies: Limb Girdle Muscular Dystrophy type 2B (LGMD2B), Miyoshi myopathy (MM) and anterior compartment myopathy (DAT) (DYSF, OMIM*603009, Bashir *et al.,* 1998; Liu *et al.,* 1998). When dysferlin was cloned it displayed homology to the *C.elegans* protein FER-1, which is implicated in the fusion of large membranous vesicles in developing sperm. FER-1 mutations lead to defective vesicle fusion in spermatocytes and insterility in worms (Achanzar and Ward, 1997). The proposed name given to the "dysferlin" gene reflected its significant homology to the FER-1 and the impact of the mutations leading to dystrophic related phenotypes (Bashir *et al.,* 1998 and Liu *et al.,* 1998). Following the identification of dysferlin, mammalian homologues were identified sharing high structural and sequence homology and collectively they were called the 'ferlins', which are described below (Bashir *et al.,* 1998).

1.2 Structural features of the ferlins

There are six mammalian ferlins, which are evolutionary conserved **(Figure 1.1).** The ferlins are characterized by the presence of multiple C2 domains and a C-terminal transmembrane anchor (Achanzar and Ward, 1997; Davis *et al.,* 2002; Bansal and Campbell, 2004; Doherty and McNally, 2003). C2 domains are protein domains, which fold into an eight-stranded ß-sandwich comprising 120-140 amino acid residues that can adopt two different topologies known as type-I and type II in which the N-and C-termini domains are located at opposite edges of the ß-sandwich resulting in a circular permutation of the strands **(Figure 1.2A).** The type I domain contains three loops (L1-L3) and the type II domain has four loops (L1-L4). The ligand-docking surface is the calcium binding region, which is formed by variable interstrand loops on one edge of the beta sandwich **(Figure 1.2B).** The C2 domains were initially defined as the second-constant sequence in protein kinase C and hence the name C2. They are present in 1000s of proteins and are generally implicated in proteins involved in (i) signal transduction pathways for example, cytoplasmic phospholipases A2 and protein

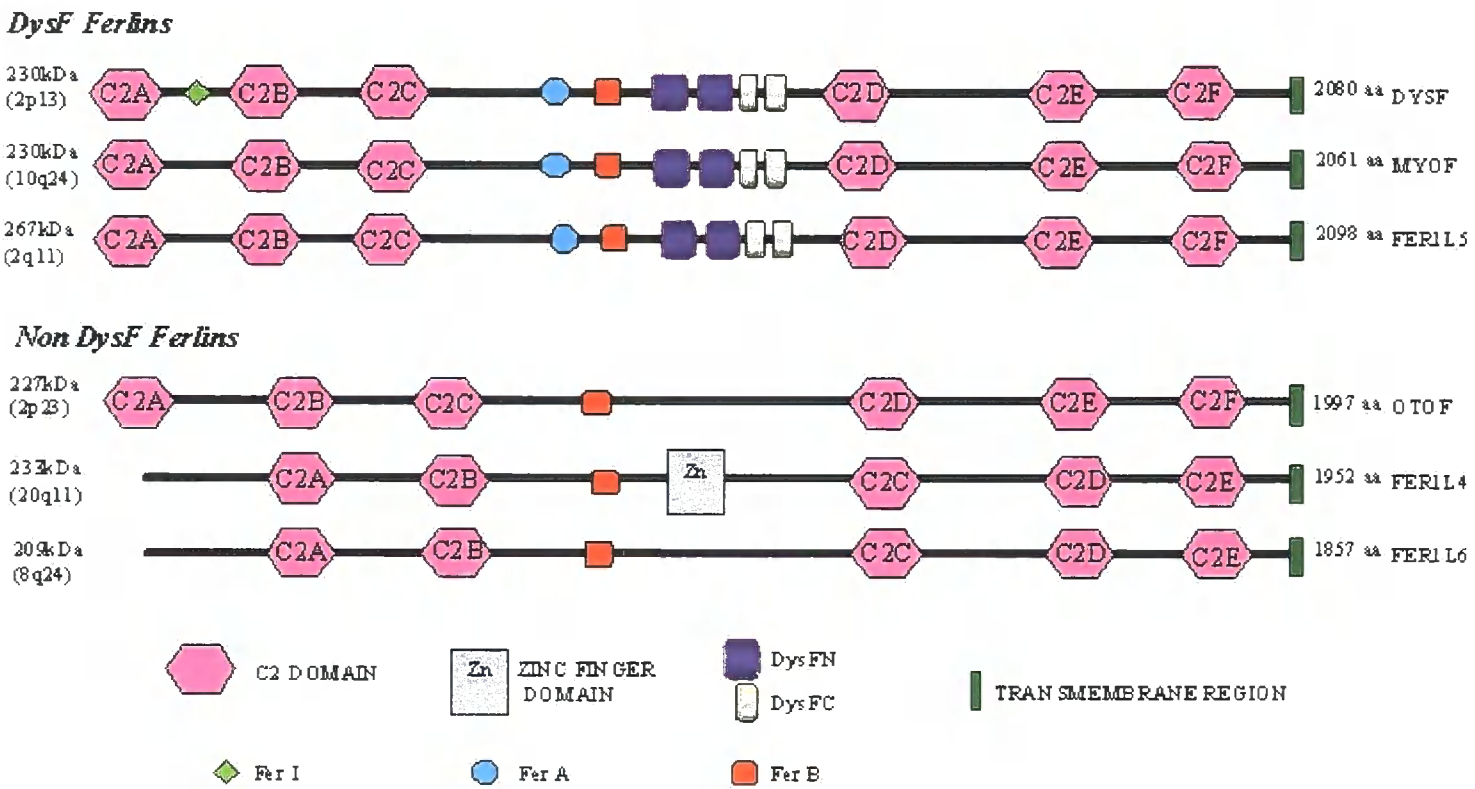
DysF Ferlins
230kDa (2p13)
C2A
C2B
C2C
C2D
C2E
C2F
2080 aa DYSF
230kDa (10q24)
2061 aa MYOF
267kDa (2q11)
2098 aa FER1L5
Non DysF Ferlins
227kDa (2p23)
1997 aa OTOF
233kDa (20q11)
Zn
1952 aa FER1L4
209kDa (8q24)
1857 aa FER1L6
C2 DOMAIN
ZINC FINGER DOMAIN
DysFN
DysFC
TRANSMEMBRANE REGION
Fer I
Fer A
Fer B

Figure 1.1. Schematic showing the structural similarities and subgrouping of the human ferlin protein family. *All proteins contain tandem C2 domains (pink) and C-terminal transmembrane domain (blue). The subgrouping is based on the presence or absence of the nested DysFC (highlighted by dark grey colour) and DysFN (highlighted by violet colour). The dysferlin domain is present in dysferlin, myoferlin and FER1L5. Other predicted domains also found in the ferlins are Fer A (bluish green), Fer B (red) and Fer I (light green). FER1L4 has a zinc finger domain between C2B and C2C. The long isoform of FER1L5 and otoferlin are shown.*

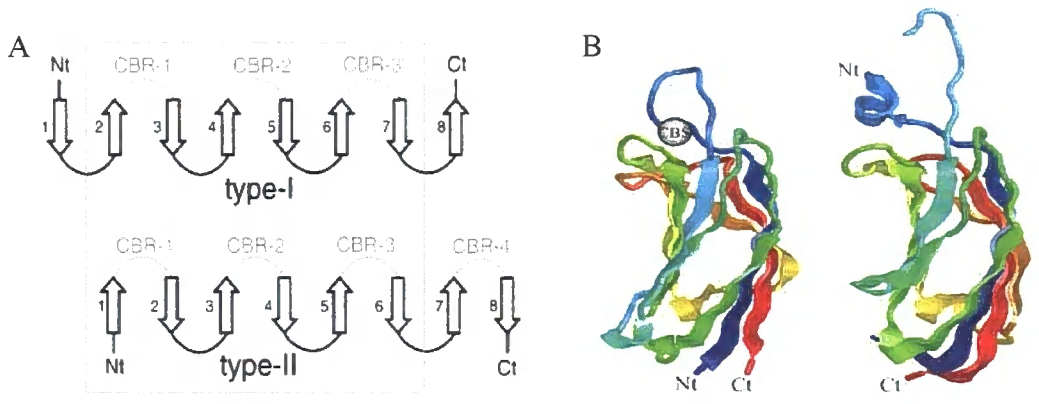

Figure 1.2. A. *Topological arrangement of ß-strands of type I C2 domain (Protein kinase C) and type II C2 domain (Synaptotagmins).* ***B.*** *Ribbon structures of type I (left) and type II (right) C2 domain of phospholipase C –d1 and protein kinase e. Nt: N- terminus; Ct: C- terminus; CBR: Calcium binding region; CBS: Calcium binding sequence. Adapted from Jiménez and Bashir, (2007).*

kinase C and (ii) vesicle trafficking/membrane fusion for example, synaptotagmins, rabphilin 3A, munc 13, DOC2 proteins and RIM (Cho and Stahelin, 2006; Rizo and Sudhof, 1998; Chacon *et al.*, 2001; Davis *et al.*, 2002). The topology in the C2 domain of protein kinase C is generally that of type I, the synaptotagmin C2 domains generally show a type II topology (Nalefski and Falke, 1996). The C2 domains of the ferlins exhibit type II topology (Davletov *et al.*, 1993; Davis *et al.*, 2002; Jiménez and Bashir, 2007). C2 domains are capable of binding Ca^{2+}, phospholipids, inositol polyphosphates, phosphotyrosines and they also participate in a Ca^{2+} dependent and independent protein-protein interactions (Cho and Stahelin, 2006; Rizo and Sudhof, 1998, Fernandez-Chacon *et al.*, 2001; Davis *et al.*, 2002). Some of the C2 domains have calcium binding regions (CBR) and the binding of calcium to the C2 domains primarily involves aspartyl side-chains that act as bidentate ligands for these ions (Davletov *et al.*, 1993).

The C2 domains most studied and best characterized are those present in synaptotagmins, membrane associated proteins, which are thought to function as Ca^{2+} sensors during synaptic membrane fusion (Chapman *et al.*, 1998). The C2 domains in the ferlin proteins have been shown to be the most similar to those present in the synaptotagmins (Davis *et al.*, 2002; Bansal and Campbell, 2004; Doherty and McNally, 2003; Therrien *et al.*, 2009). Based on the homology with FER-1 and the similarities of the C2 domains with those of synaptotagmin the ferlin proteins are predicted to be involved in membrane fusion (Bansal and Campbell, 2004; Doherty and McNally, 2003). The six mammalian ferlins genes are dysferlin, otoferlin, myoferlin, FER1L4, FER1L5 and FER1L6 located on human chromosomes 2p13, 2p23, 10q24, 20q11, 2q11 and 8q24 respectively. Of these, dysferlin, myoferlin and otoferlin have been characterized. Dysferlin and otoferlin are implicated in genetic diseases namely muscular dystrophy (Bashir *et al.*, 1998; Liu *et al.*, 1998) and nonsyndromic deafness respectively (Yasunaga *et al.*, 1999; Yasunaga *et al.*, 2000). Sequence analysis of the three characterized ferlin genes has identified the molecular signature of the ferlin protein family, which resides in the last two C-terminal C2 domain sequences located before the transmembrane domain (Britton *et al.*, 2000) **(Figure 1.3).** Using these C2 domain sequences our group and work of others have identified novel ferlin genes and shown that there are only six ferlins in the human and also other mammalian genomes.

Dysferlin, myoferlin, otoferlin and FER1L5 (long isoform) proteins have six C2 domains designated C2A to C2F and FER1L4 and FER1L6 have five C2 domains corresponding to C2B to C2F of the dysferlin, myoferlin and FER1L5 C2 domains. Otoferlin has two isoforms, the long isoform containing six C2 domains and the short isoform containing three C2 domains (Yasunaga *et al.*, 2000). Evidence is also emerging of dysferlin, myoferlin and FER1L5 isoforms (Pramono *et al.*, 2006; McNally *et al., 2000*; http://www.ncbi.nlm.nih.gov). Comparison of all ferlin C2 domains has shown that the last two C-terminal domains (C2E and C2F) share strong similarity across the entire ferlin family (Jiménez and Bashir, 2007). But the C2A is quite divergent between the ferlins indicating functional flexibility. *In vitro* studies have shown that of the six C2 domains in dysferlin and myoferlin, only the C2A domain is capable of binding phospholipids in a Ca^{2+} dependent manner. The other C2 domains are predicted to be involved in Ca^{2+} dependent and independent interactions (Davis *et al.*, 2002; Doherty *et al.*, 2005). The three domains, C2C, C2D and C2F contain putative calcium-binding regions and the cation-binding residues binding Ca^{2+} appear to be strongly conserved (Jiménez and Bashir, 2007). The central region of the ferlins (between C2C and C2D) shows differences amongst the ferlin proteins. In some of the ferlins there is an additional novel domain designated, DysF, which is located between the C2C and C2D domains and is present in dysferlin, myoferlin and FER1L5. The dysferlin domain is conserved during evolution and is also present in FER-1, *Drosophila* hypothetical sequence CG32226PA, yeast peroxisomal proteins and other hypothetical proteins (Ponting *et al.*, 2001; Davis and Delmonte, 2000; Jiménez and Bashir, 2007). Many disease-causing dysferlin mutation have been mapped to this domain (Patel *et al.*, 2008). The ferlins contain two copies of the DysF domain, one DysF nested within a second DysF domain. Hence the two DysF domains have been classified as DysFC (C-terminal region) and DysFN (N-terminal region). The function of the DysF domain is not known yet but the structure of the myoferlin DysF has been resolved recently and appears to be a unique fold, which is held together by stack of arginine and tryptophan residues (Patel *et al.*, 2008). The ferlins also have ferlin-specific domains of unknown function referred as: Fer I, Fer A and B (Glover and Brown, 2007); Fer I is only present in dysferlin and located between C2A and C2B domains. Fer A and Fer B are located in the central regions and inserted between C2C and C2D domains. Fer A is present in dysferlin, myoferlin and FER-1. Fer B is located adjacent to Fer A and is present in all ferlins. **(Figure 1.1).** The

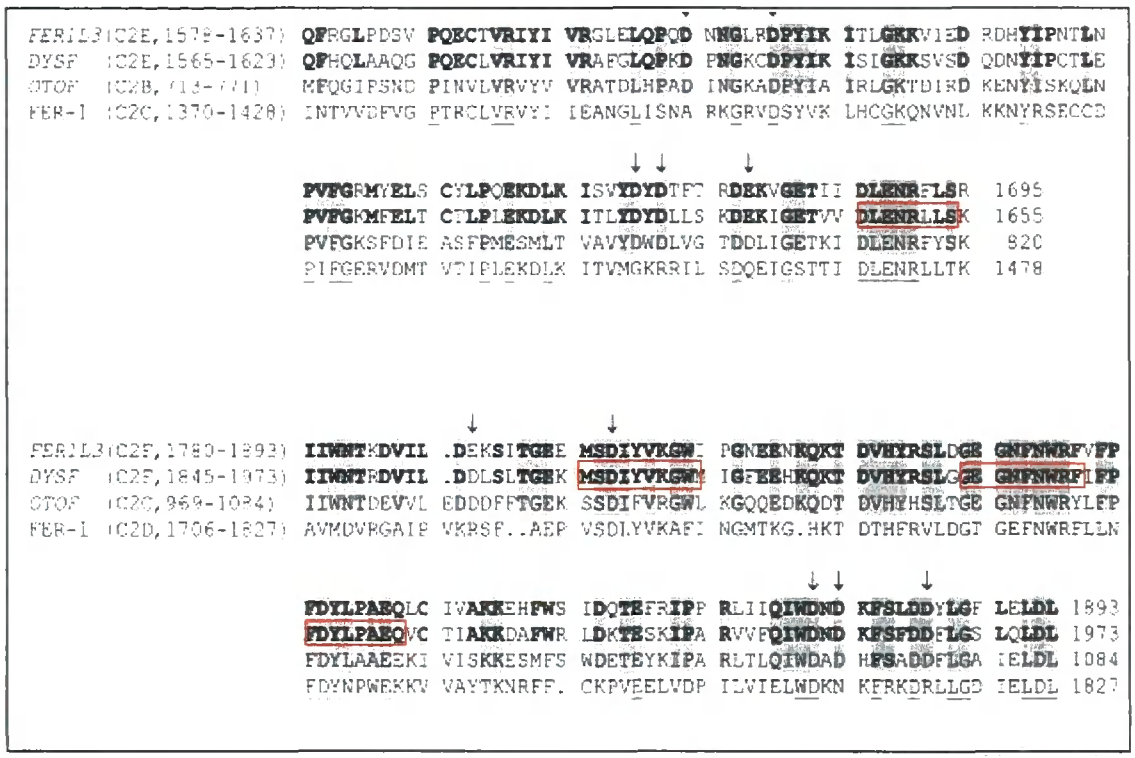

Figure 1.3. Molecular signatures of the ferlins. *Multiple sequence alignment showing the two highest conserved C2 domains of dysferlin (DYSF), myoferlin (FER1L3) and otoferlin (OTOF) in comparison with the worm ferlin (FER-1). The sequences shown in rectangular boxes are conserved in all the ferlins. Shaded amino acids shown here are conserved in all the human ferlins. The shared amino acids between dysferlin and myoferlin are indicated in bold. Highly conserved calcium binding residues are highlighted by arrows. Taken from Britton et al., (2000).*

homology between the ferlins is highlighted in **Table 1.1**.

Phylogenetic analysis of the ferlins C2 domains has shown that the ferlin protein family can be subgrouped into dysferlin-like and otoferlin-like. Dysferlin, myoferlin and FER1L5 form the dysferlin subgroup and otoferlin, FER1L4 and FER1L6 form the otoferlin subgroup. Within the dysferlin subgroup myoferlin is most similar to dysferlin and within the otoferlin subgroup FER1L6 shares highest homology to otoferlin **(Figure 1.4).**

1.3 Evolutionary conservation of the ferlins

The ferlin family is strongly conserved in evolution. Using a combination of database searches, BLAST analysis, Dr. Bashir's group has examined the presence of evolutionary homologues of the ferlins. The data generated is shown in **Table 1.2.** There are six ferlin genes in higher mammals (for example, chimpanzee, cattle, buffalo, dog, horse, cat, sheep, pig and rodents) with a similar structure as the human genes. The rodent genome contains six ferlins corresponding to the mammalian genes but mapping to different chromosomes. The mouse and the rat ferlin genes share significant sequence homology with the human ferlins and an identical protein structure with respect to the number and positions of the C2, DysF, transmembrane and the novel Fer I, A and B domains **(Table 1.2)**. The Fer B domain is conserved in most of the ferlin genes identified so far but the Fer I and B domains are present only in some of the evolutionary ferlin homologues. In zebrafish, BLAST analysis has identified dysferlin, myoferlin, otoferlin and FER1L4 but there appears to be no evidence for the existence of FER1L5 and FER1L6. The Zebrafish genome has two ferlins one representing the dysferlin subgroup and other representing the otoferlin subgroup. In the *Xenopus* genome there is clear evidence for the existence of myoferlin and FER1L6 (otoferlin-like) by BLAST analysis. The existence of other ferlin genes is not yet known because the sequencing of the *Xenopus* genome is incomplete. The *Drosophila* genome has a single ferlin gene, which shares >40% sequence homology to dysferlin, myoferlin and otoferlin. In the *Plasmodium falciparum* genome there are two ferlins, one most homologous to dysferlin/myoferlin and the other sharing most similarity with otoferlin. The data suggests that gene duplication is responsible for the emergence of the ferlin proteins in higher mammals.

*Table 1.1. Molecular genetic summary of the human ferlin genes and their similarities. * Predicted data. [b]-long isoform*

Human Ferlins	Chromosomal Mapping	Exons	Amino acids (aa)	Sequence homologies (% similarity) DYSF	OTOF[b]	MYOF
DYSF	2p13	55	2080	-	64	68
OTOF	2p23	47	1997	64	-	49
MYOF	10q24	55	2061	68	49	-
FER1L4*	20q11	45	1952	47	55	47
FER1L5*	2q11	52	2098	54	44	54
FER1L6*	8q24	40	1857	49	57	45

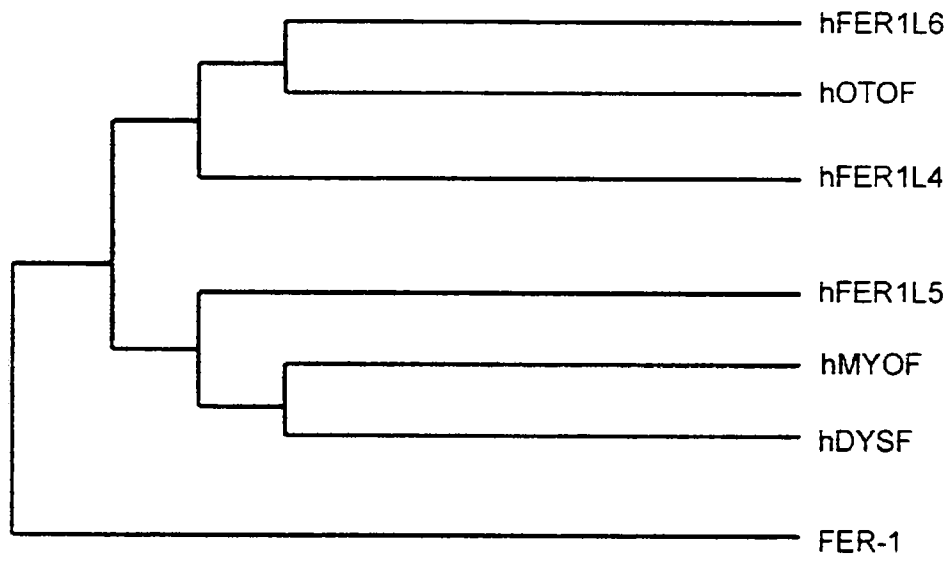

Figure 1.4. Ferlin C2 domain phylogeny. *The tree is constructed based on human ferlin C2 domain sequences aligned using Clustal W. The tree shows the relationships between and within the dysferlin and otoferlin subgroups. Myoferlin is most similar to dysferlin than FER1L5. Likewise, FER1L6 shows highest homology to otoferlin than FER1L4.*

Table 1.2. Evolutionary conservation of the ferlins.

	Map position	Size (aa)	C2 domains C2A	C2B	C2C	C2D	C2E	C2F	TD	DysF Domain	Fer I	A	B	Additional information
Human														
Dysferlin	2p13	2080	+	+	+	+	+	+	+	+	+	+	+	
Otoferlin'b'	2p23	1997	+	+	+	+	+	+	+	-	+		+	
Myoferlin	10q24	2061	+	+	+	+	+	+	+	+	+	+	+	
FER1L4	20q11	1952		+	+	+	+	+	+	-			+	
FER1L5	2q11	2098	+	+	+	+	+	+	+	+	+	+	+	
FER1L6	8q24	1857		+	+	+	+	+	+	-			+	
Mouse														
Dysferlin	6C3	2069	+	+	+	+	+	+	+	+	+	+	+	>90% identity with human.
Otoferlin'b'	5	1997	+	+	+	+	+	+	+	-	+		+	>90% "
Myoferlin	19C2	2061	+	+	+	+	+	+	+	+	+	+	+	>80% "
FER1L4	2H1	1784		+	+	+	+	+	+	-			+	>80% "
FER1L5	1B	2022	+	+	+	+	+	+	+	+	+	+	+	>70% "
FER1L6	15D1	1863		+	+	+	+	+	+	-			+	>80% "
Rat														
Dysferlin	4q34	1967	+	+	+	+	+	+	+	+	+	+	+	>90% "
Otoferlin	7q31	2054	+	+	+	+	+	+	+	-	+		+	65% identity with human long isoform.
Myoferlin	1q54	2370	+	+	+	+	+	+	+	+	+	+	+	>75% identity with human.
FER1L4	3q41	1934		+	+	+	+	+	+	-			+	>80% identity with human; Zn-NFX domain absent.
FER1L5	9q54	2035	+	+	+	+	+	+	+	+	+	+	+	>80% identity with human.
FER1L6	7q33	1890		+	+	+	+	+	+	-			+	>80% identity with human.
Danio rerio- zebrafish														
Dysferlin	?	2087	+	+	+	+	+	+	+	+	+	+	+	>68% similarity with human ferlins
Myoferlin	13	2032	+	+	+	+	+	+	+	+	+	+	+	>68% similarity with human ferlins
Otoferlin	20	1992	+	+	+	+	+	+	+	-	+		+	>66% similarity with human ferlins
FER1L4	11	1895		+	+	+	+	+	+	-			+	>50% similarity with human ferlins
Xenopus tropicalis														
Dysferlin/	?	?												
Otoferlin	?	?												
Myoferlin	?	1929	+	+	+	+	+	+	+	+	+	+	+	>79% similarity with human ferlins
FER1L6	9	1803		+	+	+	+	+	+	-			+	>50% similarity with human ferlins
Plasmodium Dysferlin/ Myoferlin Homologue	8	1870	+	+	+		+	+	+	-	-	-	-	43% similar to human dysferlin, 32% similar to human myoferlin 2 C-terminal transmembrane regions adjacently located.
Otoferlin Homologue	14	1904	+	+	+		+	+	+	-	-	-	-	39% similar to human otoferlin
Fly-*Drosophila*	3L	1782	+	+	+	+	+	+	+	-		-	-	>40% similarity with human ferlins
Worm FER-1	1	2034			+	+	+	+	+	+		+	+	>30% similarity with human ferlins

TM: Transmembrane domain; 'b':Otoferlin long isoform; aa: amino acid; ? : not known

Myoferlin and otoferlin appear to be the ancestral ferlins from which the two subgroups have emerged.

1.4 FER-1 and the mammalian ferlins

1.4.1 FER-1

The *C.elegans* FER-1 is a 230 kDa protein to which dysferlin shared homology when the gene was identified (Achanzar and Ward, 1997; Aoki *et al.*, 2001). Sharing a similar structure to dysferlin, FER-1 is predicted to function in vesicle fusion during maturation of spermatozoa. FER-1 is defective in mutant spermatocytes and FER-1 mutants show a sterile phenotype (Achanzar and Ward, 1997). Currently ten mutations have been identified in the *fer-1* gene and all are missense mutations of which five (*hc136, hc136, b232ts, hc82ts, hc24ts*) map to the predicted C2 domains and two include map to the DysF domain suggesting that these domains are essential for FER-1 function (Washington and Ward, 2006). Ultrastructural studies have shown that the first C2A domain of FER-1 is required for the fusion of large vesicles termed membranous organelles (MOs) to the plasma membrane (PM), during sperm maturation. An antibody raised to FER-1 shows punctate staining at the plasma membrane of the spermatids and in MO (Washington and Ward, 2006). No FER-1 staining pattern was observed in FER-1 mutant sperm. Defective fusion of the MO is hypothesized to lead to immotile sperm. This was tested in the spermatids carrying FER-1 mutations in the C2 domain and the ability of these spermatids to trigger MO fusion was determined.

MO fusion assays were developed using the dye FM1-43. When the dye partitions in the outer membrane leaflet of spermatids the PM of the spermatids fluoresces. Fusion of the MO with the fluorescent PM, leaves a fluorescent puncta around the cell body periphery and this was used to quantify the MO fusion. Using this assay MO fusion was demonstrated in wild type spermatids and MO fusion was shown to be dependent upon internal calcium because depletion of calcium in the wild type spermatids using calcium chelators blocked MO fusion (Washington and Ward, 2006). In the presence of calcium MO fusion was shown to be blocked in FER-1 mutants indicating that FER-1 is required for the active fusion of MO with the sperm PM, a process dependent upon the C2 domains and internal calcium.

1.4.2 Dysferlin

1.4.2.1 Molecular genetics of dysferlin

Dysferlin was the first mammalian ferlin to be identified (Bashir *et al.*, 1998; Liu *et al.*, 1998). The dysferlin gene is located on chromosome 2p13 (Bashir *et al.*, 1998), spanning at least 55 coding exons (Aoki *et al.*, 2001; Liu *et al.*, 1998) and a genomic region of >150kb (Aoki *et al.*, 2001; Bashir *et al.*, 1998; Pramono *et al.*, 2006). The dysferlin cDNA contains 6,243 bp encoding a protein comprising 2,080 amino acids with a predicted molecular mass of 230kDa (Aoki *et al.*, 2001). The dysferlin gene and its protein is expressed in a variety of tissues with the highest expression in skeletal and cardiac muscle (Bashir *et al.*, 1998; Liu *et al.*, 1998). Fifteen different isoforms of dysferlin are now recognized, which are thought to be produced by alternative splicing (http://www.genecards.org). Several monoclonal antibodies (designated NCL-hamlet, NCL-hamlet 2) have been raised to dysferlin and they detect a 230kDa protein, which shows ubiquitous expression with high levels in muscle and heart (Anderson *et al.*, 1999). Dysferlin localizes at the muscle cell membrane (sarcolemma) **(Figure 1.5)** and is also present intracellularly and is thought to be in vesicles (Piccole *et al.*, 2000; Bansal *et al.*, 2003; Ampong *et al.*, 2000). Dysferlin is not associated with the dystrophin-glycoprotein complex (DGC) based on the observations that normal expression of the various DGC components is observed in dysferlin-null mice and dysferlin deficient patient muscle **(Figure 1.5)**. In dysferlin deficient mice the DGC complex is stable and functional (Ampong *et al.*, 2000; Bansal *et al.*, 2003).

1.4.2.2 Dysferlin and Muscular dystrophy

Mutations in the dysferlin gene *(DYSF)* cause three clinically distinct autosomal recessive muscular dystrophies; LGMD2B (Limb Girdle Muscular Dystrophy type 2B) (Bashir *et al.*, 1998), MM (Miyoshi myopathy) (Liu *et al.*, 1998) and DMAT (Distal anterior compartment myopathy) (Aoki, 2006) collectively called the dysferlinopathies (Illa *et al.*, 2001; Vilchez *et al.*, 2005; Urtizberea *et al.*, 2008).

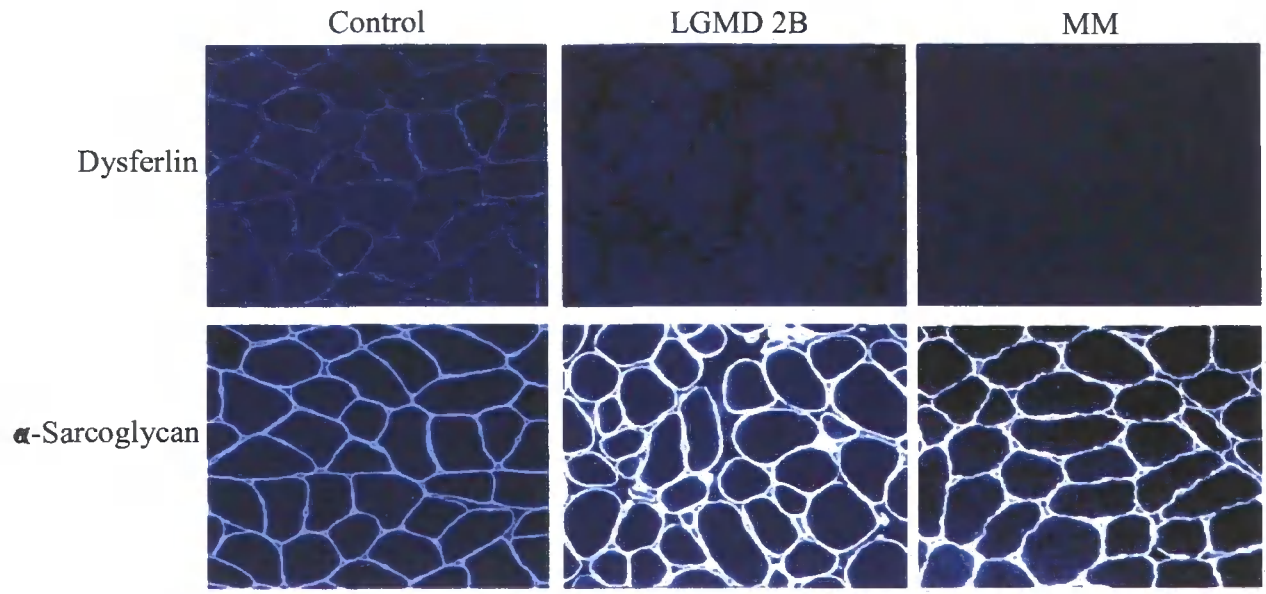

Figure 1.5. Immunofluorescence analysis of dysferlin and α-sarcoglycan in muscle biopsies of patients with LGMD2B and MM. *In the MM/LGMD2B patients the staining for dysferlin is absent but the control muscle shows staining at the sarcolemma. MM/LGMD2B muscle shows a normal staining pattern for a-sarcoglycan. Taken from Matsuda et al., (1999).*

Muscular dystrophies are a heterogeneous group of muscular disorders, characterized by progressive loss of muscle strength and integrity (Emery, 2002). LGMD2B patients show characteristically a predominant proximal muscle weakness and wasting in the late teens and often have normal mobility during childhood with a slow progression (Bashir *et al.,* 1998; Linssen *et al.,* 1997; Mahjneh *et al.,* 2001). In contrast, MM is targeted distally to gastronemius muscles of the lower limbs in late teens and subsequently there is little early involvement of anterior muscle group with an early symptom of impaired toe-standing by affected patients (Liu *et al.,* 1998). DMAT affects anterior tibial muscles (Illa *et al.,* 2001; Vilchez *et al.,* 2005). Despite their distinct symptoms, there are some remarkable overlapping features of these disorders such as an autosomal recessive inheritance, age of onset with slow disease progression and early, severe elevations of serum creatine kinase levels (Matsuda *et al.,* 1999; Illa *et al.,* 2001).

To date, at least 200 mutations (Leiden Muscular Dystrophy database, http://www.dmd.nl/) have been identified in the dysferlin gene. Many different types of dysferlin mutations have been identified in dysferlinopathy eg. missense, deletion and frameshift (Cagliani *et al.,* 2005; Nguyen *et al.,* 2005). Some of the mutations in the dysferlin gene are listed in **Table 1.3.** Overall the mutations are widely spread throughout the coding sequence of the gene without any mutational "hot spot" (Cagliani *et al.,* 2005, Nguyen *et al.,* 2005) and there are no evident genotype-phenotype correlations (Cagliani *et al.,* 2005). It has been reported that a wide inter and intra-familial variation in clinical phenotype can be associated with the same dysferlin mutation (Caglian *et al.,* 2003). Regardless of the phenotype or the mutation dysferlinopathy patients typically have severely reduced levels or a complete loss of dysferlin in skeletal muscle when analyzed by immunohistochemistry (as shown in **Figure 1.5**) and by western blotting (Anderson *et al.,* 1999, Vainzof *et al.,* 2001 and Aoki *et al.,* 2001; Matsuda *et al.,* 1999; Piccolo *et al.,* 2000). Dysferlin also shows cytoplasmic staining in the skeletal muscle fibers (Ampong *et al.,* 2005). Ultrastructural studies of normal muscle show that dysferlin is localized at the sarcolemma but in patients with dysferlin deficiency there is a subsarcolemmal accumulation of vesicles (Selcen *et al.,* 2001; Cenacchi *et al.,* 2005).

Table 1.3. Mutations in the dysferlin gene.

Description	Geographical origin	Type of disease	State/Mutational event	Nucleotide change	References
DYSF, G605TER	France	Miyoshi myopathy	Homozygous nonsense mutation	codon 605, a CAG-to-TAG transition at nucleotide 2186 (Q605X).	Liu et al. (1998)
DYSF, 1-BP DEL, 5966G	Spanish	distal myopathy with anterior tibial onset	Homozygous frameshift.	deletion of 5966G	Liu et al. (1998)
DYSF, I298V	Italian	MM/ LGMD	Heterozygosity for 2 missense mutations	ATG-to-GTC transition at nucleotide 4265 (I298V) and CGT-to-TGT transition at nucleotide 6497 (R2042C)	Liu et al. (1998)
DYSF, 5-BP DELETION AND 4-BP INSERTION, NT4872	Libyan Jewish	LGMD2B	a) Homozygous/ frameshift b) insertion/deletion	1-bp deletion of guanine and a C-G transversion at codon 1322, resulting in premature stop codon at position 1331 4872delinsCCCC	Bashir et al. (1998) Therrien et al. (2006)
	Italy	LGMD2B	1)Homozygous insertion/deletion	1-bp deletion (4872delG) and a 4876G-C transversion	Bashir et al. (1998); Sinnreich et al. (2006)
DYSF, 23-BP INS	Palestinian Arab	LGMD2B with congenital form of muscular dystrophy	Insertion represented a tandem duplication resulting from replication slippage frameshift	23-bp insertion at codon 1386, premature termination at codon 1427	Mahjneh et al. (1992), Bashir et al. (1998)
DYSF, P791R	Canadian aboriginal	LGMD2B/ MM	Homozygous missense mutation	Pro791-to-Arg	Weiler et al. (1996), (1999)

Description	Geographical origin	Type of disease	State/Mutational event	Nucleotide change	References
DYSF, NT5711, G-A, +5	Yemenite Jewish descent	LGMD2B	Homozygous	G-to-A change predict to affect position 5 in the intron following amino acid 1686 (5711bp) of the dysferlin cDNA sequence	McNally et al. (2000)
DYSF, V67D	Russian	LGMD2B/ MM	Homozygous	TG-to-AT change at nucleotides 573-574 resulting in val67-to-asp substitution	Illarioshkin et al. (1996), 2000
DYSF, W999C	Patients in General	Miyoshi myopathy	Transversionand substitution	G-T transversion in exon 28 3370 resulting in a W999C substitution.	Matsumura et al. (1999)
DYSF, R1905TER	Sueca, Spain	MM, DMAT, LGMD2B	Homozygous	C-T transition in exon 51 6086 resulting in R1905X substitution	Vilchez et al. (2005)
DYSF, D625Y		LGMD2B	Compound heterozygosity Heterozygous	1) G-T transversion in exon 20 1873 resulting in an D625Y substitution 2) A-G transversion in exon 47 5201resulting in a E1734G and D625Y substitution	Illa et al. (2007)
DYSF, G519R		MM	Homozygous/ Heterozygous G519R mutation	G-A transition in exon 18 1555 resulting in G519R substitution	Illa et al. (2007)
DYSF, IVS31DS, A-G, -33		LGMD2B	Compound heterozygosity	1)A-to-G transition in intron 31, resulting in the in-frame skipping of exon 32	Sinnreich et al. (2006)

TER: Terminator; DEL: Deletion

Dysferlin deficient muscle is also characterized by inflammation correlating with the upregulation of major histocompatibility complex (MHC) class I antigens at the peripheral regions of the fibres (Gallardo *et al.*, 2001; Confalonieri *et al.*, 2003; Kostek *et al.*, 2002), plasmalemmal defects, thickened basal lamina, replacement of the plasma membrane by one to multiple layers of small vesicles, papillary projections, small subsarcolemmal vacuoles, some undergoing exocytosis and infrequent subsarcolemmal regions containing rough endoplasmic reticulum and abundant free ribosomes (Cenacchi *et al.*, 2005).

1.4.2.3 Mouse models of dysferlinopathy

There are several mouse models of dysferlin deficiency. The SJL/J (SJL-*Dysf*) was the first mouse model of dysferlin to be identified and is a naturally occurring mouse model that was used extensively prior to the identification of dysferlin to examine inflammatory diseases (Festing, 1979). SJL/J mice are susceptible to many induced autoimmune diseases such as experimental autoimmune encephalitis (EAE) and inflammatory muscle diseases. SJL mice develop progressive muscle weakness, an increased regeneration capacity and the spontaneous occurrence of inflammatory myopathy, which is accompanied by loss of muscle strength (Bittner *et al.*, 1999). Histopathological studies in this mouse at different ages identified the features compatible with a progressive muscular dystrophy including degeneration and regeneration. The muscle fibres at 3 weeks of age showed signs of progressive muscle weakness and necrotic fibrosis (Bittner *et al.*, 1999). The myopathic phenotype was shown to be inherited as an autosomal recessive trait and mapped to mouse chromosome 6 to a region syntenic with human 2p13, where the dysferlin gene mapped. The identification of mutations in the dysferlin gene highlighted that dysferlin was the causative gene responsible for the myopathy in SJL/J. Mutational screening revealed a 171bp deletion (spanning aa 1628-1685) in the dysferlin gene, which had resulted from a homozygous mutation in the 3' splice junction of exon 45 resulting in removing 57 amino acids including part of the conserved C2E domain (Bittner *et al.*, 1999). Protein analysis showed loss of dysferlin from SJL/J (SJL-*Dysf*) muscle (Bittner *et al.*, 1999; Vafiadaki *et al.*, 2001).

In addition to SJL/J there are three additional mouse models of dysferlin deficiency, A/J, Dysf^{tm1Kcam} and Dysf-/- (Brown) (Bansal *et al.*, 2003; Ho M, *et al.*, 2004). A/J is a naturally occurring mouse model of dysferlin deficiency where the mutation is an insertion of a 5-6kb retrotransposon in intron 4 of the dysferlin gene that is present as homozygous (Ho, *et al.*, 2004). The Dysf^{tm1Kcam} mouse has been generated to contain a deletion spanning exons 53-55 (aa 1983-2080) of the dysferlin gene. This deletion would remove the transmembrane domain of the protein and is present as homozygous (Bansal *et al.*, 2003). The Dysf-/- (Brown) mouse is a knockout mouse generated to contain a deletion of exon 45 (aa 1628-1685) of the dysferlin gene. This deletion removes part of the fifth C2 domain (C2E) of the protein and is present as homozygous (Ho *et al.*, 2004). Another mouse C57BL/10.SJL-*Dysf* carries the same mutation as SJL/J mice except that this mutation has been transferred to the C57BL/10 background by repeated backcrossing (von der Hagen *et al.*, 2005). Disease progression in SJL/J, Dysf-/- (Campbell), Dysf-/- (Brown), and C57BL/10.SJL mice is similar; proximal muscles are more severely affected than distal muscles but A/J mice show a slower disease progression and abdominal muscles are also affected as in Dysf-/- (Brown) mice (Ho *et al.*, 2004). Ultrastructural analysis of dysferlin-deficient muscle from Dysf -/-, A/J and SJL mice shows marked thickening and focal duplication of the basal lamina, isolated areas of membrane discontinuity, accumulation of vesicles near the sarcolemma but the contractile apparatus, thin and thick filaments and the neuromuscular junction appear normal (Ho *et al.*, 2004). Behavioral differences were also noticed in all three dysferlin-deficient mice. Severe bite wounds were consistently noticed on SJL female mice that were mated with a SJL male. The extreme aggressive behavior of the SJL mouse was not noticed in Dysf -/- nor A/J mice (Ho *et al.*, 2004). These studies suggested that there could be additional genetic defects in the SJL strain or that there is a unique combination of alleles in the SJL background to account for the aggressive behaviour (Ho *et al.*, 2004). Western analysis from all the mouse models showed no dysferlin expression or severely reduced dysferlin expression at the sarcolemma but control mice showed strong immunoreactivity for dysferlin (Vafiadaki *et al.*, 2001; Bansal *et al.*, 2003; Ho *et al.*, 2004). Immunolocalization of dysferlin in control Balb/c mice showed sarcolemmal staining for dysferlin but also cytoplasmic staining in muscle fibers **(Figure 1.6)** (Ampong *et al.*, 2005). By biochemical fractionation dysferlin was shown to be enriched in sarcolemmal but also in the T-tubule, SR muscle membranes and in

intracellular vesicles from the muscle of control mice. In SJL/J mouse, dysferlin was absent in the different membrane fractions (Ampong *et al.*, 2005).

1.4.2.4 Dysferlin and muscle membrane repair

Membrane tears are a common physiological event in muscle and heart. Muscle has an active membrane repair mechanism. To withstand the rigors of contraction, muscle fibers have a specialized protein machinery that protects the muscle membrane against mechanical stress. This mechanism is rapidly activated after injury. Cells will die if injured muscle is not repaired. Recent progress toward elucidating the mechanism involved in membrane repair has led to the 'Patch Hypothesis' explaining how cells reseal large tears on their surfaces. The 'Patch Hypothesis' states that Ca^{2+} flooding through a membrane disruption site will trigger the accumulation and fusion of vesicles at the wound site leading to the formation of a 'patch' membrane, which is added to the disruption site by Ca^{2+} dependent exocytosis (reviewed in McNeil *et al.*, 2003). The vesicles involved in membrane repair are being identified and are endomembrane derived. Examples of the type of vesicles shown to be involved in membrane repair include the yolk granules in sea urchin eggs, lysosomes in fibroblasts, NRK, CHO, L6E9 and 3T3 cells, enlargeosomes in PC12 cells and endocytic axolemmal vesicles in neurons (McNeil *et al.*, 2003; Terasaki *et al.*, 1997; Augustine, 2001; Bai and Chapman, 2004; Yasunaga *et al.*, 1999; Chakrabarti *et al.*, 2003). Lysosomes had been considered to be the principle source of endomembrane for membrane repair in mammalian cells (Reddy *et al.*, 2001) based on the evidence that wounded cells showed surface expression of the lysosomal marker Lamp-1, in a calcium dependent manner following resealing (Reddy *et al.*, 2001). Lysosomal exocytosis was shown to be Ca^{2+} dependent and regulated by the synaptotagmin, Syt-VII (Reddy *et al.*, 2001). In addition Syt-VII-deficient mice were shown to develop an inflammatory myopathy with extensive fibrosis, high serum creatine kinase levels and progressive muscle weakness, which was associated with defective membrane repair (Chakrabarti *et al.*, 2003). Enlargeosomes are exocytic vesicles represented by the giant protein AHNAK (also known as desmoyokin), which have been implicated in cell membrane enlargement, differentiation, repair and signal transduction (Hohaus *et al.*, 2002; Gentil *et al.*, 2003; Borgonovo *et al.*, 2002; Cocucci *et al.*, 2004). These are

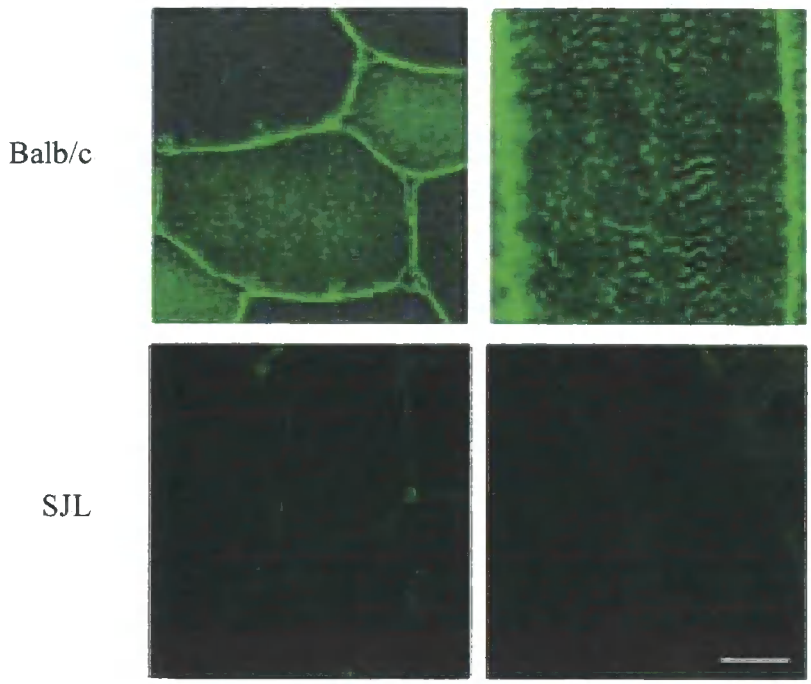

Figure 1.6. Immunohistochemical analysis of dysferlin in skeletal muscle fibers. *Immunofluorescent images of transverse and longitudinal sections respectively of the tibialis anterior (TA) muscles of mice Balb/c and SJL stained with monoclonal antibody against dysferlin showed staining for dysferlin at the sarcolemma and in the cytoplasm in control muscle sections. No staining or severely reduced staining is detected in muscle sections from SJL mice. Scale bar, 20μm. Taken from Ampong et al., (2005).*

novel vesicles, which have been shown to be resistant to nonionic detergents and mediating in endocytosis and recycling via a nonacidic route distinct from classical endosomal vesicles (Cocucci *et al.*, 2004). The participation of enlargeosomes in the enlargement of cell membrane was shown by the increased surface expression of AHNAK following elevation of intracellular calcium during cell differentiation and plasma membrane repair (Borgonovo *et al.*, 2002; Cocucci *et al.*, 2004).

In muscle cells dysferlin vesicles are thought to be the primary membrane repair vesicles. The role of dysferlin in muscle membrane repair was investigated because ultrastructural studies on dysferlin deficient patient muscle biopsies demonstrated membrane tears, duplication of the basal lamina and accumulation of vesicles under the membrane (Cenacchi *et al.*, 2005) similar to those observed in *C. elegans fer-1* mutants, which showed defective MO fusion (Washington and Ward, 2006). Additionally biochemical studies of dysferlin indicated that the C2A domain is capable of binding phospholipids similar to the C2A domain of synaptotagmin (Davis *et al.*, 2002). Together these findings led to the examination of membrane repair in the $Dysf^{tm1Kcam}$ knock out mouse of dysferlin. Laser induced membrane wounding assays were performed on single muscle fibers from wild-type and dysferlin-deficient mice in the presence and absence of calcium and using the dye FM1-43. The laser wounding assay involves creating a membrane disruption using a 10-W Argon/Ti:sapphire laser multiphoton confocal microscope in the presence of the dye FM1-43 and in the presence or absence of calcium. FM1-43 is a membrane-impermeant dye, which fluoresces when it binds to internal membranes (McNeil, 2003). The increase in FM1-43 fluorescence near the wounded site is imaged and measured over a time course (approximately a few minutes) (McNeil, 2003). Resealing of the membrane halts the increase in FM1-43 fluorescence intracellularly. In wounded wild type muscle fibres the entry of FM1-43 dye was efficiently excluded in the presence of calcium indicating that the cells had resealed their torn membranes after laser wounding (Bansal *et al.*, 2003). The Ca^{2+} dependency of membrane repair was shown by wounding in the absence of calcium when the dye continuously entered the muscle cell indicating a failure to reseal. Wounding of dysferlin deficient fibres in the presence of Ca^{2+} did not stop the increase in FM1-43 fluorescence demonstrating that dysferlin-null fibres are defective in membrane repair (Bansal *et al.*, 2003). In parallel

with laser wounding experiments strong staining of dysferlin was observed at the wound sites in wild type muscle fibers (Bansal *et al.*, 2003).

Further evidence of a role of dysferlin in membrane repair was shown from the studies by Lennon *et al.*, (2003). Wild type myotubes from SWR/J mice and myotubes from dysferlin-null SJL/J mice were injured after the cells were preloaded with a fluorescent Ca^{2+} indicator, Indo1-AM. In loaded cells changes in Ca^{2+} were monitored fluorescently following membrane injury. This showed that there was a transient marked elevation of Ca^{2+} in response to membrane disruption in the myotubes from SWR/J cells and levels of Ca^{2+} returned to normal levels within a few seconds highlighting efficient resealing of the disrupted membranes. In the absence of dysferlin the return to the normal Ca^{2+} levels monitored by Indol-AM fluorescence and reflecting membrane repair in SJL/J myotubes was shown to be considerably reduced (Lennon *et al.*, 2003). Co-staining of the lysosomal marker Lamp-1 and a 488-nm fluorophore bound to the dysferlin antibody was performed in myotubes from wild type and SJL/J to show that dysferlin is involved in lysosomal exocytosis (Lennon *et al.*, 2003). Co-staining showed that the sarcolemmal expression of Lamp-1 was detected on 86% of dysferlin-positive myotubes in wild type (SWR/J) membrane in the presence of calcium but this was not observed on intact cells. Chelation of Ca^{2+} with EGTA (1mM) in SWR/J myotubes resulted in a significant reduction (48%) in the amount of surface Lamp-1 after post-injury. In the presence of Ca^{2+}, 60% of cultured dysferlin deficient SJL/J myotubes showed surface Lamp-1 expression after post-injury (Lennon *et al.*, 2003). However, other studies have not shown impaired lysosomal exocytosis in dysferlin deficient muscle cells and studies by McNeil *et al.*, (2003) have shown that dysferlin is not present in lysosomal vesicles.

Further studies have provided additional evidence that dysferlin has a role in membrane repair. In wounded C2C12 myotubes dysferlin has been shown to accumulate in vesicular structures at wound sites, where they colocalize with the T-tubule marker protein, Bin1 (Klinge *et al.*, 2007). T-tubules are beaded tubular invaginations of the plasma membrane, which form a specialized membrane system facilitating excitation contraction coupling reactions (Klinge *et al.*, 2007; Carozzi *et al.*, 2000). T-tubules have been recognized as an endomembrane source of vesicles (Lee *et al.*, 2002). Furthermore, the T-tubule system was shown to be involved in

membrane elongation and repair of the sarcolemma (Engel and Franzini-Armstrong, 2004). The colocalization of dysferlin with Bin1 and other T-tubule markers (Ampong *et al.*, 2005) has led to suggestion that the source of the dysferlin vesicle involved in membrane repair may be the T-tubule system (Klinge *et al.*, 2007).

Recent work has shown that dysferlin's role in membrane repair is not only restricted to skeletal muscles but also extends to cardiac muscle (Han *et al.*, 2007). A Japanese LGMD2B patient has been described suffering from ventricular enlargement and diffuse hypokinesia and carrying a 3370G-T missense mutation in the dysferlin gene (Kurn *et al.*, 2004). These findings prompted the examination of membrane damage in heart muscle from dysferlin knock out mice ($Dysf^{tm1Kcam}$). Cardiac function tests and myocyte membrane repair capacity of dysferlin null mice hearts showed that dysferlin deficiency greatly reduces the membrane repair efficiency of cardiac muscle membrane (Han *et al.*, 2007). Aged dysferlin-null mice manifested hallmarks of cardiomyopathy, for example, elevated serum cardiac troponin T levels, cardiac necrosis and cardiac fibrosis (Han *et al.*, 2007). This suggests a model in which dysferlin might play a role in membrane repair by responding directly to a Ca^{2+} signal triggering vesicle fusion thereby resealing the membrane of cardiomyocytes (Han *et al.*, 2007). It was suggested that the dysferlin role in membrane repair of cardiomyocytes protects the heart from stress-induced left ventricular injury (Han *et al.*, 2007).

1.4.2.4.1 Interacting proteins of dysferlin

The following proteins have been shown to interact with dysferlin in muscle or be part of the dysferlin complex involved in membrane repair.

Caveolin-3: Caveolin-3 is localized to the sarcolemma and is responsible for the formation and maintenance of caveolae, which are specialized lipid raft like, small (50–100nm) invaginations of the plasma membrane present in many vertebrate cell types, especially endothelial cells and adipocytes (Williams and Lisanti, 2004). Caveolin-3 was identified as the first interacting protein of dysferlin in skeletal muscle by immunoprecipitation studies (Matsuda *et al.*, 2001). Mutations in the caveolin-3 (CAV3) gene cause many different muscular dystrophies leading to a deficiency of

caveolin-3 from patient muscle. These muscular dystrophies are called caveolinopathies (Bruno *et al.,* 2007). In the caveolin-3 deficient patient muscle biopies dysferlin expression was shown to be altered but not absent (Matsuda *et al.,* 2001). Caveolin-3 has been shown to regulate the surface trafficking of dysferlin using caveolin 3 null cells and by expressing caveolin-1 and 3 mutant proteins (Hernandez *et al.,* 2006). The caveolins were shown to mediate the trafficking of dysferlin from the Golgi complex to the plasma membrane. In muscle cells expressing caveolin mutants the exit of both mutant and wild type dysferlin from the Golgi complex was shown to be inhibited resulting in the retention of dysferlin in the Golgi complex (Hernandez *et al.,* 2006). The endocytosis of dysferlin was also shown to be rapid in caveolin null cells (Hernandez *et al.,* 2008). Recent studies have shown that caveolin-3 functions with MG53, a novel muscle membrane repair protein (see below) to regulate the surface trafficking of dysferlin (Cai *et al.,* 2009[b]).

Annexin A1 and A2: Microarray studies of dysferlin deficient muscle have reported the upregulation of Annexin A1 and A2 (Butte *et al.,* 2000; Campanaro *et al.,* 2002; Lennon *et al.,* 2003). Consistent with this data the expression of both annexin A1 and A2 has been shown to be higher in dysferlin-deficient (SJL/J) mouse muscle (Lennon *et al.,* 2003). These results led to investigations to examine the expression and function of annexin A1/A2 in skeletal muscle cells. Annexins are calcium and phospholipid binding proteins, which are widely expressed (Gerke and Moss, 2002). Annexins comprise a large protein family and are implicated in a variety of functions such as membrane organization, membrane aggregation and fusion, membrane trafficking, exocytosis, endocytosis, ion fluxes, signal transduction, inhibition of phospholipase A_2 and cell-matrix interactions (reviewed in Gerke and Moss, 2002; Moss and Morgan, 2004). Annexin A1 and A2 have been shown to aggregate intracellular vesicles and lipid rafts in a Ca^{2+} dependent manner at the cytosolic surface of plasma membranes in many cell types (Babiychuk and Draeger, 2000; Lambert *et al.,* 1997). Annexin A1 binds to S100A11 protein by forming a heterotetramer to mediate the aggregation of vesicles (Gerke and Moss, 2002). Annexin A2 has been postulated to have a similar relationship with S100A10 (Gerke and Moss, 2002). By immunolocalization and immunoprecipitation studies annexin A1 and A2 have shown to associate with dysferlin in a Ca^{2+} dependent fashion in intact skeletal muscle cells and the association has been shown to be mediated through

the unique N-terminal domains of annexins A1 and A2 (Lennon *et al.*, 2003). The interaction between annexins and dysferlin was confirmed using Fluorescence Lifetime Imaging Microscopy (FLIM), which measures the decay half life of fluorescent molecules immunologically attached to individual proteins and allows sensitive measurement of protein-protein interactions on a spatial scale of <10nm (Bacskai *et al.*, 2003). The role of annexin A1 in membrane repair has been demonstrated. Annexin A1 function was inhibited in HeLa and BS-C-1 cells by loading cells with annexin A1 antibody, by peptide competition experiments and expression of dominant negative annexin A1 mutants. Laser and glass bead wounding assays were used to show that disruption of annexin A1 expression impedes membrane repair (McNeil *et al.*, 2006). A model describing the role of dysferlin and its interacting partners proposed by Glover and Brown, (2007) is shown in **Figure 1.7A.**

AHNAK1: AHNAK1 (also called desmoyokin) is a nucleoprotein composed of three structural domains, the central domain composed of multiple IgG repeating units. Unique-sequence domains at the two ends of the protein flank a large internal domain (approximately 4300 amino acids), which is composed of highly conserved repeated elements and most of which are 128 amino acids in length (Shtivelman *et al.*, 1993). AHNAK is a novel family of two proteins (AHNAK and AHNAK2), which are characterized by common amino acid sequences and of exceptionally huge size (~600-700 kDa) (Komuro *et al.*, 2004). AHNAK1 binds with G-actin and cosediments with F-actin and has been implicated in the organization of the subsarcolemmal cell architecture (Cocucci *et al.*, 2004). Regulation of cellular AHNAK content in correlation with cell membrane remodeling and specialization has already been demonstrated in epithelial and endothelial cells (Benaud *et al.*, 2004). In these cells, AHNAK stabilization was shown to be dependent on its recruitment to the plasma membrane through interaction with its partner proteins, including the annexin2/S100A10 complex (Benaud *et al.*, 2004). In normal human skeletal muscle fiber AHNAK is known to be localized at the plasma membrane by immunohistochemistry and immunofluorescence experiments (Gentil *et al.*, 2003).

Figure 1.7A. The model of dysferlin-mediated membrane repair in skeletal muscle. ***a)*** *In normal muscle dysferlin is localized at the plasma membrane and cytoplasmic vesicles, where it interacts with AnxA1 and AnxA2, AHNAK, affixin and caveolin-3.* ***b)*** *Upon membrane injury the intracellular* Ca^{2+} *concentration is increased creating a zone of high calcium around the disruption site, triggering the membrane patch response. The high intracellular calcium levels activate proteases such as calpain 3 leading to the remodeling of the cortical cytoskeleton, which removes this physical barrier to fusion events.* ***c)*** *Dysferlin repair vesicles traffic to the wound site, where they accumulate and fuse with one another and with the plasma membrane in the presence of elevated calcium at the wound site. This requires interaction with annexin A2, other dysferlin molecules and other unknown proteins. Affixin is predicted to mediate vesicle trafficking through reorganization of the cortical cytoskeleton at the injury site.* ***d)*** *Fusion of the dysferlin repair vesicles with plasma membrane forms a membrane patch at the membrane disruption, resealing injured plasma membrane and preventing further influx of* Ca^{2+}*. Taken from Glover and Brown, (2007).*

A

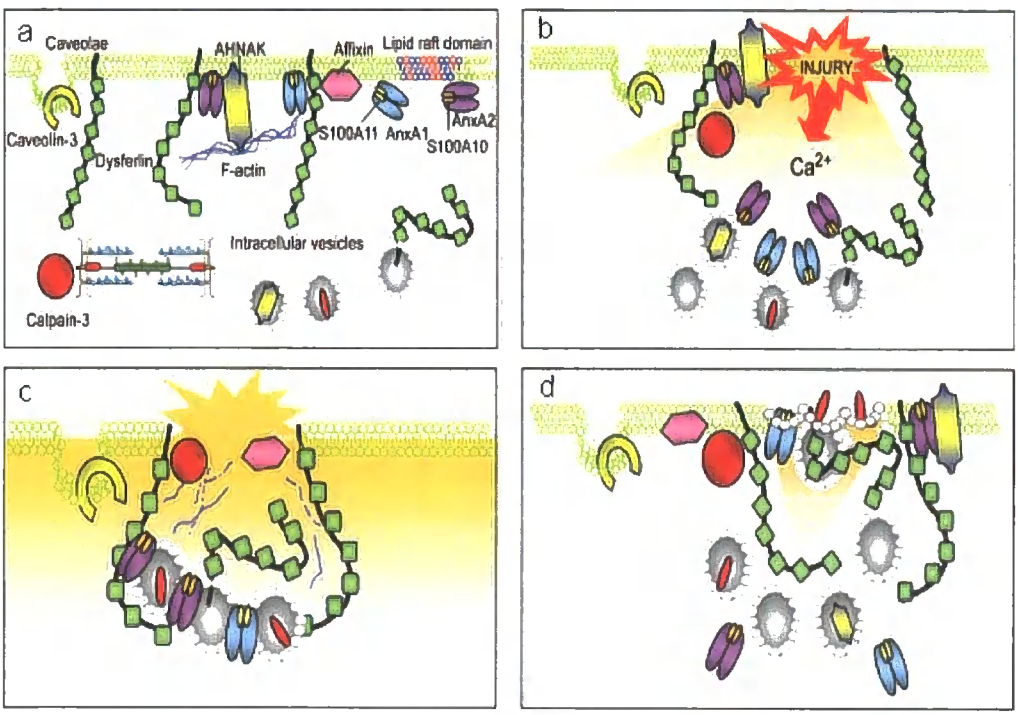
a
Caveolae
AHNAK
Affixin
Lipid raft domain
Caveolin-3
Dysferlin
F-actin
S100A11
AnxA1
AnxA2
S100A10
Intracellular vesicles
Calpain-3
b
INJURY
Ca^{2+}
c
d

Figure 1.7B. A model showing the role of MG53 in skeletal muscle membrane repair. *Extracellular calcium and extracellular oxidants enter the cell at membrane injury site triggering vesicle trafficking to the wound site. Dysferlin vesicles migrate towards the injury site probably using kinesin, motor proteins. Aggregation and fusion of dysferlin vesicles with each other form a 'patch' vesicle membrane. Vesicle docking is mediated by oxidized MG53. Fusion is mediated by annexin and dysferlin activated by calcium and probably by SNARE proteins. The 'patch' membrane fuses with the plasma membrane resealing the injured membrane. Taken from Mc Neil, (2009).*

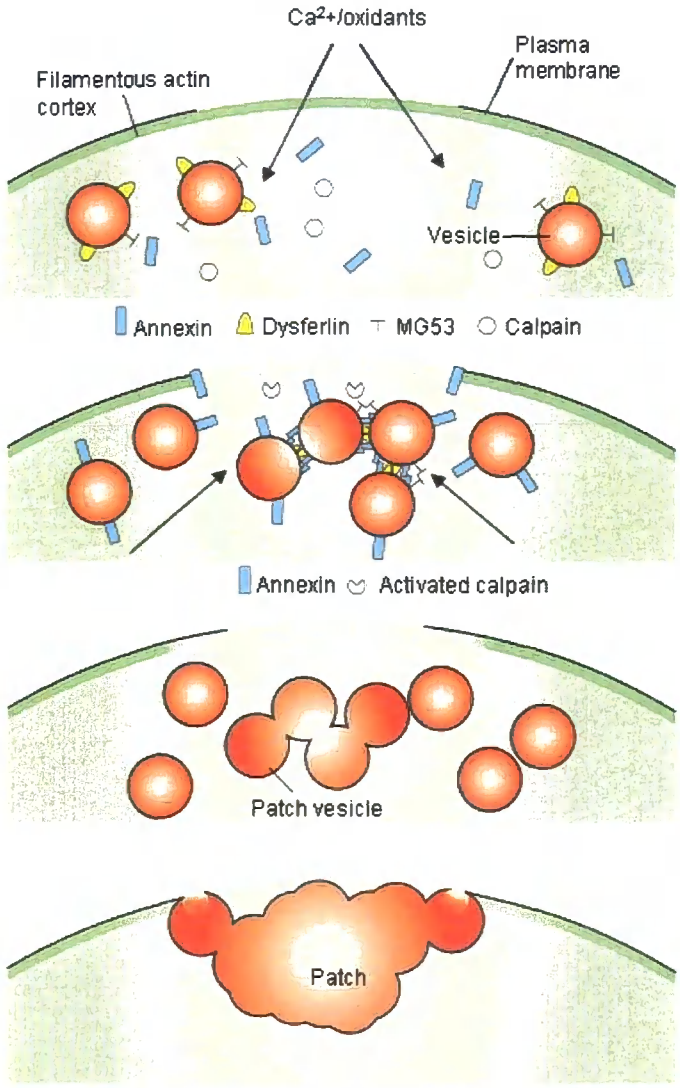
Ca2+/oxidants
Plasma membrane
Filamentous actin cortex
Vesicle
Annexin
Dysferlin
MG53
Calpain
Annexin
Activated calpain
Patch vesicle
Patch

AHNAK has been shown to form a complex with dysferlin in skeletal muscle by coimmunoprecipitation experiments (Huang *et al.*, 2007). It is not clearly mentioned which isoform of the AHNAK interacts with dysferlin but we believe that AHNAK refers to the isoform AHNAK1. In human skeletal muscle, AHNAK localized at the sarcolemmal membrane was shown to colocalize with dysferlin and the dihydropyridine receptor (DHPR) subunit of the L-type Ca^{2+} channel by immunofluorescent analysis (Huang *et al.*, 2007). In dysferlinopathy, reduction or absence of dysferlin was shown to result in a secondary muscle-specific reduction in AHNAK (Huang *et al.*, 2007). Glutathione S-transferase (GST) pull-down assays of different recombinant GST AHNAK and dysferlin fusion proteins has demonstrated that the binding site of dysferlin and AHNAK is between the C-terminus of AHNAK and the N-terminal C2A domain of full length dysferlin (Huang *et al.*, 2007). AHNAK and dysferlin were shown to be in a complex (Huang *et al.*, 2007). In regenerating muscle the levels of AHNAK and dysferlin were elevated and there was a redistribution of both proteins from the sarcolemma to the cytoplasm (Huang *et al.*, 2007). The role of AHNAK in membrane repair is unclear because the absence of AHNAK containing exocytotic vesicles does not impair membrane repair whereas AHNAK positive enlargeosomes have been shown to undergo Ca^{2+} regulated exocytosis following plasma membrane disruption (Cocucci *et al.*, 2004).

Affixin: Affixin (beta-parvin) is a novel, integrin-linked kinase-binding protein that is involved in the linkage between integrin (a cell adhesion molecule that mediates cell-extracellular matrix and cell-cell interactions) and the cytoskeleton (Yamaji *et al.*, 2001). It is highly enriched in skeletal and cardiac muscle (Yamaji *et al.*, 2004). Affixin was shown to colocalize with dysferlin at the sarcolemma of normal human skeletal muscle and co-immunoprecipitates with dysferlin (Matsuda *et al.*, 2005). The immunoreactivity of affixin was shown to be reduced at the sarcolemma of MM and LGMD2B patient muscles, although the total amount of the affixin protein levels were unchanged (Matsuda *et al.*, 2005). Affixin was shown to interact with dysferlin in mouse and human skeletal muscles by coimmunoprecipitation. Using immunoprecipitation with deletion mutants of dysferlin the C-terminal intracellular region of dysferlin was identified as the apparent affixin binding domain and the CH1 domain of affixin was identified as the dysferlin-interacting region (Matsuda *et al.*,

2005). The role of affixin in membrane repair has not been elucidated and no other studies have identified affixin in a dysferlin complex.

MG53: MG53 (mitsugumin 53) is a newly discovered protein belonging to the tripartite motif/RING B box Coil Coil (TRIM/RBCC) family of proteins that is expressed specifically in skeletal and cardiac muscle (Sardiello *et al.*, 2008; Cai *et al.*, 2009[a]). Mice lacking MG53 develop a dystrophic phenotype, which is linked with defective membrane repair (Cai *et al.*, 2009[a]). MG53 is localized to intracellular vesicles and the sarcolemma through binding with the lipid phosphatidylserine (Cai *et al.*, 2009[a]). MG53 vesicles were shown to traffic to the cell surface and fuse with the cell membrane and overexpression of MG53 enhances vesicle fusion and formation of filopodia like structures (Cai *et al.*, 2009[b]). The exocytosis of MG53 vesicle was shown to be dependent upon caveolin-3 (Cai *et al.*, 2009[b]). Further studies by Cai *et al.*, (2009[b&c]) demonstrated the role of MG53 in membrane repair. MG53 vesicles were shown to translocate to muscle membrane injury sites and analysis of MG53 deficient muscle by electron microscopic analysis confirmed that MG53 is involved in vesicle trafficking during membrane repair because vesicle translocation was shown to be lacking at muscle injury sites in MG53 deficient muscle. Further studies on MG53 revealed that the function of MG53 during membrane repair is dependent upon the redox state of the cell. In the presence of an oxidative environment such as that found extracellularly MG53 undergoes oligomerization. A model was proposed whereby oxidation-dependent oligomerization of MG53 acted as a signal to facilitate the recruitment of MG53 vesicles to membrane injury sites because MG53 was shown to act independent of Ca^{2+} unlike other known membrane repair proteins including dysferlin and annexins (Cai *et al.*, 2009[a]; McNeil and Kirchhausen, 2005; Bansal *et al.*, 2003; Lennon *et al.*, 2003). The relationship of MG53 and dysferlin is emerging and a recent paper on MG53 has demonstrated that MG53 regulates the surface trafficking of dysferlin through its interaction with caveolin-3 (Cai *et al.*, 2009[c]). *Mg53*$^{-/-}$ mice show retention of dysferlin containing vesicles in the post Golgi compartment indicating that the translocation of dysferlin vesicles to the injury site requires MG53 and also caveolin-3. In this first study of MG53, Cai *et al*, (2009[b]) demonstrated that MG53 and caveolin-3 colocalize in muscle cells and that MG53 regulates membrane budding and exocytosis. A physical interaction between caveolin-3 and MG53 was demonstrated and shown to mediate the trafficking of dysferlin

vesicles to the injury site during membrane repair (Cai *et al.*, 2009[c]). Expression of caveolin-3 mutants was shown to cause retention of wild type caveolin-3 in the Golgi complex and this also resulted in an aberrant localization of MG53 and dysferlin, which was associated with defective membrane repair (Cai *et al.*, 2009[c]). Therefore MG53, dysferlin and caveolin-3 appear to form a functional complex in muscle that is involved in the recruitment of vesicles to the membrane wound site. The recent model of membrane repair includes the involvement of MG53 and its interaction with dysferlin and caveolin is shown in **Figure 1.7B** (Mc Neil, 2009).

1.4.2.5 Dysferlin and muscle inflammation

In dysferlinopathy inflammation has been shown to be a key feature with patients often misdiagnosed with polymyositis (Nguyen *et al.*, 2007). Endomysial and perivascular infiltrates have been shown to be common in necrotic dysferlin deficient fibres, consisting mostly of $CD4^+$ and $CD8^+$ T-cells and macrophages (Selcen *et al.*, 2001; Nguyen *et al.*, 2007; McNally *et al.*, 2000; Gallardo *et al.*, 2001). Non necrotic dysferlin-deficient fibers are free of all types of infiltrates (Gallardo *et al.*, 2001). There is upregulation of major histocompatibility complex (MHC) class I antigens in dysferlin deficient muscle (Gallardo *et al.*, 2001; Selcen *et al.*, 2001) and there is an increased number of macrophages and T lymphocytes in patients indicating an active inflammatory response (Gallardo *et al.*, 2001; Confalonieri *et al.*, 2003; Cenacchi *et al.*, 2005). In all of the mouse models of dysferlin deficiency high numbers of necrotic and regenerating fibers were observed and there was infiltration of mononuclear cells into intact fibers, phagocytosis and marked variation of fiber size as observed in dysferlinopathy patients (Ho *et al.*, 2004). Ultrastructural studies demonstrated that some macrophages and lymphocytes were tightly adhered to the sarcolemma (Kostek *et al.*, 2002; Gallardo *et al.*, 2001, Confalonieri *et al.*, 2003) **(Figure 1.8)**. It has been now recognized that dysferlin is normally expressed in $CD14^+$ monocytes and that $CD14^+$ monocytes from LGMD2B and MM patients are deficient for dysferlin (Gallardo *et al.*, 2001). Detection of dysferlin in monocytes has become a diagnostic test for the dysferlinopathies (Gallardo *et al.*, 2001). Monocytes differentiate into macrophages and in these cells, membrane fusion events are critical for phagocytosis and cytokine release (Nagaraju *et al.*, 2008). Recently, it has been demonstrated that monocytes from patients with dysferlinopathy show increased

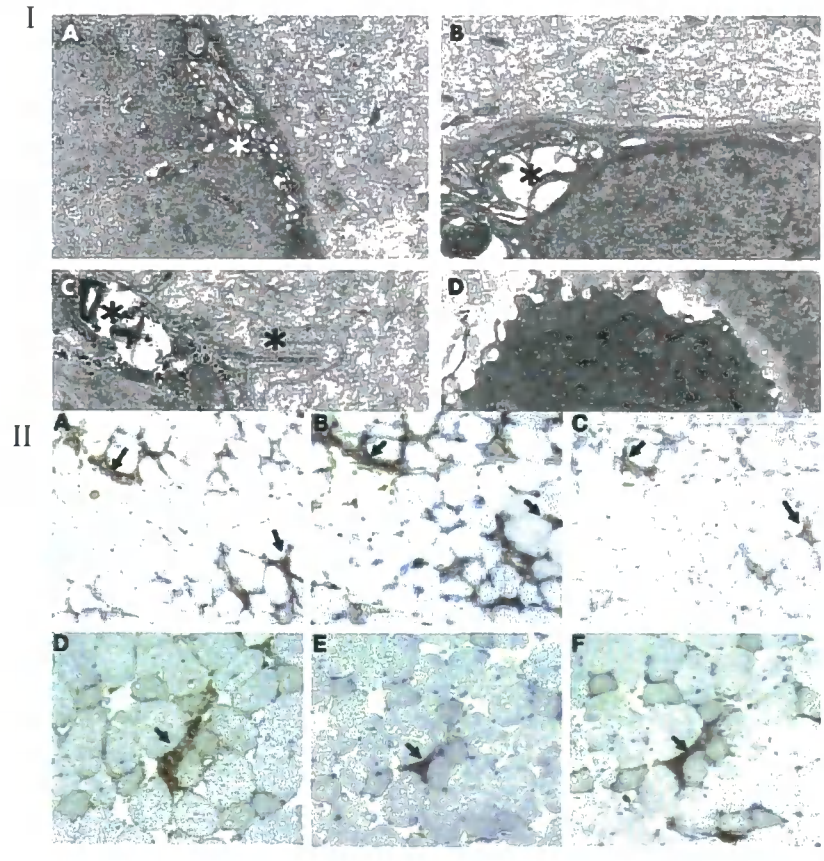

Figure 1.8. Ultrastructural analysis of skeletal muscle from a patient with dysferlinopathy. I) *Features include subsarcolemmal accumulation of vesicles indicated by asterisk in image A, swollen cisternae indicated by asterisk in image B, presence of vacuoles and microvilli-like projections (indicated by left and right asterisks respectively in image C) and infiltration of lymphocytes (shown in image D).* ***II)*** *Infiltration of activated macrophages in muscle from dysferlin-deficient patients (A-C) and SJL/J mouse (D-F). Macrophage activation markers HLA-DR (A), HLA-A, -B, -C (B), CD86 (C) MOMA-2 (D), CD11c (E), and ICAM-1 were used (F). Images I and II taken from Cenacchi et al., (2004); Nagaraju et al., (2008) respectively.*

bacterial phagocytosis compared to control cells (Nagaraju *et al.*, 2008) **(Figure 1.8).** Monocytes and peritoneal macrophages from normal control C57BL/6 and dysferlin-deficient SJL/J mice strains were tested for their ability to phagocytose fluorescently-labeled *E.coli* and showed enhanced phagocytic activity (Nagaraju *et al.*, 2008). The phagocytic activity of the monocytes was also demonstrated by siRNA mediated knock down of dysferlin using the J774 macrophage cell line, which also exhibited significantly higher bacterial phagocytosis (Nagaraju *et al.*, 2008). In SJL mice strong upregulation of endocytic proteins CIMPR, clathrin, adaptin-a and small Rho family GTPases RhoA, Rac1 and Cdc 42 was also observed in splenocytes and macrophages of dysferlin-deficient AJ mice (Nagaraju *et al.*, 2008). Abnormal signaling and phagocytosis was predicted to be the cause of the inflammation in dysferlinopathy (Nagaraju *et al.*, 2008). To identify which signaling pathways were active in dysferlin deficient muscle, microarray studies were performed, which highlighted that loss of dysferlin in muscle activates compensatory membrane trafficking pathway, the Slp2a and Rab27A pathway (Kesari *et al.*, 2008). This pathway is normally inactive in muscle and normally operates in melanocytes and T-cells. Examination of dysferlinopathy patients has shown that in dysferlin deficient muscle T-cells are more activated (Kesari *et al.*, 2008). These findings have led to suggestions that following muscle injury in dysferlin deficient patients there is an exaggerated immune response triggered by the loss of dysferlin in monocytes and activation of compensatory vesicle trafficking pathways in muscle and this exacerbates the dystrophic phenotype (Kesari *et al.*, 2008).

1.4.2.6 Dysferlin and muscle regeneration

Several studies analyzing dysferlin deficient patient muscle and mouse models of dysferlinopathy have highlighted the role of dysferlin in muscle regeneration. Dysferlin was shown to be highly expressed in satellite cells in dystrophic muscle biopsies and expression of dysferlin was shown to increase in activated satellite cells (Luna *et al.*, 2004). In differentiating myoblasts, dysferlin mRNA and protein expression was elevated reaching maximal levels in mature myotubes. Inhibiting myoblast fusion using drugs resulted in a decrease in dysferlin expression (Luna *et al.*, 2004). These preliminary studies hinted at the role of dysferlin in muscle regeneration. Further studies demonstrated that myoblast fusion was delayed in siRNA transfected

C2C12 cultures showing dysferlin knock down (Luna *et al.*, 2006). Dysferlin deficient patient muscle cultures also showed delayed myoblast fusion as demonstrated by measuring the fusion index of the cultures. A functional link between dysferlin and myogenin during muscle regeneration was highlighted. During muscle differentiation knockdown of dysferlin using siRNA was shown to correlate with reduced myogenin levels (Luna *et al.*, 2006). Myotubes formed from dysferlin deficient cultures also showed reduced expression of myogenin mRNA. In addition to its role in membrane repair dysferlin was proposed to function in a myogenic signaling pathway (Luna *et al.*, 2006). In rats, muscle regeneration can be studied by cardiotoxin treatment, which induces muscle regeneration after muscle damage (Harris *et al.*, 1974). In wild type mice, notexin treated muscle can be repaired within 3 or 4 days post injection by muscle regeneration (Harris *et al.*, 1974). In normal rat muscle dysferlin was shown to localize at the sarcolemma where it colocalized with AHNAK (Huang *et al.*, 2007). After notexin treatment both dysferlin and AHNAK were shown to redistribute in the cytoplasm of regenerating muscle fibres (Huang *et al.*, 2007). In dystrophic muscle a cytoplasmic localization of dysferlin and increased protein expression has also been observed in regenerating muscle fibres (Lo *et al.*, 2008). However it must be pointed out that dysferlin mislocalization in dystrophic muscle is not only linked to fibre regeneration but may also be due to defective membrane targeting of dysferlin (Lo *et al.*, 2008). A recent study by Chiu *et al.*, (2009) has demonstrated that muscle biopsies from dysferlinopathy patients show an excess of immature fibers indicating that muscle regeneration is delayed. Notexin was used to induce muscle damage in dysferlin deficient SJL/J mice and attenuated muscle regeneration was demonstrated, which was associated with delayed removal of necrotic fibres, an extended inflammatory phase and delayed functional recovery (Chiu *et al.*, 2009). In their collection of dysferlin deficient muscle biopsies from patients they observed an inflammatory cell infiltrate with reduced neutrophil levels in muscle. Following muscle injury of SJL dysferlin deficient mice using notexin or by needle wounding Chiu *et al.*, (2009) confirmed that there was a reduction in early neutrophil recruitment in muscle from dysferlin deficient C57BL/10.SJL-*Dysf* mice. Satellite cell activation and myoblast fusion during regeneration was shown to be normal. Using dysferlin deficient myoblast cultures cytokine release upon stimulation was shown to be reduced. Collectively these findings have led to suggestions that dysferlin is not only involved in vesicle fusion but also secretion of cytokines from skeletal muscle.

The inflammatory response following muscle damage has been shown to be critical for muscle regeneration. Neutrophils are recruited first to the muscle injury site and signaling from neutrophils and satellite cells then recruit monocytes, which undergo phagocytosis to remove cell debris (Gallardo *et al.*, 2001; Fanin and Angelini, 2002; Luna *et al.*, 2004). The monocytes recruited to the injury site first acquire an inflammatory phenotype to release proinflammatory cytokines, which activate satellite cell proliferation but then they switch phenotype to become anti-inflammatory stimulating myoblast fusion (Arnold *et al.*, 2007). Depletion of neutrophils and monocytes in wild type muscle has been shown to delay muscle regeneration (Teixeira *et al.*, 2003). A model has been proposed to suggest that in dysferlinopathy there is defective membrane repair but the reduced secretion of cytokines in the absence of dysferlin leads to impaired muscle regeneration and this then acts as the final trigger for the development of the dystrophic pathology (Chiu *et al.*, 2009).

1.4.2.7 Dysferlin function in non-muscle cells

Recent publications have extended the knowledge of dysferlin expression in non muscle cells. Dysferlin has been shown to be highly expressed in the apical plasma membrane of the syncytiotrophoblasts (STBs) in human placenta with some expression in blood vessels, leaky endothelial cells of circumventricular organs of CNS and glomeruli of kidney cells (Vandré *et al.*, 2007; Hochmeister *et al.*, 2006; Hassane *et al.*, 2006). The expression of dysferlin in the human placental microvillous STBs was first identified through proteomic studies (Vandré *et al.*, 2007). Dysferlin was shown to be prominent within the apical plasma membrane with lesser expression in the basal membranes (Vandré *et al.*, 2007). This study also demonstrated trafficking of dysferlin to both apical and basal plasma membrane of the STB through a caveolin-independent mechanism based on the absence of both a and ß isoforms of CAV1 staining in the STB by double labeling experiments. This suggested that dysferlin may be involved in polarized trafficking. Additionally, Vandré *et al.*, (2007) have shown that dysferlin expression is highly increased in fusing and multinucleated syncytial cells and not in mononuclear cytotrophoblasts that had not fused with syncytial structures (Vandré *et al.*, 2007).

In the study by Hochmeister *et al.*, (2006), dysferlin expression in endothelial cells was detected in inflamed and non inflamed vessels in patients with multiple sclerosis

(MS). In the inflamed CNS of patients with MS or in animals with experimental autoimmune encephalomyelitis, dysferlin reactivity was shown to be induced in endothelial cells and the expression was shown to associate with vascular leakage (Hochmeister *et al.*, 2006). In addition, many blood vessels with perivascular inflammatory infiltrates were shown to lack dysferlin expression in inactive lesions or in the normal-appearing white matter. In vitro analysis showed that expression of dysferlin in endothelial cells can be induced by stimulation with tumor necrosis factor-alpha (Hochmeister *et al.*, 2006). Hence, in this study dysferlin was shown to be a new marker for leaky brain vessels (Galvin *et al.*, 2006).

Expression of dysferlin in the kidney has been reported in patients with LGMD2B and these patients also showed renal abnormalities characterized by glomerular proteinuria (Hassane *et al.*, 2006). Analysis of urinary protein levels detected high levels of microalbuminuria, which was associated with an absence of dysferlin in the glomerular regions of the kidney. In kidney of patients with idiopathic minimal change nephropathy or healthy controls no loss of dysferlin was observed in the glomerular regions of renal biopsies (Hassane *et al.*, 2006). The presence of dysferlin in glomeruli has been associated with glomerular permeability.

1.4.3 Myoferlin

Myoferlin was the first protein identified that shares the highest similarity to dysferlin (Davis *et al.*, 2000). Like dysferlin, myoferlin is located at the sarcolemma of skeletal muscle and is also present in cytoplasmic vesicles, the nucleus and at the nuclear membrane (Davis *et al.*, 2000). Myoferlin is a ubiquitously expressed protein and shows high expression in muscle, heart, kidney, spleen and lung. Initial studies investigated the expression of myoferlin in dystrophic muscle and although no significant changes in expression were observed in dysferlin deficient muscle (Inoue *et al.*, 2006) the sarcolemmal expression of myoferlin was increased in *mdx* skeletal muscle (Davis *et al.*, 2000). Since *mdx* muscle undergoes several rounds of degeneration and regeneration myoferlin was implicated in muscle regeneration (Davis *et al.*, 2000). Subsequent studies on myoferlin null mice showed defective myogenesis and the loss of myoferlin was shown to result in reduced muscle mass with the loss of large diameter myofibers (Doherty *et al.*, 2005). Myoferlin null

muscle cultures displayed a reduced myogenic index compared to controls (Doherty *et al.*, 2005). Using cardiotoxins to induce muscle regeneration it was demonstrated that mice lacking myoferlin were impaired in their ability to regenerate skeletal muscle after injury (Doherty *et al.*, 2005). Staining of dystrophin showed many irregularly shaped small muscle fiber in myoferlin null muscle similar to a dystrophic phenotype. An increased expression of dysferlin was also observed in myoferlin null muscle (Doherty *et al.*, 2005). In the C2C12 model of myoblast fusion myoferlin was expressed abundantly in myoblasts primed for fusion, "prefusion" myoblasts. Myoferlin was found in vesicular structures in the cytoplasm and at the plasma membrane. In myoblasts fusing with myotubes myoferlin was shown to concentrate at sites of membrane merging (Davis *et al.*, 2002; Doherty *et al.*, 2005). Recently dysferlin has also been shown to concentrate at membrane fusion sites of myoblast/myotube undergoing fusion suggesting that both myoferlin and dysferlin are required for membrane merging (Huang *et al.*, 2007). So far, myoferlin has not been shown to be directly linked to any human disease but the expression of myoferlin is upregulated in dystrophin-deficient (*mdx*) skeletal muscle and also in regenerating muscle (Davis *et al.*, 2000; Haslett *et al.*, 2002). Myoferlin shares biochemical similarities to dysferlin; its C2A domain has been shown to bind phospholipid in a calcium dependent manner like the dysferlin C2A domain (Davis *et al.*, 2002). The second C2 domain of myoferlin C2B binds the membrane recycling protein EHD2 (Doherty *et al.*, 2008). EHD2 levels are reduced in myoferlin null muscle cells and by examining the endocytosis of transferrin, delayed membrane recycling was demonstrated in myoferlin null myoblasts (Doherty *et al.*, 2008). Consistent with this the expression of a dominant negative EHD2 protein in myoblasts was shown to result in sequestration of myoferlin and inhibition of myoblast fusion (Doherty *et al.*, 2008). These studies have highlighted that myoferlin is involved in membrane recycling during myoblast fusion.

Proteomic analysis of endothelial cell (EC) caveolea/lipid rafts microdomains has demonstrated that myoferlin is strongly expressed in EC and vascular tissues (Bernatchez *et al.*, 2007). Subsequent studies of myoferlin null EC demonstrated that in cultured EC cells myoferlin was found at the cell surface and predominantly localized at the sarcolemma and lining of intact blood vessels. The loss of myoferlin was shown to reduce the levels of vascular endothelial growth factor receptor-2

(VEGFR-2) and its autophosphorylation (Bernatchez *et al.*, 2007). Myoferlin was shown to regulate the stability of vascular endothelial growth factor receptor by forming a complex with dynamin-2 (Dyn-2) and this protected the receptor from CBL-dependent degradation in cells depleted for myoferlin (Bernatchez *et al.*, 2007; Bernatchez *et al.*, 2009). Consistent with this myoferlin knock out mice showed impaired VEGF permeability effect in vivo (Bernatchez *et al.*, 2007). Further studies by Bernatchez *et al.*, (2009) have provided further evidence that myoferlin has a role in endocytosis. The interaction of myoferlin with dynamin-2 prompted studies in endothelial cells to determine whether myoferlin is involved in receptor dependent endocytosis because dynamin-2 is required for fission of endocytic vesicles from the cell membrane. siRNA knockdown of myoferlin in EC cells was shown to decrease clathrin dependent and raft dependent endocytosis. In cells overexpressing myoferlin endocytosis was increased (Bernatchez *et al.*, 2009). The role of myoferlin in endocytosis was shown to be dependent upon an interaction with dynamin-2 and caveolin-1. From these studies it appears that myoferlin is required for several endomembrane fusion events.

1.4.4 Otoferlin

Otoferlin, as the name implies is the ferlin highly expressed in the inner ear including cochlea, vestibule and brain although a low level of expression is seen in other tissues including lung, kidney, skeletal muscle and heart (Yasunaga *et al.*, 1999). By *in situ* hybridization, otoferlin staining was observed in mouse inner hair cells (IHC), outer hair cells (OHC), spiral ganglion cells, neuroepithelia of the utricle, saccule and semicircular canals at embryonic day 19.5, P0 and P2 (Yasunaga *et al.*, 2000). In the inner ear, otoferlin immunoreactivity was found highest in the IHC and the staining was shown to be associated with the basolateral region of these cells where the afferent synaptic contacts are located suggesting that otoferlin is a component of the hair cell presynaptic machinery. Ultrastructural studies have demonstrated that otoferlin is associated with synaptic vesicles surrounding the ribbon and presynaptic membranes of IHC (Roux *et al.*, 2006). Otoferlin mutations are linked with autosomal recessive non-sydromic deafness (Yasunaga *et al.*, 1999; Yasunaga *et al.*, 2000). Mutations in these patients have a type of hearing loss called auditory neuropathy, which prevents the transmission of sound from the inner ear to the brain. Otoferlin has

been implicated in synaptic exocytosis and is required for the late step of Ca^{2+} dependent synaptic vesicle exocytosis acting as the major Ca^{2+} sensor triggering synapic vesicle fusion at the IHC ribbon synapse (Roux *et al.*, 2006). Many C2 domain containing membrane proteins are present in synaptic vesicles and are implicated in synaptic vesicle exocytosis (Nalefski and Falke, 1996). Synaptotagmin I (Syt I), the most extensively studied synaptic vesicle membrane protein, has been shown to interact with the two members of the SNARE complex; syntaxin 1 and SNAP25 and is considered as the major Ca^{2+} sensor of fast synaptic vesicle exocytosis at conventional synapses (Kee and Scheller, 1996; Li *et al.*, 1995; Gerona *et al.*, 2000; Zhang *et al.*, 2002; Reviews: Chapman, 2002; Sudhof, 2004). The synaptic location of otoferlin and its predicted C2 domains suggested that otoferlin might play a similar role in IHC synaptic vesicle fusion and otoferlin may also interact with syntaxin 1 and SNAP25. This was demonstrated in *Otof-/-* mice, which were shown to have a profound hearing impairment (Roux *et al.*, 2006). *Otof-/-* IHCs lacked the fast component of the exocytotic burst even in increased concentration of Ca^{2+} compared to control IHCs, which showed fast exocytotic burst in the presence of Ca^{2+}. The experiments also showed that the deafness in otoferlin-deficient mice appeared to be caused by an almost complete loss of calcium mediated exocytosis from IHC suggesting that otoferlin functions as the calcium sensor during synaptic exocytosis in IHC. Interaction of otoferlin with syntaxin 1 and SNAP25 was demonstrated by coimmunoprecipitation studies using protein extracts from mouse cochlear sensory epithelium and confirmed by pull down assays using GFP otoferlin fusion proteins. These experiments demonstrated a direct binding of SNAP25 and syntaxin 1, which was also shown to be calcium dependent. Otoferlin and SNARE protein interactions have been confirmed and the interacting site on otoferlin for the SNARE interactions is the C2F domain (Ramakrishnan *et al.*, 2009). Expression of otoferlin C2F mutations, which are linked with deafness impaired the ability of otoferlin to bind SNARE proteins indicating that these interactions with otoferlin regulate IHC synaptic exocytosis (Ramakrishnan *et al.*, 2009).

1.4.5 FER1L5

Belonging to the ferlin family, FER1L5 is subgrouped with dysferlin and myoferlin based on the sequence and structural homology **(see section 1.2, Figure 1.1 and**

Figure 1.4). The FER1L5 sequence was assembled by Dr. Bashir's group in 2005 and annotated sequences of FER1L5 are also deposited in Entrez Gene. The annotated sequence shows very good overlap with the sequence assembled by the Bashir's Laboratory, which represents the long FER1L5 isoform. In Entrez Gene, sequences to a long and short isoform of FER1L5 are deposited. The long isoform of the FER1L5 gene has a 6297 base pair sequence encoding a protein of 2098 amino acids with a predicted molecular mass of 242 kDa. The short isoform of the FER1L5 gene has a 2536 base pair sequence encoding a protein of 802 amino acids, which shares 98% sequence similarity with long isoform of the FER1L5. The short isoform is predicted to have the last C2 domains present in the long isoform corresponding to C2E and C2F **(see Figure 1.9A)**. FER1L5 shares 38% identity and 54% similarity with human dysferlin and myoferlin respectively (Table 1.1). The FER1L5 gene is conserved in evolution and is present in the rodent, frog, fly, and worm genomes (Table 1.2). FER1L5 has a similar structure to dysferlin and myoferlin and contains six C2 domains corresponding to the C2A to C2F domains in dysferlin and myoferlin. It also has the dysferlin domain DysFN domain. The FER1L5 genome is organized across fifty two exons. The gene expression profile of FER1L5 during C2C12 differentiation was shown by Dr. Bashir's group to be similar to that of dysferlin and myoferlin, with expression increasing in differentiating myoblasts **(Figure 1.9B)**. From these findings it was predicted that FER1L5 may be involved in muscle membrane fusion.

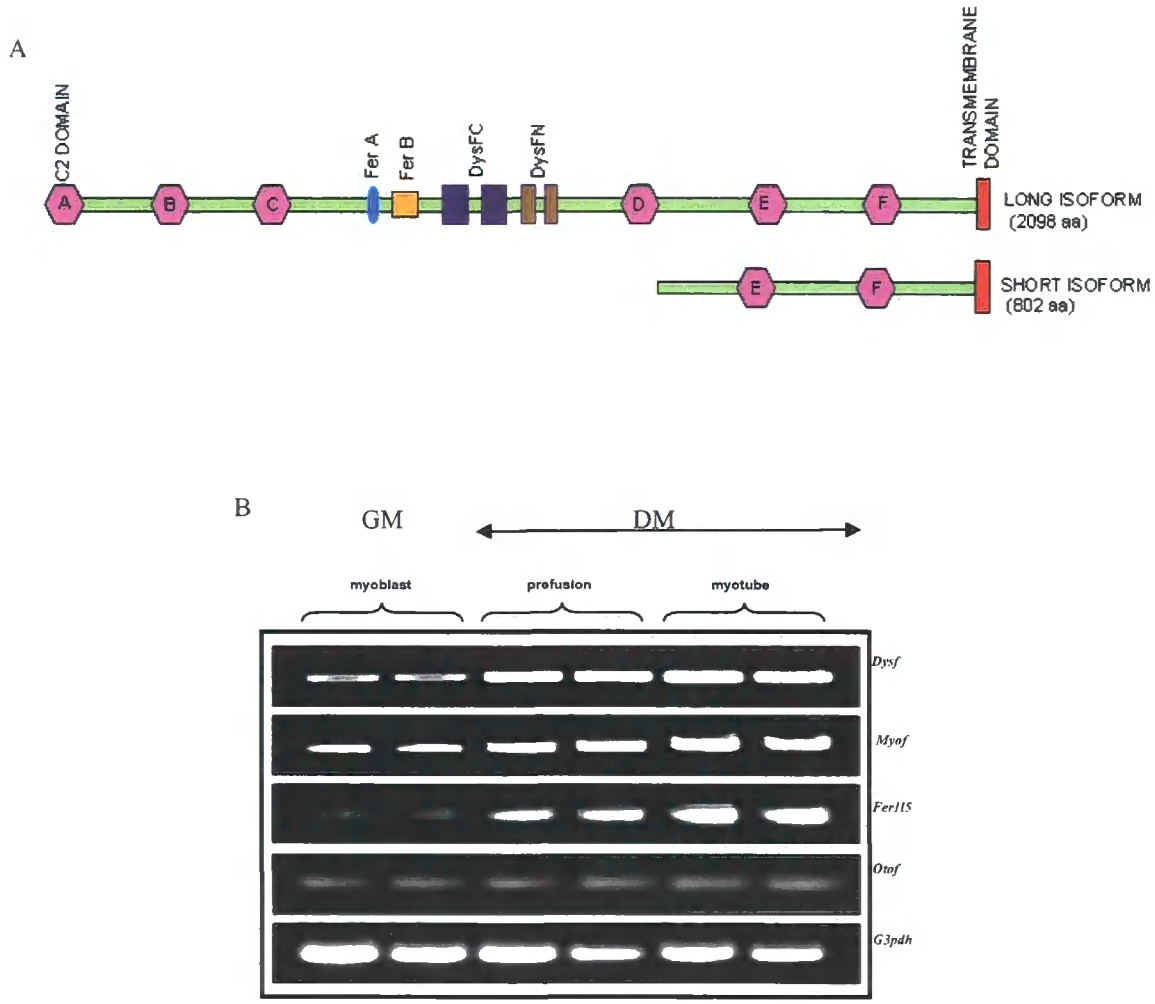

Figure 1.9. A) Figure illustrating the different domains present in the long and short isoform of FER1L5. B) Gene expression profile of the ferlin genes during C2C12 differentiation. *Dysferlin, myoferlin and FER1L5 showed highest expression in the myotubes compared with proliferating myoblasts. A similar expression profile was observed for dysferlin and myoferlin. Otoferlin expression was not changed in the different stages of myoblast fusion. G3pdh expression was used to normalize the cDNAs. GM- growth media, DM- differentiation media. The primers used for the RT-PCR are described in Appendix B.*

1.4.6 Aims of the project

By performing homology modeling of the ferlin C2 domains, analyzing the ferlin sequences and by examining the gene expression of FER1L5 during muscle differentiation FER1L5 has been shown to be similar to dysferlin and myoferlin. It was hypothesized that FER1L5 has a role in muscle membrane fusion. FER1L5 is a novel ferlin and very little is known about this protein, its subcellular distribution in muscle and function in muscle cells. The Bashir laboratory had generated a polyclonal antibody to FER1L5 using N-terminal specific peptides to the long isoform of FER1L5 **(see section 2.1.2A).**

The aims of the project were to investigate whether FER1L5 has a role in muscle membrane fusion by

1) Examining the subcellular distribution of FER1L5 in muscle tissue and in the C2C12 muscle cell lines.
2) Determining if FER1L5 shares a similar membrane distribution to dysferlin and myoferlin in muscle cells.
3) Determining the expression of FER1L5 during C2C12 muscle differentiation.
4) Investigating whether inhibition of FER1L5 impairs myoblast fusion and membrane repair.

CHAPTER II: MATERIALS AND METHODS

2.1 Chemicals and antibodies

2.1.1 Chemicals

The chemicals used for my investigation were of analytical grade and purchased from VWR, Sigma and BDH.

2.1.2 Antibodies

Polyclonal antibodies to FER1L5 and myoferlin were generated by Dr. Bashir's laboratory. The monoclonal myoferlin was generated by the late Louise Anderson and was gifted to Dr. Bashir. The antibodies listed in **Table 2.1** and **Table 2.2** were bought from commercial suppliers. The following antibodies were gifts from C. J. Hutchison (lamin A), R. A. Quinlan (β-tubulin), Angus Lamond (coilin) and Hannelore Haase (AHNAK KIS).

A. FER1L5 antibody

Since our group had assembled the novel FER1L5 sequence and no antibody was available this was generated by the company CovalAb. A polyclonal antibody was generated using two N-terminal peptides, LAPLPRPCMSIDFRD and TRIEKHQNRQYGLC corresponding to amino acids 15-30 (LAPLPRPCMSIDFRD) and 482-496 (TRIEKHQNRQYGLC) respectively in the Genbank FER1L5 sequence AY461813 corresponding to the long FER1L5 isoform **(Appendix A)**. The peptides that were used showed minimal homology with dysferlin and myoferlin sequences **(Figure 2.1)**. For immunofluorescence analysis the affinity purified antibody (generated by CovalAb) was used and for the western analysis the final bleed was used. For peptide blocking equal amounts of each FER1L5 peptide was incubated with the FER1L5 antibody (final bleed or affinity purified antibody). Other controls tested included preimmune serum. Tubes containing antibody and peptide were incubated with agitation at room temperature for 30 minutes and the immunoadsorbed mixture was dialyzed. The specificity of the FER1L5 polyclonal antibody is described in chapter III.

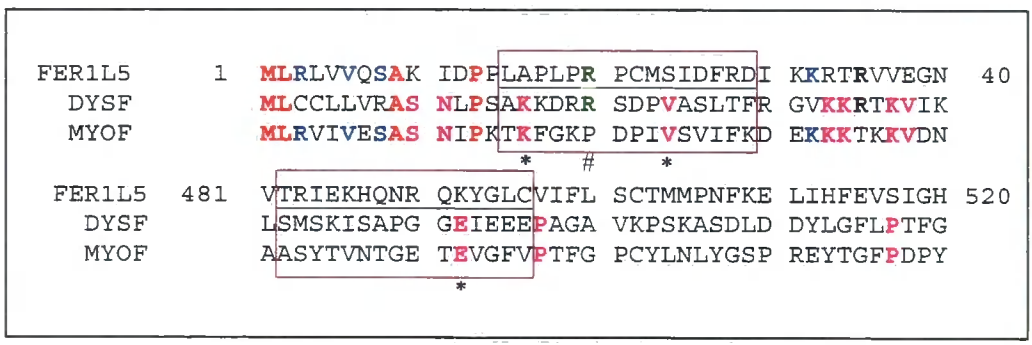

Figure 2.1. Multiple sequence alignment highlighting the FER1L5 amino acid sequences used to generate the FER1L5 antibody. *The underlined sequences correspond to the peptides used for antibody generation, which show least similarity with the corresponding dysferlin and myoferlin sequences. Out of 15 amino acids in each FER1L5 peptide only one amino acid showed identity to dysferlin (indicated by #). Asterisks indicate similar amino acids.*

B. Myoferlin antibodies

For myoferlin we used two antibodies, a monoclonal antibody, FER1L3 was generated to the peptide sequence GDEPPPERRDRDNDSDDVE corresponding to amino acids 326-344 in the myoferlin sequence AAH52617.1. This antibody has been previously characterized (Jaiswal *et al.*, 2007). The polyclonal antibody to myoferlin was generated to sequences previously described in Davis *et al.*, (2000) to the peptide SEDGSRIRYGGRDYSLD corresponding to amino acid residues 1692–1708 in the myoferlin sequence (AF182316.1). Affinity purified polyclonal myoferlin antibody was used for the immunofluorescence studies. The specificity of this antibody was checked by immunoadsorption as described for the FER1L5 antibody.

2.2 Cell culture

2.2.1 C2C12, NRK, HeLa, HDF and RD cells

C2C12 is a murine skeletal muscle myoblast cell line (Jasmer and Kwak, 2006; Riquelme *et al.*, 2006), which is commonly used to study myoblast fusion (Yaffe and Saxel, 1977). Proliferating C2C12 cells were grown in DMEM supplemented with 10% FCS and 0.2% antibiotic at 37° C. When the proliferating cells approached 70% confluence they were either passaged using trypsin EDTA with washes in 1X PBS or grown in differentiation media which contained DMEM supplemented with 2% donor horse serum. For immunolabelling, differentiating C2C12 cells were cultured on 13mm glass coverslips (SLS # MIC3306) coated with laminin (5µg/ml). The cell lines NRK (Normal Rat Kidney cell), HeLa and human dermal fibroblasts cells (HDF) were cultured in DMEM supplemented with 10% FCS and 0.2% antibiotic. Human RD (human rhabdosarcoma) cell line was cultured in DMEM supplemented with 20% FBS. Cells were passaged using trypsin EDTA and all washes were performed with 1X PBS.

2.2.2 Cryopreservation of cultures

All cells were routinely cryopreserved in liquid nitrogen for longer storage. Sub-confluent cultures were detached by trypsinisation and pelleted by centrifugation as described above. For T75 flasks, $1x10^6$ cells were resuspended on ice in 5ml of

complete media containing 2% dimethyl sulfoxide (DMSO) and 1 ml aliquots were transfected to cold cryotubes (kept at -20° C overnight). Cryotubes were then placed at -80°C overnight before storage at -140° C the following day. To re-establish cultures, cell suspensions were thawed quickly in a 37°C water bath and diluted into the appropriate media. Fresh media was added the following day.

2.2.3 Passage of cells

Confluent (70-80%) cells were briefly washed with 0.5 M EDTA in PBS and then treated with 0.5ml trypsin for approximately 1 min at 37°C. The trypsin activity was neutralized by adding 10 ml PBS. The cells were centrifuged at 1000 rpm for 5 minutes and resuspended in 5 ml of PBS. 20µl cell aliquots were diluted with 20µl of trypan blue, mixed and single cell suspensions were counted using a Neubauer hemocytometer in duplicate. Cells were diluted in an appropriate volume of fresh DMEM containing 10% FCS with antibiotics and seeded into culture flasks.

2.3 Immunohistochemistry

Eight micron cryostat adult human muscle cross sections were obtained from late Dr. Louise Anderson. Ethical permission was obtained for these and the work was performed in accordance with the Human Tissue Act (2007). The sections were fixed in 100% cold acetone for 5 minutes and permeabilized in PBS containing 0.2% TritonX-100 for another 5 minutes at room temperature. The sections were washed with 1X PBS for a few times and incubated with primary antibodies overnight at 4°C. The primary antibodies were applied in double staining combinations: polyclonal FER1L5/monoclonal dysferlin and polyclonal FER1L5/monoclonal myoferlin respectively. Following this, sections were incubated with the secondary antibodies, anti-rabbit Alexa 546 and anti-mouse Alexa 488 respectively for 1 hour at room temperature. The sections were then washed with PBS and stained with Mowiol containing DAPI for microscopy.

2.4 Immunofluorescence

Cells were seeded onto sterile glass coverslips held in 24 well or 6 well plates in appropriate media. For differentiating C2C12 cells we used laminin coated coverslips. Following washing of cultured cells in 1X PBS the cells were fixed at the appropriate

Table 2.1. Primary antibodies used in this study

Antibody	Dilution		Antibody type		Source
	IF	IB	IF	IB	
FER1L5 (AP/ FB)	1: 5/ 1:100*	1:50	p	p	-
Myoferlin (AP/ FB)	1: 5	1:50	p	p	-
Myoferlin	Neat	1:50	m	m	-
Dysferlin	Neat	1:500	m	m	Novocastra Laboratory Ltd.
Coilin	1: 350		P		-
Caveolin-3	1:100	1:100	m	p	BD Biosciences/ Transduction Laboratories
Cyclin D3	1:100	1:300	m	p	Calbiochem
Actin	1:100	1:500	m	p	Sigma
β-tubulin	Neat		m		-
β-dystroglycan	1:15		m		Novocastra Laboratory Ltd
Fibrillarin	1:500		m		Abcam
AHNAK KIS	1:15p/ 1:100m	1:100p	p/m	p	-
Transferrin	1:100	1:1000	m	m	Abcam
Lamin A (Jol5)	1:100	1:200	m	m	-
Bin 1	1:100	1:100	m	m	Abcam
GAPDH		1:1000			Abcam
Desmin	1:100		m		-

Immunofluorescence (IF) microscopy Immunoblotting (IB) m-monoclonal, p-polyclonal, AP-affinity purified, FB and * - Final Bleed)

Table 2.2. Secondary antibodies used in this study

Antibody	Dilution IF	IB	Antibody type	Source
Alexa 546 goat anti-rabbit IgG	1:200		Rabbit/p	Invitrogen
Alexa 488 goat anti-mouse IgG	1:200		Mouse/m	Invitrogen
FITC donkey anti-rabbit IgG	1:50		Rabbit/p	STRATECH
TRITC donkey anti-mouse IgG	1:50		Mouse/m	STRATECH
Donkey anti-rabbit HRP		1:2000	Rabbit/p	Jackson Immunoresearch
Donkey anti-mouse HRP		1:2000	Mouse/m	Jackson Immunoresearch

time points in 4% paraformaldehyde (PFA) in 1X PBS for 10 minutes at 4°C. Fixed cells were washed three times for 5 minutes in 1X PBS at 4°C and permeabilized with 0.5% TritonX-100 in 1X PBS for 5 minutes at 4°C. For immunostaining of microtubules we followed a specialized method for cell permeabilization and fixation (Prescott et al., 1992). Cells were permeabilized for 30 seconds in permeabilization buffer (50mM Pipes, 50mM KCl, 0.5mM MgCl2, 1mM EGTA, 1mM mercaptoethanol, 1% Triton X-100, 4% polyethyleneglycol 40,000 at pH 6.8) and washed with PBS and then fixed with 90% methanol in MES buffer (100mM-2-(Nmorphilino)-ethane sulphonic acid, 1mM EGTA, 1mM $MgSO_4$, pH 6.9) at -20° C for 5 minutes. Washed cells were then extracted with 1% Nonidet P40 in PBS for 10 minutes at room temperature. Following permeabilization of fixed cells, cells were washed in PBS for 5 minutes at 4°C and blocked in blocking buffer (5% FCS in 1X PBS) for 30 minutes at room temperature prior to incubation with primary antibody. The coverslips were placed on parafilm for the antibody application. The primary antibodies used and their dilutions are described in Table 2.1. All primary antibodies were diluted in blocking buffer and applied for 1hr at room temperature followed by three 30 minute washes in blocking buffer to remove excess antibody. Following this the appropriate fluorescently labelled secondary antibody was applied in the dark for 1 hour followed by three 30 minute washes in blocking buffer. Following application of secondary antibody coverslips were briefly dried and cells were mounted in Mowiol containing DAPI (5µl of 2 mg/ml) for confocal microscopy.

2.5 Microscopy

2.5.1 Confocal Imaging

Upright Confocal laser scanning LSM 510 META (Carl Zeiss equipped with a cooled CCD camera) microscope at 40X and 63X/1.10 lens was used for imaging. Z-series were collected in Multi-track mode using sequential and simultaneous scanning averaging the background 4-7 times at a scan speed of 7 and a resolution of 1024x1024. Each Z-stack had a thickness of 0.9µm. All montages were assembled in ImageJ software and Adobe Photoshop 6.0.

2.5.2 Live Cell Imaging

C2C12 myotubes were cultured in six well plates. Prior to imaging myotubes were treated with 2mM methyl-β-cyclodextrin (MCD) to deplete cholesterol from membranes. In other experiments 2mM MCD was applied after labeling myotubes with the lipid raft dye, Alexa Fluor 488 labeled cholera toxin subunit B (Vybrant Lipid Raft Labeling Kit, Molecular Probes) by incubation, at a dilution of 1:500 at 37°C for 60 minutes. Following labelling of the lipid rafts, myotubes were treated with 2mM MCD for 45 minutes. Imaging was performed using Zeiss AxioVision microscope. Images were acquired at 5 second intervals over a period of 60 minutes using a 20X objective. Images were assembled using AxioVision 4.5 software and then processed further by ImageJ and photoshop 6.0.

2.6 Protein Analysis

2.6.1 Whole Cell Protein Extraction

All protein analysis was performed on ice. Whole cell protein was extracted from monolayer cells after washing 3 times in ice cold 1X PBS using RIPA (Sigma) buffer containing Complete Mini Protease Inhibitor Cocktail (Roche Molecular Biochemicals, 1 tablet/10ml). Cells were scraped off dishes using a cell scraper and transferred to 1.5 ml centrifuge tubes where the cells were vortexed briefly 2 or 3 times followed by incubation on ice for 20 minutes. Following this cells were centrifuged at 13000 rpm for 10 minutes at 4°C. The supernatant was removed for protein quantification or aliquoted for storage at -80°C until needed.

2.6.2 Protein Quantification

The Lowry method was used to determine the protein concentrations of the extracted proteins. Each sample was analyzed in duplicate using 5mg/ml BSA as the standard protein. BSA concentrations of 5µg, 10µg, 20µg and 40µg per ml were used to generate standard curves. Protein samples were used at dilutions from 1 µl to 3µl in the colorimetric assay. Samples were read in Beckman DU-600 spectrophotometer at 595nm. The unknown protein concentrations were calculated using the standard curve: Y= mX. (Y = protein concentration in µg/µl, m = gradient of the line and X = Abs at 595 nm).

2.6.3 Western Blot Analysis

A) Preparation of the SDS-PAGE Gel

SDS gel electrophoresis was performed to separate proteins using the Mini-Protean 3 gel system (BioRad Mini PROTEAN & Mini TransBlot). The concentration of the acrylamide resolving gel varied dependenting upon the molecular weight of the protein to be analysed **(Table 2.3A)**. For dysferlin, myoferlin and FER1L5, 6% gels were used. For lamin A (70 kDa), actin (42kDa) and G3PDH (30 kDa) 5-10% gels were used. **Table 2.3B** describes the constituents of the SDS gels, which were immediately poured between glass plates held on the casting ring. The gel was overlaid with saturated butanol to obtain a smooth interphase between the resolving and the stacking gel. Following polymerization the stacking gel mixture (4% acrylamide, 0.5mM Tris HCl pH 6.8, 20% SDS, 10% APS) was poured on top of the resolving gel (the resolving butanol was removed prior to this) and the combs were inserted between the plates. After the gel had polymerized the combs were removed and the wells were washed with distilled water before use. Approximately 20–30µg of purified protein samples were denatured using an equal volume of 2X loading buffer (0.5M Tris-HCl, pH 6.8, 10% glycerol, 70mM lauryl sulphate, 5% 2-mercaptoethanol, 15µl bromophenol blue) by incubation at 95°C for 5 minutes. Samples were briefly centrifuged prior to gel loading. Electrophoresis was performed (according to standard protocol) for 2 hours at 100V followed by 150V for 2 hours. The prestained protein markers (BioRad) were used to monitor the electrophoresis.

B) Immunoblotting

This was performed using the Transblot (BioRad). Following SDS-PAGE gels were removed from the plates, rinsed in transfer buffer and electroblotted onto 0.45µM nitrocellulose membranes (Amersham Biosciences) in transfer buffer for 1 hour at 150V at room temperature with cooling. Post transferred nitrocellulose membranes were incubated for 1 hour in 3% milk powder (w/v) in PBS containing 0.2% Tween-20 and rinsed briefly 3 times for 5 minutes with 5% non fat milk/0.2% Tween-20 to reduce non-specific binding sites. The blocked membranes were incubated with primary antibody appropriately diluted in 3% non fat milk (w/v) in PBS for 24hr at

4°C with constant shaking and washed three times in 2.5% to 3% non fat milk for 5 minutes. Immunoreactive bands were detected by sequential incubations with appropriate HRP conjugated secondary antibody diluted in non fat milk for 1 hour at room temperature with constant agitation, followed by three 5 minute washes with 3 % skimmed milk/0.2% Tween-20 and a final wash in 1X PBS. For immunodetection, the ECL-enhanced chemiluminescence reagents were mixed at a ratio of 1:1 (v/v) and applied to the blots. The labeled blots were exposed to X-OMAT films (Kodak) for different times and adjusted accordingly depending on the results.

2.6.4 Densitometry

To estimate the protein proportion of each band, densitometry was performed using UVI bandmap software (UVItec, Cambridge, UK). The values of the each specific band from three different blots (triplicate) were obtained separately by calculating the protein proportions against the background as a control. The percentage values of each band were obtained by calculating the mean percentage from these three values.

2.7 Subcellular Fractionation

A) Intracellular membrane fractionation

1x107 C2C12 cells cultured in 12 x 90mm dishes were washed with cold PBS to remove media and homogenized in HES buffer (255mM sucrose, 20mM HEPES, 1mM EDTA at pH 7.4) containing protease inhibitor using a hand held Dounce homogenizer by applying 15-20 strokes. The homogenates were centrifuged at 19,000g for 20 minutes at 4°C using a Beckman JA-20 rotor and the supernatants were used to prepare the intracellular membrane fractions. The pellet was retained on ice for preparation of the plasma membranes. The 19,000g supernatant was recentrifuged at 40,000g for 20 minutes to obtain the low density microsomal pellet. The 40,000g supernatant was further centrifuged at 180,000g for 90 minutes in a Ti–50 rotor to obtain the high density microsomal pellet. All pellets were resuspended in HES buffer containing protease inhibitors and aliquots stored at -80°C. The pellet obtained from the 19,000g centrifugation was resuspended in HES buffer containing 1.12M sucrose and layered onto 10mls of 1.12M sucrose for centrifugation at 100,000g for 60 minutes. The white fluffy plasma membrane layer was aspirated and diluted in sucrose free HES buffer for centrifugation to obtain sucrose free plasma membrane fractions.

Table 2.3.A. Western Blotting Solutions

Tank Buffer (Running Buffer)

	1X	10X
Tris	3.03g	30.28g
Glycine	14.41g	144.1g
SDS	1.0g	10g
Total vol.	1 litre	1 litre

Transfer Buffer

	1X
Tris	3.03g
Glycine	14.41g
Methanol	200ml
Total vol.	1 litre

2X Sample Buffer (pH adjusted to 6.8 and filtered)

	2X
Tris	0.303g
SDS	0.4g
DTT	6.2mg
Glycerol	4.0ml
Bromophenol blue	36.0µl
Total vol.	20.0ml

Table 2.3B. Constituents of SDS-PAGE electrophoresis gels

	6% Resolving	10% Resolving	12% Resolving	5% Stacking
Sterile dH_2O	5.8 ml	5.3 ml	4.3 ml	2.72 ml
Acrylamide	1.5 ml	2.0 ml	3.0 ml	625 µl
1.5M Tris pH 8.8	2.5 ml	2.5 ml	2.5 ml	-
0.5M Tris pH 6.8	-	-	-	650 µl
10% SDS	100 µl	100 µl	100 µl	50 µl
10% APS	100 µl	100 µl	100 µl	50 µl
TEMED	4 µl	4 µl	4 µl	5 µl
Total Volume	10 ml	10 ml	10 ml	5 ml

The 100,000g pellet obtained was the mitochondrial/nuclear fraction. All pellets were resuspended in HES buffer containing protease inhibitors. Equal volumes of equal fraction were analysed by western blotting.

B) Sucrose gradient ultracentrifugation

$1x10^7$ C2C12 myoblasts were trypsinised and the cell pellet was homogenised using a hand held Dounce homogeniser in 1.5ml of homogenization buffer (HEPES 20mM pH 7.4, 150 mM NaCl, 5mM $MgCl_2$, 2.5mM EGTA, 5% sucrose + protease inhibitor cocktail). The lysed cells were centrifuged at 1000g for 15 minutes. Following centrifugation 1 ml post nuclear supernatant was loaded on top of sucrose gradient ranging from 20-40% and ultracentrifuged at 166,000g in a SW41 rotor (Beckman) for 12 hr. 1ml fractions were collected carefully from top of the gradient and aliquoted and stored at -80°C until required.

C) Floatation sucrose gradient centrifugation

C2C12 myoblast pellets were obtained by centrifugation of $1x10^7$ lysed cells at 1000g for 15 min. The pellets were resuspended in 0.32M sucrose, 5mM HEPES pH 7.4 containing protease inhibitors supplemented with 0.5% final concentration of Triton X-100. After incubation on ice for 30 minutes the mixture was loaded onto a floatation sucrose gradient over two cushions of 1M and 1.3M sucrose respectively. After centrifugation at 166,000g for 18hr in a SW-41 rotor (Beckman) 1 ml fractions were collected, aliquoted and stored at -80 °C for further analysis.

2.8 Analysis of conditioned medium for FER1L5 vesicles

C2C12 cells were cultured and at 70% confluence were switched from growth media to differentiation media. 7ml of differentiation media was added to each dish. Conditioned media was aspirated from each dish at days 0, 2, 4, 8 following serum withdrawal. The aspirated media was centrifuged at 2000g for 15 minutes to remove any floating cells and cell debris. After a further low speed centrifugation at 4000g for 15 minutes the supernatant was subjected to ultracentrifugation using a SW41 rotor at 150,000g for 90 minutes. The invisible pellets were resuspended in 100µl 1 X PBS containing protease inhibitor cocktail and analyzed by western blotting.

2.9 siRNA studies

2.9.1 Generation of C2C12 stably expressing myoferlin siRNA

RNA interference was performed in C2C12 cells using the mammalian expression vector pSUPER.gfp/neo (Oligogene) for the direct synthesis of siRNA transcripts using the polymerase H1-RNA gene promoter. The vector co-expresses green fluorescent protein (GFP) to allow detection of transfected cells. To knock down endogenous myoferlin the following gene specific sequences to myoferlin were designed using the RNA design tool Oligoengine. Murine myoferlin 5' CCCTCTGAGCTCATGGATG 3'; Human myoferlin 5' TGCGAACGGCGATAAAGCA 3'; Human and murine myoferlin 5' TTCAGTTTGAAGTCAGCAT 3'. Scrambled siRNA with no predicted target site in the murine and human genome 5' TAGTTGTACCGGTCATTAA 3' was used as a negative control. The oligos were designed with *Hin*dIII sites to allow cloning into the vector. The sense and the antisense sequences were separated by TCTCTTGAA spacer sequences. The sense and antisense oligos were annealed and cloned at the *Bgl*I and *Hin*dIII site in the p-SUPER vector. Cloning and purification of myoferlin plasmids were carried out by Maria Hill. To perform myoferlin knock down $1x10^6$ C2C12 myoblasts were cultured in DMEM containing 10% FBS and transfected with 3μg of the each of the myoferlin siRNA and scrambled siRNA plasmids respectively in 100μl of nucleofector solution and electroporated using specified conditions for C2C12 cells. Following electroporation 1ml of growth media was added to the electroporated cells and they were transferred into 6-well plates. 24 hours after transfection cells were switched to growth media containing G418 (0.5mg/ml) for 10-15 days. Media was refreshed every 4 days. The G418 resistant cells were then seeded into 96 well dishes to establish single cell colonies and subsequently transferred to 24 well, 6 well and 90 mm dishes for further propagation. Seven independent single cell colonies were taken further for culturing and then cells were analyzed for myoferlin expression by performing immunofluorescence and western analysis.

2.10 FER1L5 antibody loading

A whole range of single and pooled siRNAs specific for FER1L5 were used and transfection of C2C12 were performed using the Amaxa nucleofection. Transient

knockdown of FER1L5 did not result in reduction of FER1L5 protein levels (information provided by Dr. Khalil Saleki). Therefore a different approach was adopted to inhibit FER1L5 function, by loading C2C12 cells with FER1L5 antibody by nucleofection. The Amaxa electroporation protocol for C2C12 cells was modified in that the appropriate electroporation buffer supplied for C2C12 cells was replaced with preimmune serum, FER1L5 peptide blocked serum and FER1L5 antiserum respectively. Prior to antibody introduction into C2C12 cells, the uptake into C2C12 cells of large molecules such as fluorescent dextran was possible in serum rather than the nucleofector buffer using the electroporation conditions specified for C2C12 cells. Following transfection of fluorescent dextran (or a control GFP plasmid in serum) in some cases transfection of up to 50% of C2C12 cells was observed. The same electroporation conditions as used for the fluorescent dextran or GFP plasmid were applied to C2C12 cells incubated separately with each of 100µl preimmune serum, FER1L5 peptide blocked serum and FER1L5 antiserum respectively. Equal densities of each group of C2C12 cultures were grown in differentiation media on glass coverslips held in six well plates until day 9 following serum withdrawal. The cells were then fixed, permeabilised and immunolabelled with anti-desmin antibody to identify myogenic cells and mounted in Mowiol containing DAPI for confocal microscopy. The fusion index of the different C2C12 cultures loaded with preimmune serum, peptide blocked FER1L5 serum and FER1L5 antiserum respectively was quantified by analyzing twenty fields on the coverslips at 40X magnifications and counting the number of desmin positive nuclei in myotubes in respect of total number of nuclei. Statistical analysis was performed using the unpaired students t-test using Microsoft excel. "P" values were obtained by performing unpaired students t-test using Microsoft excel.

CHAPTER III: PROTEIN EXPRESSION OF FER1L5 IN MUSCLE CELLS

3.1 Introduction

C2C12 is used extensively as a cell culture model to study the function of muscle proteins *in vitro*. C2C12 cells were used to examine the role of FER1L5 in muscle membrane fusion since recent studies in C2C12 cells have been performed for dysferlin and myoferlin to study their role in membrane repair and myoblast fusion respectively (Doherty *et al.*, 2005; Klinge *et al.*, 2007; Luna *et al.*, 2006). To investigate the role of FER1L5 in muscle membrane fusion a polyclonal antibody was used. In this chapter the specificity of the FER1L5 antibody is first demonstrated and then the distribution of FER1L5 in C2C12 myoblasts and in adult human muscle sections is described.

3.2 Results

3.2.1 The specificity of the FER1L5 antibody

The specificity of the polyclonal FER1L5 antibody was examined by comparing the signal obtained following incubation with peptide blocked FER1L5 antiserum and preimmune serum respectively using C2C12 lysates for immunoblotting and C2C12 cells for immunolabelling. Following peptide blocking the immunoblotting was performed by Dr. Khalil Saleki. In C2C12 lysates, FER1L5 antiserum recognized a 267 kDa protein **(Figure 3.1A)**. The molecular mass of the FER1L5 protein was determined by comparing the relative mobility of the FER1L5 protein with that of protein markers of known molecular mass. The predicted molecular mass of the FER1L5 sequence assembled by our group was 242 kDa. The FER1L5 protein detected in C2C12 lysates corresponds to the long FER1L5 isoform. Following peptide blocking, the signal obtained with the FER1L5 antiserum by western blotting was abolished. No signal was obtained with preimmune serum. FER1L5 expression was also examined in different mammalian cell lines and the 267 kDa FER1L5 protein was detected **(Figure 3.1B,** provided by Dr. Khalil Saleki**)**. FER1L5 protein is bigger in size compared to the 230 kDa proteins reported for dysferlin (Anderson *et. al.*, 1998; Matsuda *et al.*, 1999) and myoferlin (Davis *et al.*, 2000). By immunolabelling with affinity purified FER1L5 antibody, a predominant punctate staining pattern was

Figure 3.1. Examining the specificity of the FER1L5 antibody. *Equal amounts of protein (20μg) prepared from C2C12 lysates were used to generate duplicate western blots by Dr Khalil Saleki. A) Following immunoblotting a signal was obtained with FER1L5 anti serum (blot 1) but not with peptide blocked FER1L5 antiserum (blot 2) and preimmune serum (blot 3) respectively. FER1L5 antiserum detected a 267 kDa protein (arrow indicate the position of the 250 kDa protein marker. B) The 267 kDa FER1L5 protein is detected in mammalian cell lines, HEK293 (human embryonic kidney 293 cells), SW13 (adrenal carcinoma cell line), HT29 (human colon adenocarcinoma cell line), HUVEC (human umbilical vein endothelial cells), KELOID (keloid fibroblasts) and HDF (human dermal fibroblasts) cells. C) For the immunolabelling experiments the affinity purified FER1L5 antibody (670ng/50μl) specificity was examined after incubation with equal amounts of FER1L5 competitive peptides at a final concentration of 3.4μg/50μl. C2C12 cells incubated with FER1L5 antibody showed staining (No peptide). The signal was abolished after incubation with peptide blocked FER1L5 affinity purified antibody (With peptide). DAPI was used to highlight the nuclei. Projection of merged stack confocal images is presented. Scale bar, 10μm.*

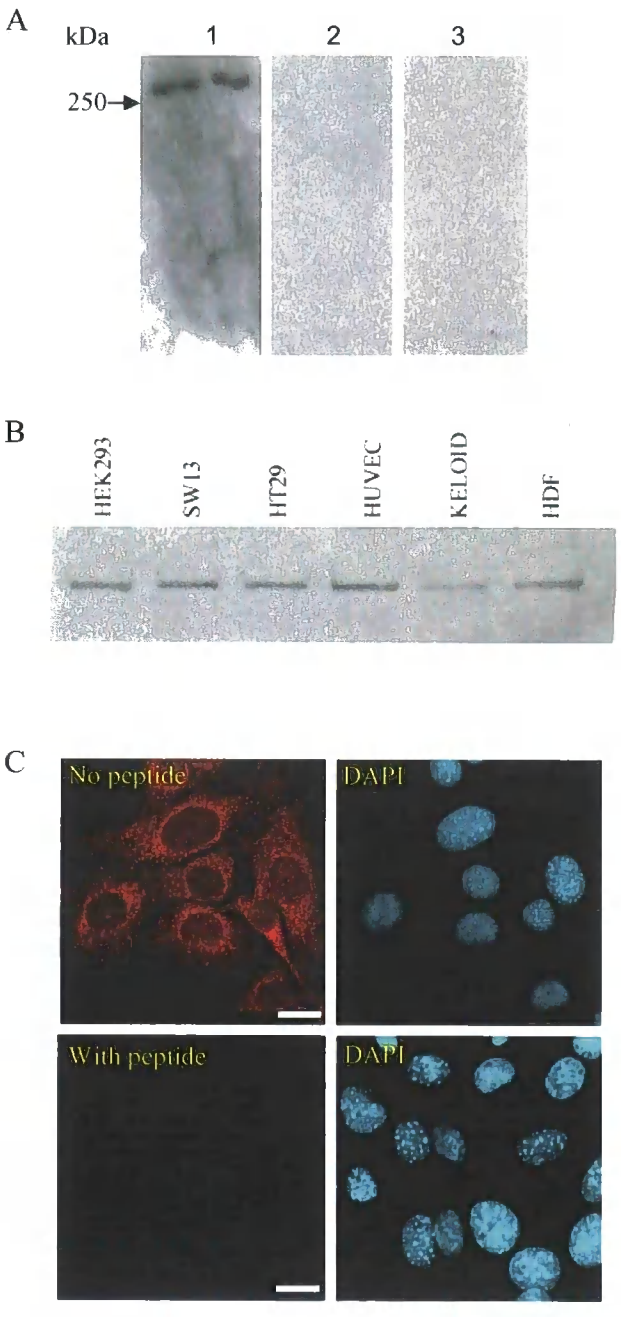
A
kDa
1
2
3
250
B
HEK293
SW13
HT29
HUVEC
KELOID
HDF
C
No peptide
DAPI
With peptide
DAPI

observed in C2C12 myoblasts indicating a vesicular localization of FER1L5 in myoblasts **(Figure 3.1C)**. In addition to the cytoplasmic staining, some FER1L5 staining was also detected in the nucleus. No staining was detected with the peptide blocked FER1L5 antibody **(Figure 3.1C)**. The FER1L5 staining pattern was also examined in different cell lines such as rhabdosarcoma (RD), HeLa, NRK (normal rat kidney cell line) and HDF. All cell types displayed a predominant punctate staining pattern throughout the cytoplasm indicating a vesicular localization. Nuclear staining of FER1L5 was also evident in these cells **(Figure 3.2)**.

3.2.2 FER1L5 expression in adult human muscle sections

Cross-sections of adult human muscle were labelled with antibodies to FER1L5, dysferlin and myoferlin respectively. Immunolabelling of FER1L5 with dysferlin and myoferlin was performed. Very weak immunostaining of FER1L5 was detected at the sarcolemma when analysed by confocal Z-series images but the staining was predominantly intracellular as shown in the projected Z-series images in **Figure 3.3Bi, Ci**. Dysferlin and myoferlin staining was observed at the sarcolemma and was higher compared to FER1L5. For dysferlin and myoferlin some intracellular staining was also observed **(Figure 3.3Bii, Cii).** Intracellular dysferlin staining in human muscle fibres has been reported (Anderson *et al.*, 1998, Matsuda *et al.*, 1999; Piccolo *et al.*, 2000; Inoue *et al.*, 2006). The staining of FER1L5 was shown to be specific because no staining was detected in the control sections stained with secondary antibody alone **(Figure 3.3A)**. In some areas, partial costaining of FER1L5 and dysferlin and FER1L5 and myoferlin respectively was observed **(Figure 3.3Biii and 3.3Ciii)**.

3.2.3 The subcellular distribution of FER1L5 in C2C12 myoblasts

Since the staining pattern obtained after immunolabelling C2C12 muscle cells with FER1L5 antibody suggested that FER1L5 is present in vesicles the distribution of FER1L5 was investigated in more detail by biochemical fractionation of C2C12 cells. First membrane fractions were generated by sucrose gradient fractionation of low speed supernatants of C2C12 lysates and equal volumes of each fraction were analysed by western blotting. I prepared the lysates and Dr. Khalil Saleki performed the western blotting. The distribution of FER1L5 was examined and compared with

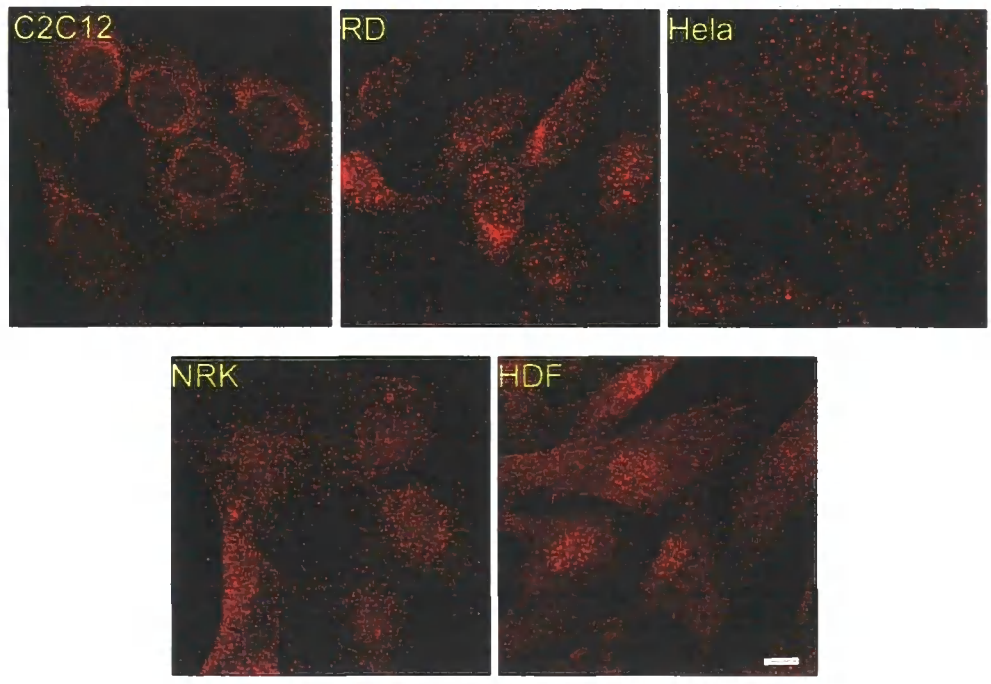

Figure 3.2. FER1L5 staining in cultured cells. *Immunolabelling of C2C12, RD (rhabdosarcoma cell line), HeLa, NRK (normal rat kidney cell line) and HDF cells using the affinity purified FER1L5 antibody. All cells showed FER1L5 staining in vesicular structures in the cytoplasm and a speckled like staining pattern was evident in the nucleus. Projected confocal images are presented. Scale bar, 10μm.*

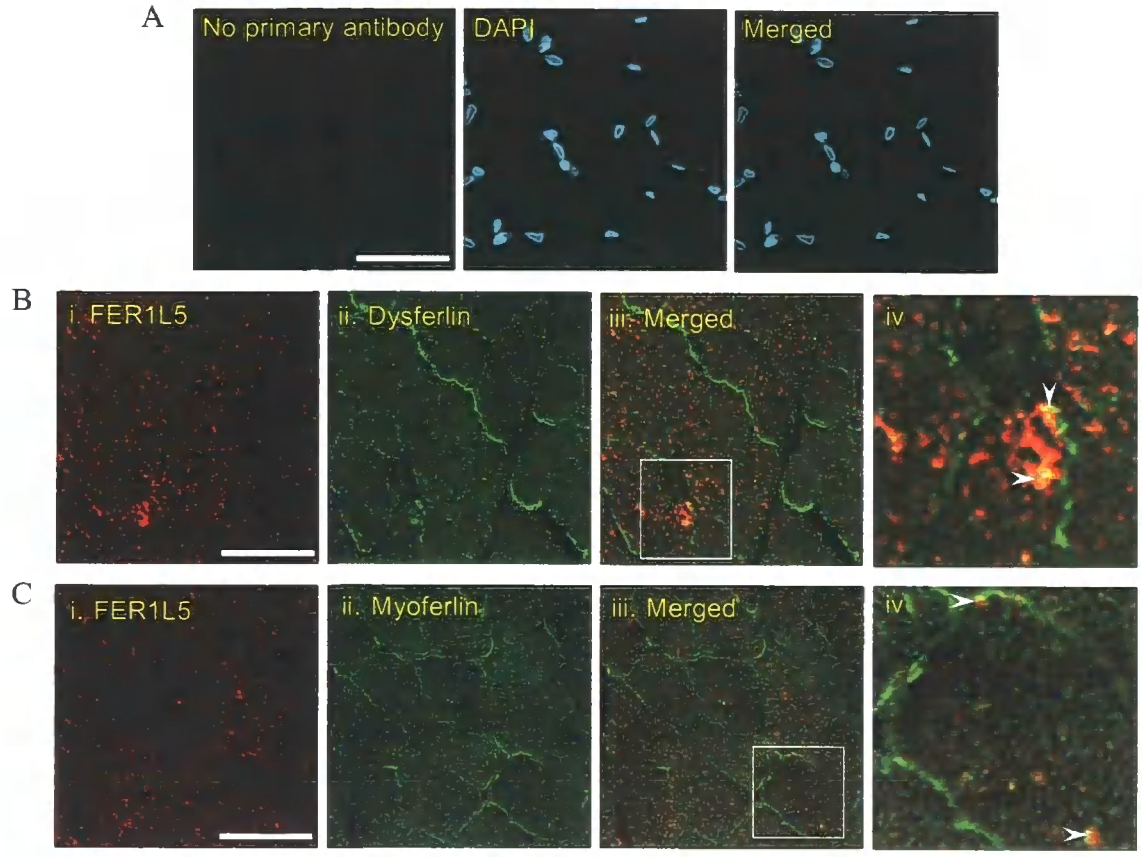

Figure 3.3. Expression of FER1L5 in adult human muscle. *The expression of FER1L5 was examined by immunofluorescence using cross sections of human muscle. FER1L5 staining was detected predominantly intracellularly (Bi and Ci). Dysferlin and myoferlin staining was detected at the sarcolemma and also intracellularly (Bii and Cii). In some areas partial co-staining of FER1L5 with dysferlin (Biii) and myoferlin (Ciii) was observed. Co-stained regions are indicated by arrow heads (Biv and Civ). Staining specificity was shown using secondary antibody as shown in (A). Projected confocal images are presented. Scale bar, 50μm.*

dysferlin and myoferlin respectively. FER1L5 immunoreactivity was detected in all membrane fractions prepared from C2C12 myoblasts, low density microsomes (LDM), high density microsomes (HDM), mitochondria/nuclei and plasma membrane fractions. A similar distribution was detected for dysferlin and myoferlin. **(Figure 3.4A).** The fidelity of the fractionation was confirmed by examining the distribution of lamin A, a nuclear lamina protein (Markiewick *et al.*, 2004) which was only detected in the mitochondria/nuclei fraction. The data highlights the dynamic intracellular membrane distribution of FER1L5 but also dysferlin and myoferlin respectively. The data indicated that FER1L5 was present in vesicles.

The properties of FER1L5 vesicles in C2C12 cells were examined next by performing continuous sucrose density ultracentrifugation. Post nuclear myoblast supernatants were prepared and loaded onto 20-40% sucrose gradients. Following ultracentrifugation equal volumes of each fraction were analyzed by western analysis. FER1L5 was predominantly detected in low density vesicles (fractions 4 and 5) although small amounts did co-sediment with dense vesicular fractions. Myoferlin and dysferlin showed an equal distribution between the lighter and denser vesicular fractions (fractions 3 to 6) **(Figure 3.4B)**. The sedimentation profiles of the proteins AHNAK, caveolin and Bin 1 were also obtained. AHNAK is a dysferlin and myoferlin interacting protein (Huang *et al.*, 2007) and a marker for enlargeosomal vesicles, which have also been implicated in membrane repair (Borgonovo *et al.*, 2002; Cocucci *et al.*, 2004). AHNAK immunoreactivity was only detected in the lighter vesicular fractions (fractions 1 and 2). For caveolin 3, a muscle membrane protein (Song *et al.*, 1996), which is thought to regulate the endocytosis of dysferlin, overlapping immunoreactivity was observed with dysferlin, myoferlin and FER1L5 respectively. Bin 1, a T-tubule marker protein (Lee *et al.*, 2002), which has been co-localized with dysferlin in C2C12 myotubes at sites of membrane wounding (Klinge *et al.*, 2007) co-sedimented in fractions 3 to 5 (low and high density fractions). The co-sedimentation profile of Bin 1 displayed overlaps with dysferlin and partially overlapped with myoferlin and FER1L5 **(Figure 3.4B)**. Overall the co-sedimentation profile of FER1L5 vesicles overlapped with those obtained for dysferlin and myoferlin vesicles suggesting that FER1L5 vesicles were similar to dysferlin and myoferlin vesicles. To obtain further evidence of this the solubility of FER1L5,

Figure 3.4. The subcellular distribution of FER1L5 in C2C12 myoblasts. A) *Membrane fractions were prepared from C2C12 lysates by sucrose gradient centrifugation. Membrane distribution was then analyzed by western blotting using FER1L5 antiserum. Equal loading of each fraction demonstrated that FER1L5 was present in high density microsomes (HDM), low density microsomes (LDM), nuclei/ mitochondria (N/M) and plasma membrane (PM). Similar profiles were obtained for dysferlin and myoferlin. Lamin A was only detected in the nuclear/mitochondrial fractions. The data is representative of three independent experiments.* ***B)*** *The buoyant properties of FER1L5, dysferlin and myoferlin vesicles was examined by fractionating on 20-40% sucrose gradients. Equal volumes of each fraction were loaded onto gels for western analysis.* ***C)*** *Floatation gradient analysis of Triton X treated C2C12 cells was examined after resuspending post nuclear C2C12 lysate pellets in buffer supplemented with Triton X-100, 0.5% final concentration. Caveolin-3 and transferrin receptor represented the markers for detergent resistant membranes and detergent soluble membranes respectively. Fractions 1-4 corresponded to the floated fractions and fractions 5-8 corresponded to the dissolved fractions respectively. Fraction 9 corresponded to the nuclear fraction. The data is representative of two independent experiments.*

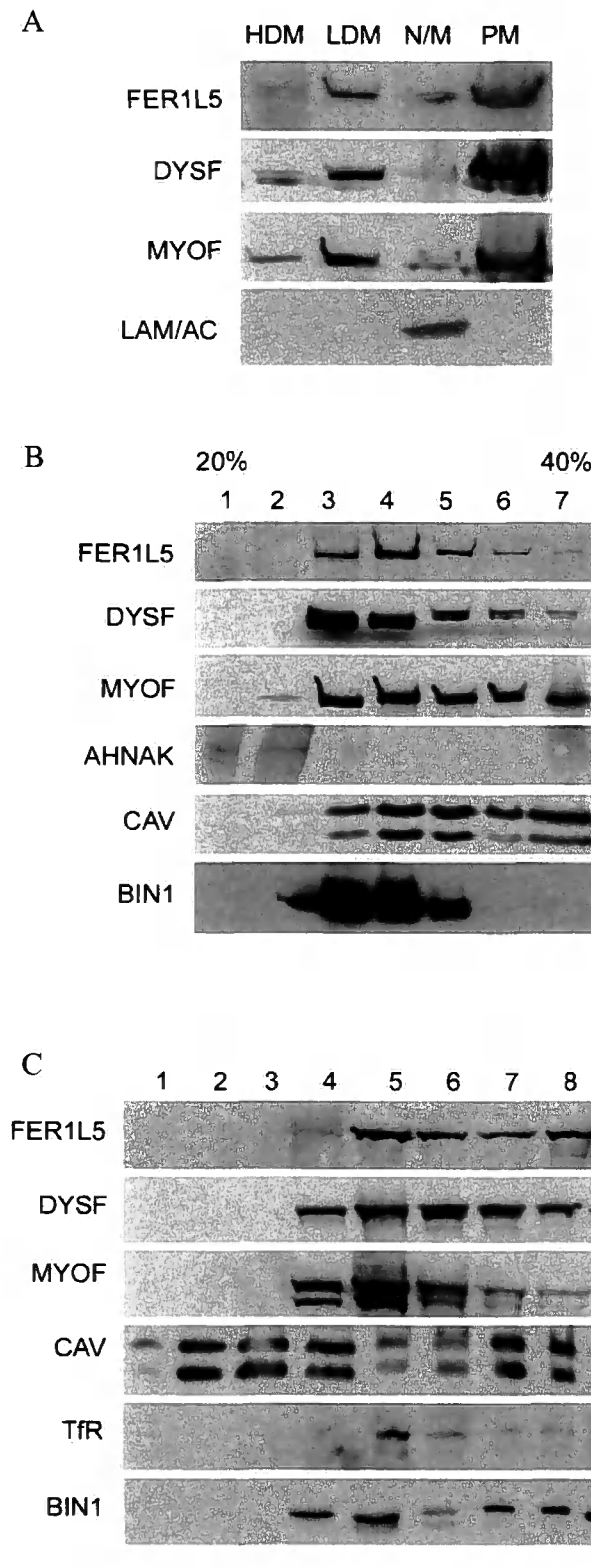
A
HDM
LDM
N/M
PM
FER1L5
DYSF
MYOF
LAM/AC
B
20%
40%
1
2
3
4
5
6
7
FER1L5
DYSF
MYOF
AHNAK
CAV
BIN1
C
1
2
3
4
5
6
7
8
9
FER1L5
DYSF
MYOF
CAV
TfR
BIN1

dysferlin and myoferlin vesicular membranes, in detergent, was examined by performing floatation sucrose gradient centrifugation of postnuclear C2C12 membranes treated with 0.5% final concentration of TX-100. Following fractionation, equal volumes of each fraction were analyzed by Western blotting. The detergent solubility profiles of the ferlin vesicular membranes were compared with two proteins, caveolin-3 a well known marker of detergent resistant membranes (van Deurs *et al.*, 2003; Cocucci *et al.*, 2004) and transferrin receptor as a marker for detergent soluble membranes respectively (Cocucci *et al.*, 2004). Dysferlin and myoferlin immunoreactivity was observed in both floated and dissolved fractions. Fraction 4 represented the interface between the floated and dissolved fractions **(Figure 3.4C)**. For FER1L5, the immunoreactivity was mostly evident in the dissolved non-floated fractions, fractions 5 to 8 suggesting that the membranes of FER1L5 vesicles are largely non-resistant to detergent. Caveolin-3 showed immunoreactivity in all of the fractions but predominantly in the floated fractions (fractions 2-4) consistent with what has been reported for this protein (Cocucci *et al.*, 2004). The sedimentation profile for transferrin receptor was consistent with what has been reported for transferrin receptor containing vesicles (recycling vesicles), which are solubilized by TX-100 (Cocucci *et al.*, 2004) with the immunoreactivity mostly recovered in the non-floated dissolved fractions, 5 and 6. Overall the co-sedimentation profiles of dysferlin, myoferlin and FER1L5 overlapped with each other suggesting that these proteins are present in similar vesicles.

3.2.4 Co-staining of FER1L5 with dysferlin and myoferlin in C2C12 cells

Based on the biochemical fractionation data FER1L5 was predicted to co-localize with dysferlin and myoferlin respectively in C2C12 cells. This was investigated by performing co-immunolabelling of C2C12 myotubes with antibodies to FER1L5/dysferlin and FER1L5/myoferlin respectively. Myotubes were used for the co-immunolabelling experiments because high dysferlin expression has not been observed in myoblasts (Doherty *et al.*, 2005; Foxton *et al.*, 2004). Confocal images representative of FER1L5/dysferlin and FER1L5/myoferlin expression in myotubes are shown in **Figure 3.5.** In myotubes, following immunolabelling with FER1L5 affinity purified antibody, FER1L5 was detected in vesicular structures in the

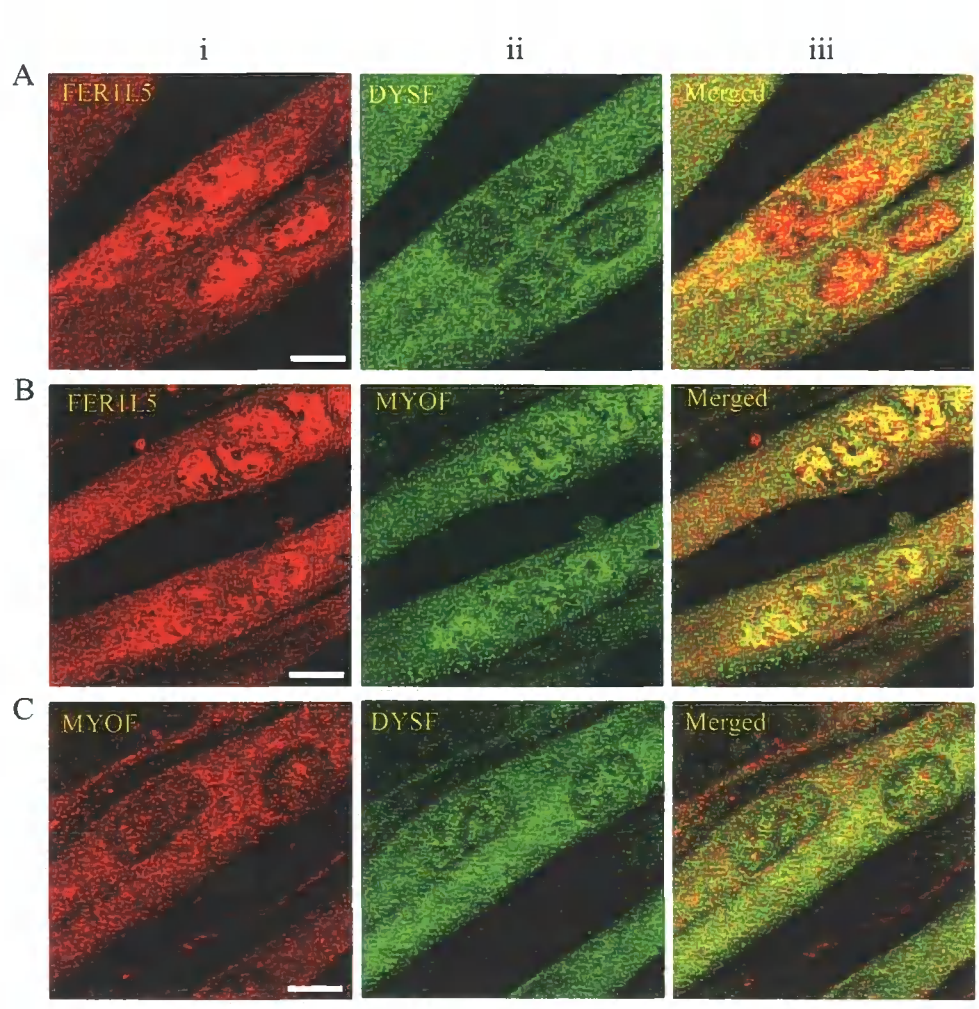

Figure 3.5. Co-localization studies. ***A)*** *Double staining of FER1L5 (red) with dysferlin (green) and* ***B)*** *FER1L5 (red) and myoferlin (green) reveals that there is co-staining in a small subpopulation of vesicular structures in the cytoplasm. Co-staining is also observed in subnuclear regions of C2C12 myotubes.* ***C)*** *Myoferlin (red) and dysferlin (green) showed minimal co-staining in the cytoplasmic and subnuclear regions in myotubes. Projected confocal images are presented. Scale bar, 12μm.*

cytoplasm and there was also a subnuclear co-staining **(Figure 3.5Ai, Bi).** Co-staining of FER1L5 with both dysferlin and myoferlin was observed in only a small subpopulation of vesicular structures in C2C12 myotubes **(Figure 3.5Aiii, Biii).** Myoferlin and dysferlin displayed minimal partial co-staining in the cytoplasm and subnuclear regions in myotubes **(Figure 3.5C).** My data indicated that FER1L5 is present in distinct ferlin vesicles in C2C12 cells. The nuclear distribution of dysferlin and myoferlin during myoblast fusion has not been reported before and was confirmed by Dr. Khalil Saleki by western blotting of nuclear fractions obtained from myoblasts and myotubes respectively. FER1L5 was detected in myotube nuclei by western blotting.

3.2.5 The organelle distribution of FER1L5 in C2C12 cells

To determine the identity of the organelle(s) positive for FER1L5, co-immunolabelling was performed in C2C12 myoblasts and myotubes using the FER1L5 affinity purified antibody and markers to known organelles such as early endosomes (EEA1), late endosomes/lysosomes (Lamp-1), enlargeosomes, (AHNAK), Golgi vesicles (TGN38), recycling vesicles (transferrin receptor), endocytic vesicles (clathrin) and T-tubule vesicles (Bin 1). No co-staining of FER1L5 with EEA1, LAMP1, TGN38, transferrin receptor and Bin 1 was observed in both myoblasts and myotubes (data not shown but available on request). Co-staining of FER1L5 with clathrin and AHNAK respectively was observed in a small population of cytoplasmic vesicles in both myoblasts **(Figure 3.6Ai, ii)** and myotubes **(Figure 3.6Bi, ii).**

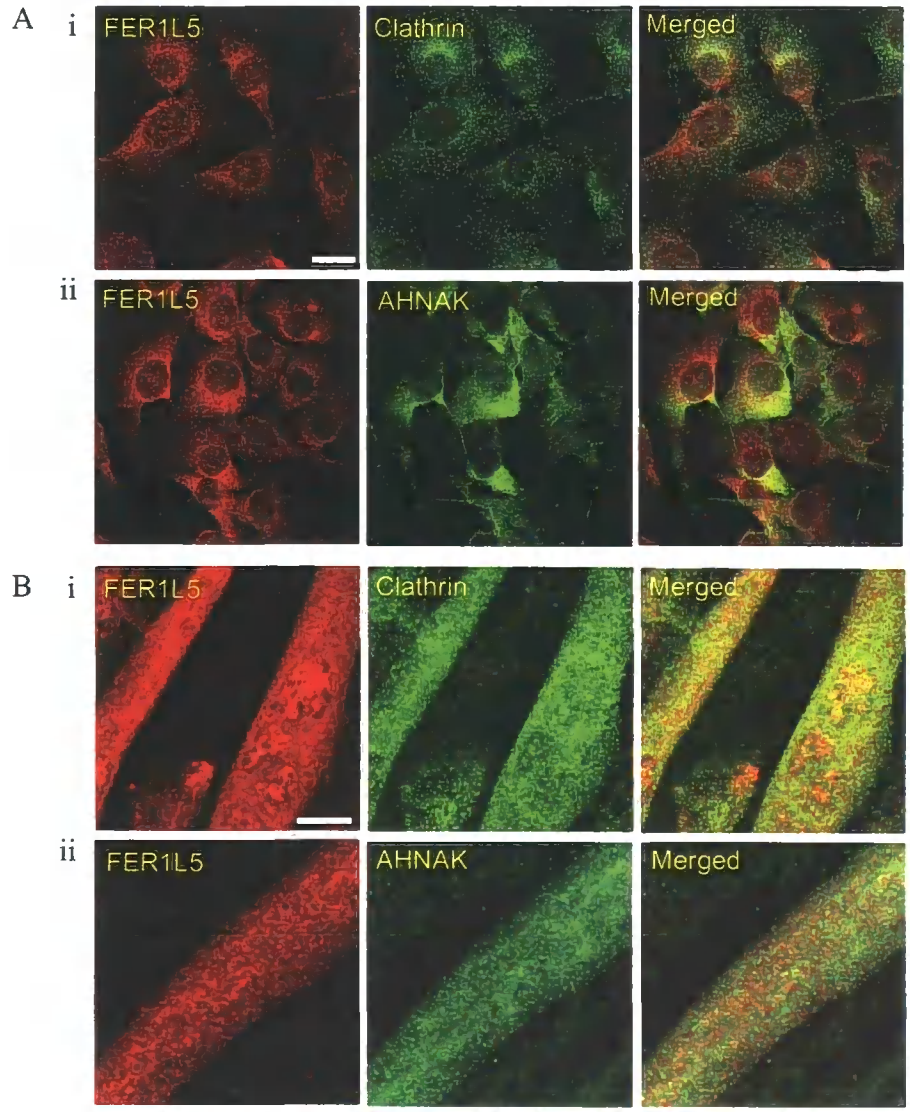

Figure 3.6. Co-localization studies of FER1L5 in C2C12 cells with markers of endocytic vesicles and enlargeosomes. *Co-immunolabelling of FER1L5 was performed in C2C12 myoblasts* ***(A)*** *and myotubes* ***(B)*** *using antibodies to (i) FER1L5 and clathrin and (ii) FER1L5 and AHNAK. Co-staining was observed in a small population of vesicles in the cytoplasm. Projected images are shown. Scale bar, 10μm for myoblasts and 12μm for myotubes.*

3.2 Discussion

In this chapter the specificity of a polyclonal FER1L5 antibody was demonstrated and following this the expression of FER1L5 was investigated by western blotting and immunolabelling. On western blots FER1L5 recognized a 267 kDa protein, which is slightly larger than the other characterized ferlins, dysferlin (230kDa) (Anderson, *et. al.*, 1998; Matsuda *et al.*,1999), myoferlin (230kDa) (Davis *et al.*, 2000) and otoferlin (220kDa) (Yasunaga *et al.*, 2000, Roux *et al.*, 2006).

The expression of FER1L5 was also examined in adult human muscle sections. Weak sarcolemmal staining was detected for FER1L5 compared to dysferlin and myoferlin from the Z-stacks of confocal microscopy but the sarcolemmal staining was not clearly observed in the projected merged image as shown in Figure 3.3. To avoid the errors in immunofluorescence to investigate the subcellular localization in detail we are generating FER1L5 GFP fusion proteins in collaboration with Dr. Martin Cann, Durham University. These alternative strategies will then be used to confirm our results. A detailed distribution of FER1L5 in adult human muscle is being performed in collaboration with Dr. Jens Reimann (Bonn, Germany) and the preliminary data supports the data presented in this chapter. In C2C12 cells, FER1L5 was shown to be present in vesicles, which share overlapping properties with dysferlin and myoferlin vesicles. FER1L5 was shown to be predominantly present in low density vesicles the membranes of which were largely non-resistant to non-ionic detergent. Dysferlin and myoferlin appeared to be more dynamic in their vesicular distribution, existing in both low and high density vesicles whose membranes showed detergent resistance and solubility. The co-sedimentation profiles of FER1L5, dysferlin and myoferlin vesicles respectively overlapped with each other and suggested that FER1L5, dysferlin and myoferlin may co-localize in C2C12 muscle cells. This was investigated by co-immunolabelling of FER1L5/dysferlin and FER1L5/myoferlin respectively in C2C12 myotubes. This demonstrated that FER1L5, dysferlin and myoferlin are present in distinct vesicles in myotubes. Interestingly, FER1L5 was also detected in myotube nuclei where it showed extensive co-localization with myoferlin compared to dysferlin. A nuclear distribution of dysferlin and myoferlin in C2C12 cells has not been reported before. The nuclear distribution was confirmed by nuclear fractionation of myoblasts and myotubes by Dr. Khalil Saleki (Presented at the 2nd Dysferlin

Conference, Puerto Rico, 2008). Dysferlin is predicted to have a role in myogenic signaling based on observations that in dysferlin deficient myotubes there is a severe reduction in the gene expression of the terminal muscle differentiation marker, myogenin, which correlates with delayed myoblast fusion highlighting that there may be a direct interaction between dysferlin and myogenin during early myogenesis. It has been suggested that dysferlin and myogenin may share a common signaling pathway during skeletal muscle differentiation (Luna *et al.,* 2006). Since this study has demonstrated that FER1L5 and myoferlin also have a nuclear distribution during myoblast fusion and these proteins show partial nuclear co-localization with dysferlin one can speculate that these ferlins may also have a role in myogenic signaling. The nuclear distribution of these proteins during myoblast fusion needs to be investigated further.

The biochemical fractionation experiments highlighted that the co-sedimentation profiles of FER1L5, dysferlin and myoferlin membranes partially overlapped with the T-tubule protein, Bin1 (Lee, *et al.,* 2002). The T-tubule membrane system has a role in excitation-contraction coupling and is also a source of vesicles (Lee *et al.,* 1993; Carozzi *et al.,* 2000). Recent studies have demonstrated that dysferlin, which is predominantly localized to the T-tubule membrane system in C2C12 myotubes accumulates with Bin 1, in vesicles at myoblast/myotube membrane fusion sites and also at sites of membrane wounding suggesting that T-tubules may be the source of the dysferlin vesicles, which participate in muscle membrane fusion (Klinge *et al.,* 2007). The co-sedimentation data presented in this chapter suggested that FER1L5 and myoferlin membranes may be derived from T-tubule membranes in C2C12 muscle cells. FER1L5 was found to show no co-staining with Bin 1 in myotubes. Co-immunolabelling was performed with markers to known vesicles. No co-staining was observed with marker to early endosomes, late endosomes, Golgi derived vesicles, transferrin receptor and T-tubule vesicles. A small population of FER1L5 vesicles co-stained with AHNAK and endocytic vesicles. Overall the data suggests that FER1L5 is present in distinct vesicles in C2C12 cells.

CHAPTER IV: FER1L5 EXPRESSION AND DISTRIBUTION DURING C2C12 MYOBLAST FUSION

4.1 Introduction

The overlapping properties of FER1L5, dysferlin and myoferlin vesicles in C2C12 cells indicated that FER1L5 may have a role in similar muscle membrane fusion events as dysferlin and myoferlin respectively, namely myoblast fusion and membrane repair. To investigate this, the expression of FER1L5 in differentiating C2C12 muscle cells, and the effects of FER1L5 inhibition on the myogenic index of these cells was examined. In this chapter the expression and distribution of FER1L5 during C2C12 myoblast fusion is described.

4.2 Results

4.2.1 FER1L5 expression during C2C12 myoblast fusion

Proliferating C2C12 myoblasts grown at 70% confluency were switched to differentiation media and the cells were then lysed at different stages of myoblast fusion (D0, D2, D4, D10 and D12 (days) following serum withdrawl). Immunoblot analysis was performed on lysates obtained from C2C12 cultures harvested at different stages of myoblast fusion. FER1L5 was shown to be expressed at all stages of myoblast fusion, from proliferating myoblasts to mature myotubes **(Figure 4.1)**. FER1L5 expression did not increase dramatically as the cultures became abundant in myotubes as has been reported for dysferlin (Doherty *et al.*, 2005: Foxton *et al.*, 2004) FER1L5 levels appeared to be slightly higher in early differentiating cultures (at day 4 following serum withdrawal) **(Figure 4.1)**. The increase in the FER1L5 expression levels were determined using densitometry by calculating the mean percentage values of each the band intensity from three different blots and compared the mean percentage values of the each band intensity. This showed that the expression levels of FER1L5 were increased 20% at D2 and 30% at D4. The lysates were also examined for dysferlin expression and this increased as cultures became abundant in myotubes (Davis *et al.*, 2002; Foxton *et al.*, 2004; Doherty *et al.*, 2005) **(Figure 4.1)**. Actin was used as a loading control. C2C12 myoblast fusion is non-synchronous and the differentiating cultures used to analyze the overall FER1L5 expression contained a mixture of cells at different stages of myoblast fusion, FER1L5 expression was also examined by immunolabelling, using an affinity purified FER1L5 antibody. In the

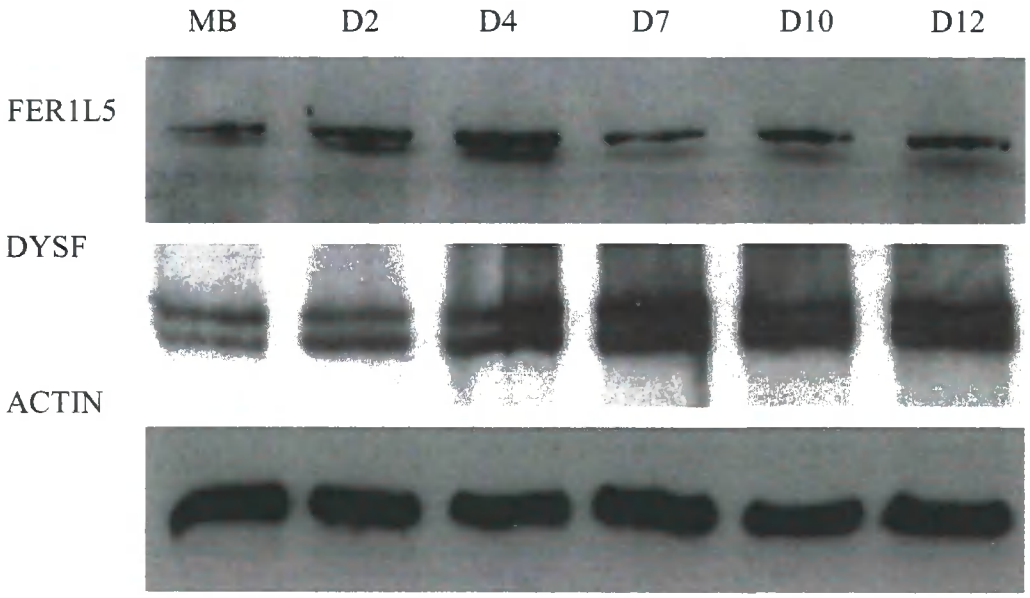

Figure 4.1. Expression profile of FER1L5 and dysferlin during C2C12 myoblast fusion. *Western analysis of lysates obtained from differentiating cultures of different time points. The expression levels of FER1L5 were increased 20% at D2 and 30% at D4 by densitometry. MB= myoblast, D= time following serum withdrawal. A doublet band was identified for dysferlin and has been reported by our group and previously by others (Jaiswal et al., 2007; Davis et al., 2002; Foxton et al., 2003).*

differentiating cultures, the expression of FER1L5 was slightly higher in prefusing myoblasts and myotubes respectively, compared with mononucleated myoblasts **(Figure 4.2A)**. In myotubes, FER1L5 was present in vesicular structures indicating that it had a similar cytoplasmic distribution as observed in myoblasts **(Figure 4.2Bi)**. In myotubes, in addition to the cytoplasmic distribution, FER1L5 was also present in the nucleus. A characteristic nuclear FER1L5 staining in aggregate like structures was observed in all myotube nuclei **(Figure 4.2A, Bii)**. The nuclear aggregates stained with FER1L5 antibody in myotubes were shown to be specific by peptide blocking **(Figure 4.2C)**. Following peptide blocking of the FER1L5 antibody no nuclear and cytoplasmic staining was observed indicating that the myotube staining was specific. In addition to the characteristic nuclear distribution of FER1L5, cytoplasmic vacuoles, largely free of FER1L5 staining were detected in C2C12 myotubes **(Figure 4.3i-iv)**. DAPI staining was used to show that these cytoplasmic vacuoles were not nuclei **(Figure 4.3ii)**. The size of these cytoplasmic vacuoles ranged from 2-3μm and they were present as single or multiple units **(Figure 4.3i, iii-iv)**. In some myotubes intercellular connections emerging from the FER1L5 free vacuoles and connecting with neighbouring myotubes were observed **(Figure 4.3v)**. FER1L5 stained intercellular connections were also observed between myotubes and between myoblasts and myotubes **(Figure 4.3vii, viii)**. In fusing myoblasts there was a concentration of FER1L5 staining in vesicular structures at membrane fusion sites **(Figure 4.4A)**, which was not observed at apposed myoblast-myotube membranes **(Figure 4.4B)** as has been reported for dysferlin and myoferlin (Klinge *et al.*, 2007; Doherty *et al.*, 2005). By co- immunolabelling differentiating C2C12 cultures with the respective antibodies to dysferlin and myoferlin the concentration of dysferlin and myoferlin at apposed myoblast-myotube membrane fusion sites was demonstrated, where they also appeared to colocalizes **(Figure 4.4C).**

4.2.2 The nuclear distribution of FER1L5 during C2C12 myoblast fusion

The nuclear expression of FER1L5 during myoblast fusion was confirmed by Dr. Khalil Saleki in the laboratory by performing nuclear fractionation and western analysis of C2C12 whole nuclear extracts generated from respective myoblast and myotube cultures. This work showed that nuclear FER1L5 levels modestly elevated in myotube cultures compared to myoblasts. The levels of nuclear myoferlin appeared to

Figure 4.2. FER1L5 expression during C2C12 myoblast fusion. ***A.*** *Images representing cultures at different stages of myoblast fusion. The DAPI staining is shown below for each time point. 0.9μm thickness Z-stack images are presented. Scale bar is 10μm for DO and D2 and 20μm for D4 and D8.* ***B. (i)*** *In myotube cytoplasm FER1L5 staining is detected in vesicular structures.* ***(ii)*** *Inset of image taken from D8 myotubes shown in 'A' to highlight the presence of FER1L5 stained nuclear aggregates.* ***C.*** *Confocal images taken at the same settings of myotubes stained with FER1L5 antibody (-peptide) and peptide blocked FER1L5 antibody (+peptide) respectively to show that the myotube staining is specific. Projected images are shown. Scale bar, 20μm.*

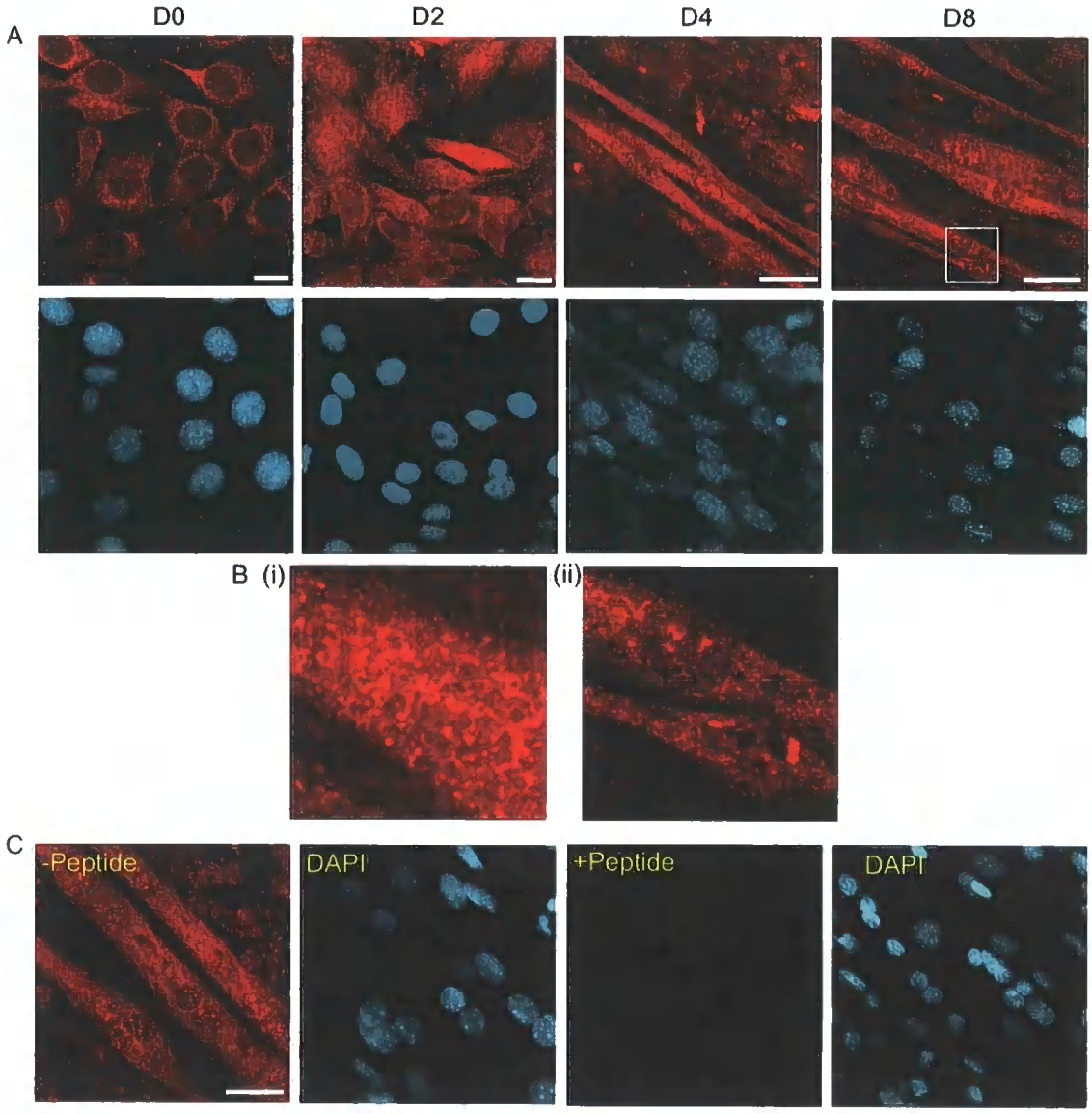
A
D0
D2
D4
D8
B (i)
(ii)
C
-Peptide
DAPI
+Peptide
DAPI

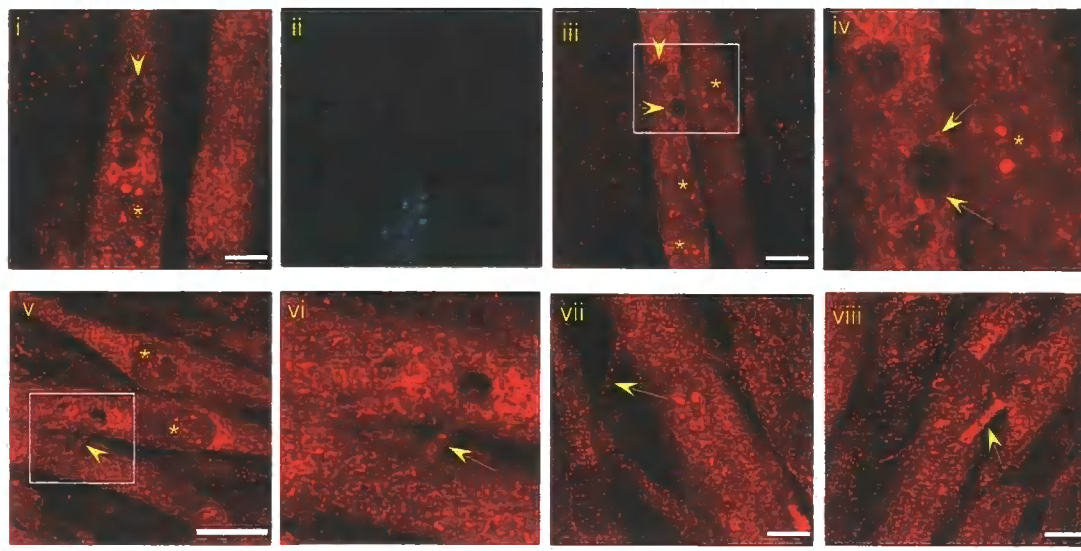

Figure 4.3. FER1L5 expression in multinucleated myotubes. *In myotubes stained with FER1L5 antibody cytoplasmic vacuoles largely free of FER1L5 staining (indicated by arrow heads) were detected as single (as described in v) or multiple units [as described in i and iii]. The merged DAPI image in (ii) shows that the cytoplasmic vacuoles (as described in [i]) are not nuclei. Myotube nuclei contained FER1L5 aggregates, which are indicated by asterisks. [iv] is an inset of [iii] and shows FER1L5 stained intercellular connections emerging from the vacuolar regions (indicated by arrows). [v-vi] show intercellular connections (indicated by arrows) extending from the FER1L5 free vacuolar region linking with an adjacently located myotube. [vi] is an inset of [v]. [vii and viii] FER1L5 stained intercellular connections were also observed between myoblast and myotubes (indicated by arrowhead). Projected images are presented here. Scale bar for images [i], [iii], [vii] and [viii] is 8μm. Scale bar for image [v] is 20μm.*

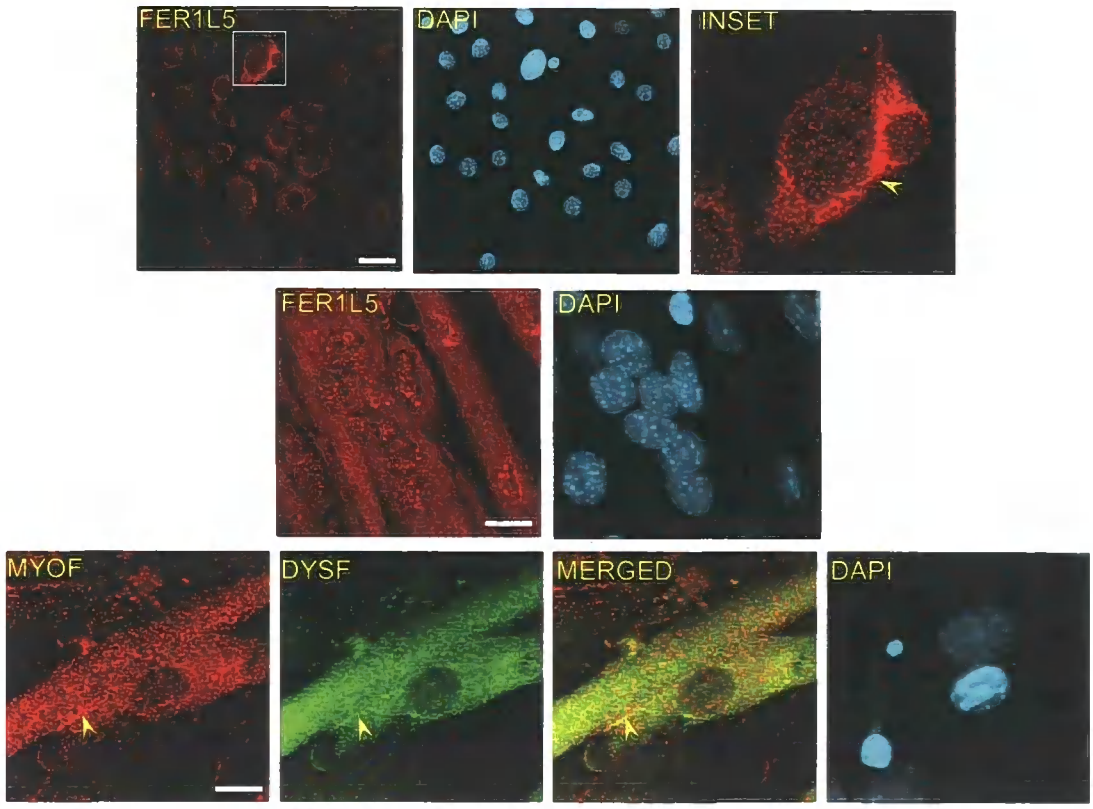

Figure 4.4. Immunofluorescence staining of cultures containing a mixture of myoblasts and myotubes. ***A)*** *Accumulation of FER1L5 stained vesicles (indicated by arrowhead in inset image) were observed at membrane fusion sites between myoblasts. Scale bar, 10µm.* ***B)*** *FER1L5 is not abundantly expressed at the apposed myotube-myoblast and myotube-myotube membranes as reported for myoferlin and dysferlin. Note the presence of FER1L5 in aggregates in myotube nuclei. Scale bar, 12µm.* ***C)*** *Enhanced staining of dysferlin and myoferlin at apposed myoblast-myotube membranes and their co-staining at these regions (indicated by arrow heads). Projected images are presented here. Scale bar, 12µm.*

be higher in myotube cultures compared to myoblast cultures but what was noteworthy was that nuclear dysferlin levels were highly elevated in myotube cultures compared to myoblast cultures. To complement the western analysis, I performed immunofluorescence analysis of myotubes to examine the nuclear expression of FER1L5 **(Figure 4.5)**. First, myotubes were stained with antibodies to the proteins, LAP2a and lamin A which have been localized to the nucleoskeleton and the nuclear lamina respectively (Cenciarelli *et al.,* 1999; Markiewicz *et al.,* 2005). The nuclear staining pattern of LAP2a and lamin A was compared with that obtained for FER1L5. FER1L5 was present in aggregates in all myotube nuclei **(Figure 4.5C)**. The staining pattern of FER1L5 was not consistent with that obtained for a nuclear lamina protein and the pattern also differed from that obtained for LAP2a **(Figure 4.5A)**. The nuclear expression pattern of FER1L5 was also compared with proteins known to be present in subnuclear bodies. The only marker available to test was the subnuclear body protein, fibrillarin (van Koningsbruggen *et al.,* 2004). Myotubes were stained with fibrillarin antibody alone to determine its expression pattern and then co-immunolabelling was performed with antibodies to coilin, another subnuclear body protein and a marker of Cajal bodies (Korie *et al.,* 2006). The staining of fibrillarin and coilin in myotubes was consistent with that reported by others (van Koningsbruggen *et al.,* 2004). Partial costaining of fibrillarin and coilin was observed in myotube nuclei **(Figure 4.6A)**. When double staining with anti-fibrillarin antibody and FER1L5 antibody was performed there was some staining overlap of FER1L5 and fibrillarin within subnuclear domains **(Figure 4.6B)**. This data suggested that FER1L5 was not localized to subnuclear domains containing fibrillarin in C2C12 myotubes. To examine the subnuclear distribution of FER1L5 further C2C12 myotubes were treated with the drug actinomycin D, which is known to disrupt the integrity of subnuclear bodies (van Koningsbruggen *et al.,* 2004). Proteins localizing to subnuclear bodies show a nucleoplasmic redistribution following actinomycin D treatment (van Koningsbruggen *et al.,* 2004). C2C12 myotubes grown on coverslips were incubated with a range of actinomycin D concentrations (0.5, 1.0, 5.0, 7.0 and 10μg/ml) to determine the optimal concentration required for the redistribution of the subnuclear body protein, fibrillarin **(Figure 4.7A)**. Following incubation with actinomycin D (for 3 hours at 37°C), fixed cells were immunolabelled with antibodies to coilin and fibrillarin **(Figure 4.7A)**. From these experiments the concentration of actinomycin D required to disrupt subnuclear body integrity was determined to be 10μg/ml.

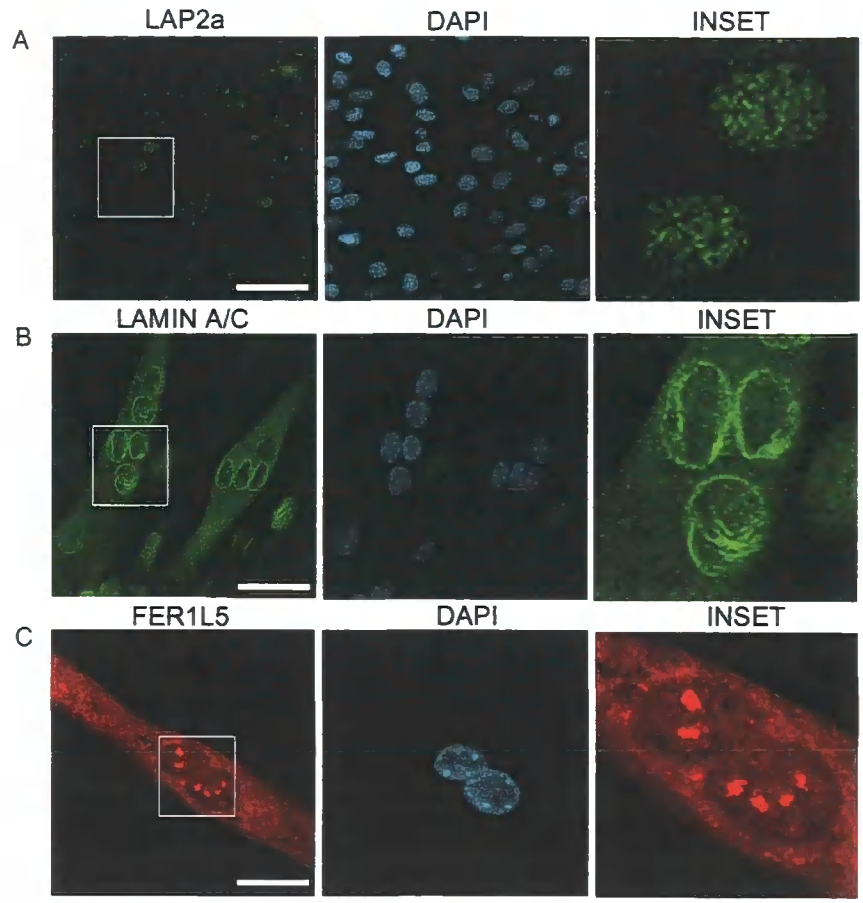

Figure 4.5. Staining of C2C12 myotubes with anti-LAP2a and anti-lamin A antibodies. ***A)*** *LAP2a showed a speckled nucleoplasmic distribution.* ***B)*** *The staining of lamin A was predominantly at the nuclear lamina and in internally bound nuclear structures.* ***C)*** *FER1L5 staining was observed in the nucleoplasm in aggregates. Projected images are presented. Scale bar, 20μm.*

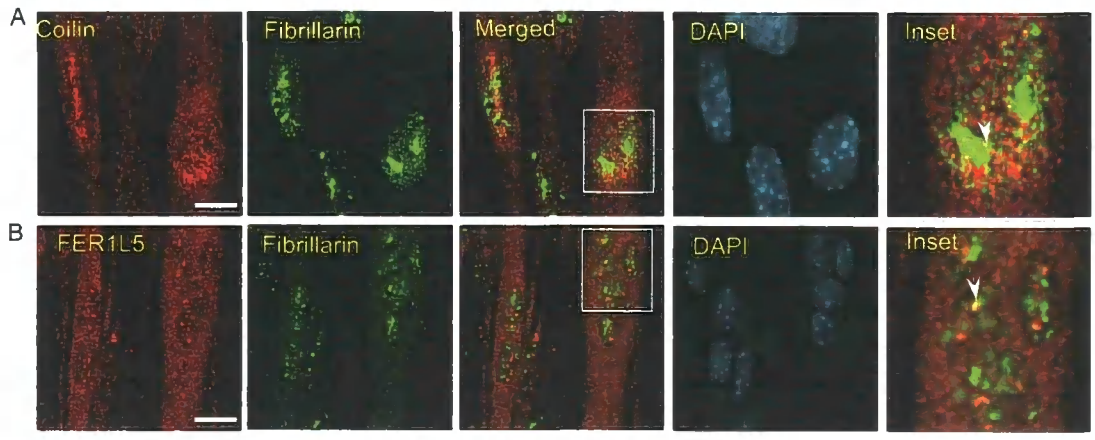

Figure 4.6. Partial co-staining of FER1L5 and fibrillarin in myotube nuclei.

A. *Co-staining of coilin and fibrillarin in myotube nuclei. Inset image shows the overlapped staining of coilin with fibrillarin in myotube nuclei.* ***B.*** *Co-staining of FER1L5 and fibrillarin revealed minimal staining overlap in myotube nuclei. Co-stained regions are indicated by arrow heads. Projected images are shown. Scale bar, 12μm.*

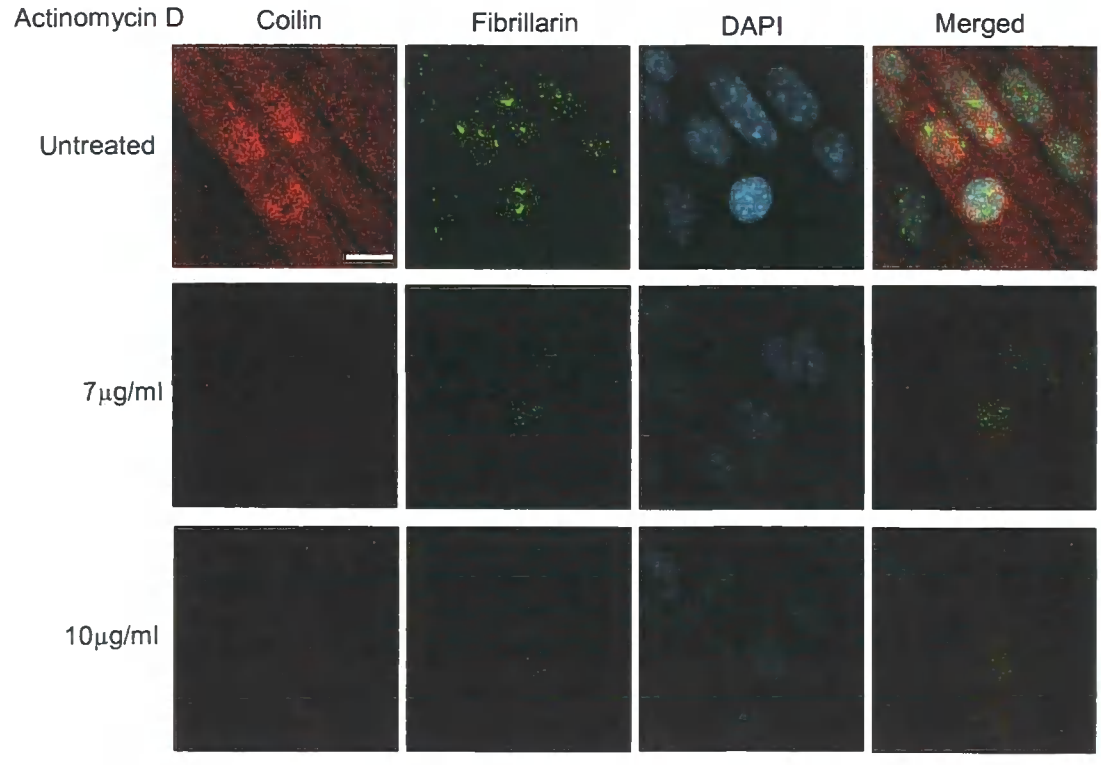

Figure 4.7A. Treatment of myotubes with actinomycin D (ActD). *Confocal imaging of untreated and ActD treated myotubes. The usual staining pattern (as described in Figure 4.6) was observed in the untreated myotubes co-stained with antibodies to coilin and fibrillarin respectively. In myotubes treated with 7μg/ml ActD, a partial nucleoplasmic redistribution of fibrillarin and coilin was observed. A complete, diffuse nucleoplasmic redistribution of fibrillarin was observed in myotubes treated with 10μg/ml ActD. Projected images are presented. Scale bar, 12μm.*

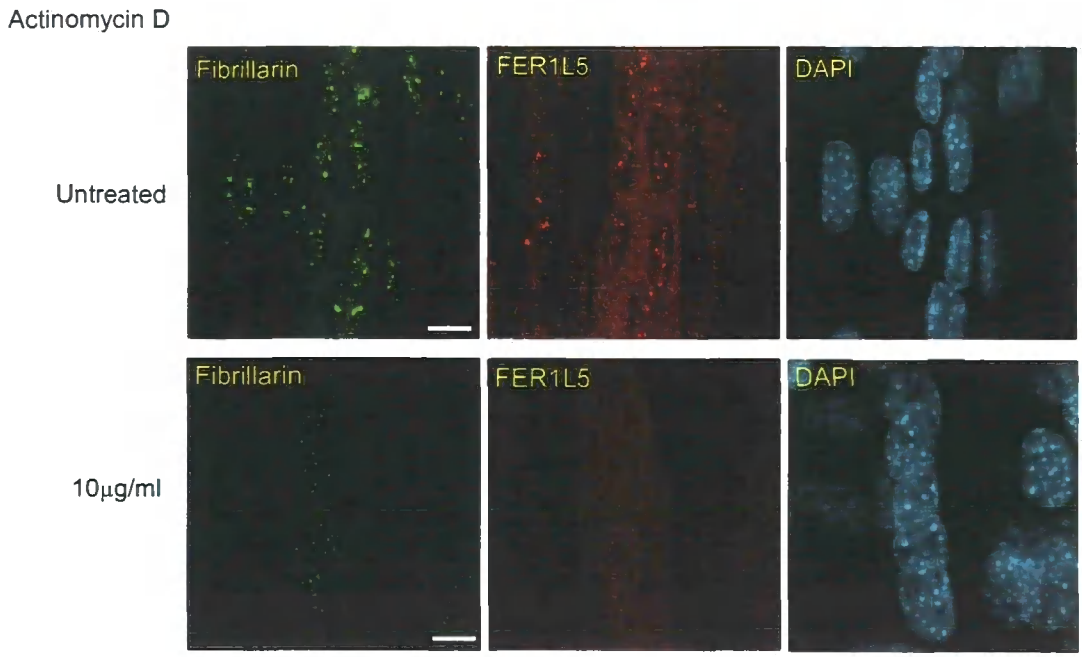

Figure 4.7B. Redistribution of FER1L5 in myotubes following ActD treatment. *Images taken from the untreated and ActD treated (10µg/ml) myotubes. Like fibrillarin, FER1L5 redistributes from aggregates to a diffuse nucleoplasmic distribution following ActD treatment. Projected images are shown. Scale bar, 12µm.*

Myotubes were then incubated with 10μg/ml actinomycin D for 3 hours at 37°C, fixed and coimmunolabelled with affinity purified polyclonal FER1L5 antibody and monoclonal anti-fibrillarin antibody **(Figure 4.7B)**. In untreated myotubes, the nuclear staining of FER1L5 was in aggregates as previously described **(Figure 4.7B)**. Upon exposure of actinomycin D, there was a redistribution of FER1L5 from the nuclear aggregates to a diffuse distribution across the nucleoplasm of C2C12 myotubes **(Figure 4.7B)**. Overall the data suggested that in C2C12 myotubes FER1L5 is localized to a fibrillarin-deficient region of subnuclear bodies that is sensitive to actinomycin D treatment. Interestingly, in addition to the nuclear redistribution of FER1L5 following actinomycin D treatment, in myotube cytoplasm, there were multiple irregular shaped cytoplasmic vacuoles free of FER1L5 staining detected as described previously **(Figure 4.7C)**.

4.2.3 Investigating whether FER1L5 is early muscle differentiation marker

Myoferlin and dysferlin have been shown to have a role in muscle regeneration as described in the Introduction. The work in our group has shown that dysferlin, myoferlin and FER1L5 are present in the nucleus during myoblast fusion. In dysferlin null myoblasts, which show impaired formation of large myotubes the reduction of dysferlin correlates with a reduction in myogenin expression. This has highlighted that dysferlin may be involved in muscle regeneration through a myogenic signaling pathway (Luna *et al.,* 2006). To explore whether FER1L5, dysferlin and myoferlin are early myogenic markers, the C3H-ER-MyoD fibroblast cell line, which has been used to identify early markers of muscle differentiation (Cenciarelli *et al.,* 1999) was used. C3H-ER-MyoD is a well characterized C3H10T1/2 cell line that stably expresses an estradiol-inducible MyoD protein (Cenciarelli *et al.,* 1999). Myogenic differentiation is induced by culturing cells in differentiation medium (DM) containing estradiol (10μM) for increasing periods of time as shown in Cenciarelli *et al.,* (1999). For this study C3H-ER-MyoD cells were cultured in differentiation media containing 10μM estradiol for 0hrs, 18hrs, 24hrs and 48hrs respectively and then cells were lysed for immunoblotting **(Figure 4.8)**. Control cells were cultured in differentiation media containing no estradiol. Equal amount of protein lysates were loaded onto gels for western analysis and the expression of FER1L5, dysferlin and myoferlin was examined. Cyclin D3 was expressed in hormone free differentiation media and in

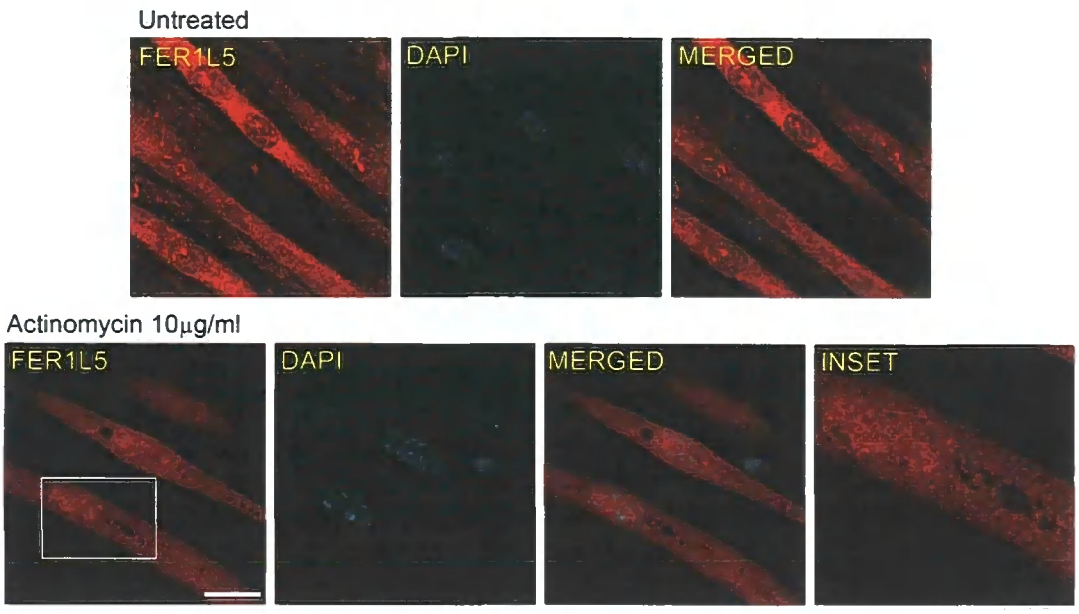

Figure 4.7C. *In actinomycin D treated myotubes multiple irregular shaped cytoplasmic vacuoles free of FER1L5 staining were detected. Projected images are presented. Scale bar, 20µm.*

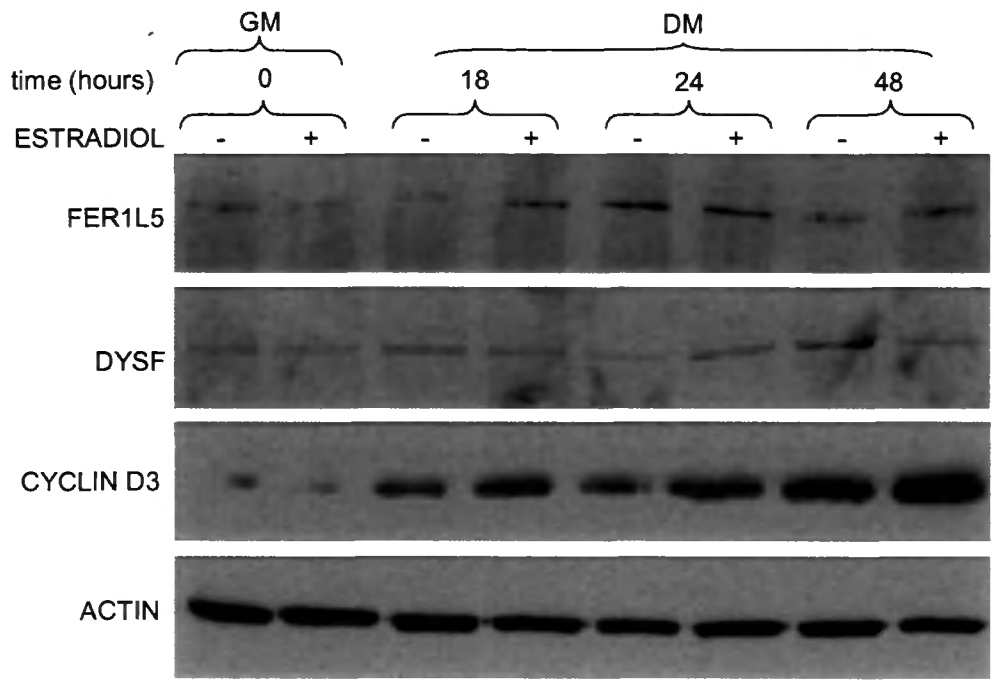

Figure 4.8. FER1L5 and dysferlin expression in C3H-ER-MyoD cells cultured in the presence and absence of estradiol (10μM). *Equal amount of proteins were taken from cell at t=0, 18, 24 and 48 hours after serum withdrawal for western analysis. Cyclin D3 expression was induced in the presence of hormone at 18, 24, and 48 hours following serum withdrawal. For FER1L5, increased expression was observed at 18 hours following serum withdrawal in the presence of estradiol. Dysferlin expression was not altered in the presence or absence of hormone, in differentiation media. GM: growth media; DM: differentiation media.*

media containing estradiol. In differentiation media containing estradiol the expression of cyclin D3 increased at 18h, 24h and 48h following serum withdrawal compared to hormone free media. This data is similar to that reported by Cenciarelli *et al* (1999) using this cell line. The same lysates showing increased cyclin D3 expression when the cells were grown in differentiation media containing hormone were then examined for FER1L5, dysferlin and myoferlin expression respectively. For FER1L5, a slight increase in expression was observed at 18h following serum withdrawal, in lysates from cells cultured in hormone containing media compared to cells cultured in hormone free media. No differences in expression between the two groups of cultures were observed at 24h and 48h, following serum withdrawal. For dysferlin no differences in expression were observed in cultures grown in hormone free differentiation media and media containing estradiol. No data was obtained for myoferlin. Overall the data obtained did not suggest that FER1L5 and dysferlin are early markers of muscle differentiation. The expression of FER1L5 in C3H-ER-MyoD estradiol treated and untreated cells grown in growth media (GM) and differentiation media was also examined by confocal microscopy. Estradiol treated and untreated cells were imaged at the same confocal settings following immunolabelling with FER1L5 and cyclin D3 antibodies. In untreated cells cultured in growth media, FER1L5 staining was observed in cytoplasmic vesicular structures and nuclear staining was also observed **(Figure 4.9A).** For cyclin D3 a speckled like staining pattern was detected in the nuclear regions consistent with published data (Cenciarelli *et al.,* 1999) and also staining was observed in the cytoplasm in aggregates **(Figure 4.9A)**. The staining in the cytoplasmic aggregates for cyclin D3 suggested an artifact because no other published literatures mentioned so far for cyclin D3 staining in the cytoplasmic aggregates. However, there was co-staining of FER1L5 and cyclin D3 in some cytoplasmic aggregates was detected **(Figure 4.9A)**. When cells were switched to differentiation media and examined at 24h following serum withdrawal, FER1L5 staining was detected at the nuclear membrane and perinuclear region in small aggregates **(Figure 4.9B)**. This staining pattern was more prominent in estradiol treated cells and there appeared to be a slight increase in FER1L5 staining in these cells. During myogenesis increased nuclear expression of cyclin D3 has been reported and shown to correlate with withdrawal of the cells from the cell cycle (Mariappan *et al.,* 2005). These cells are myogenic cells. In estradiol untreated myogenic C3H-ER-MyoD cells occasional co-staining of FER1L5 and cyclin D3 was

Figure 4.9A. Expression of FER1L5 and cyclin D3 in proliferating C3H-ER-MyoD cells analysed by immunofluorescence and confocal microscopy. *In estradiol treated and untreated proliferating cells, FER1L5 staining is detected in vesicular structures and there is also some nuclear staining. Cyclin D3 staining is predominantly detected in the cytoplasm and there is staining in aggregates in both hormone treated and untreated cells. Co-staining of FER1L5 and cyclin D3 is observed in some of the cytoplasmic aggregates (indicated by arrowheads). Scale bar, 10μm.*

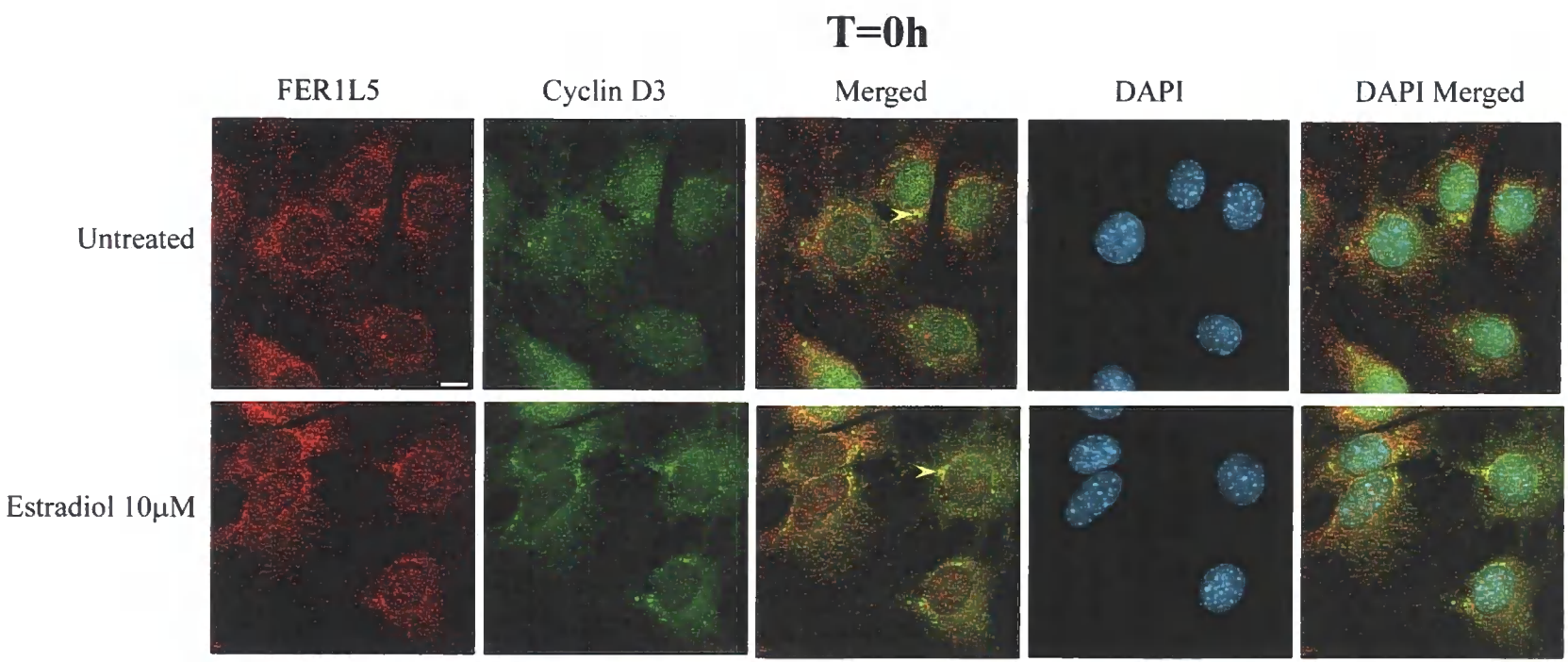
T=0h
FER1L5
Cyclin D3
Merged
DAPI
DAPI Merged
Untreated
Estradiol 10μM

Figure 4.9B. Increased nuclear expression of cyclin D3 in C3H-ER-MyoD cells following serum withdrawal. *FER1L5 staining is detected in aggregates at the nuclear membrane and perinuclear regions in untreated and estradiol treated cells but is more prominent in hormone treated cells. Myogenic cells (indicated by arrowhead) show enhanced nuclear cyclin D3 expression. In differentiating estradiol untreated cells partial co-staining of cyclin D3 and FER1L5 is observed in the cytoplasmic aggregates. In differentiating estradiol treated cells many areas of nuclear co-staining of cyclin D3 and FER1L5 are observed in myogenic cells. (indicated by arrowheads). Scale bar, 10μm.*

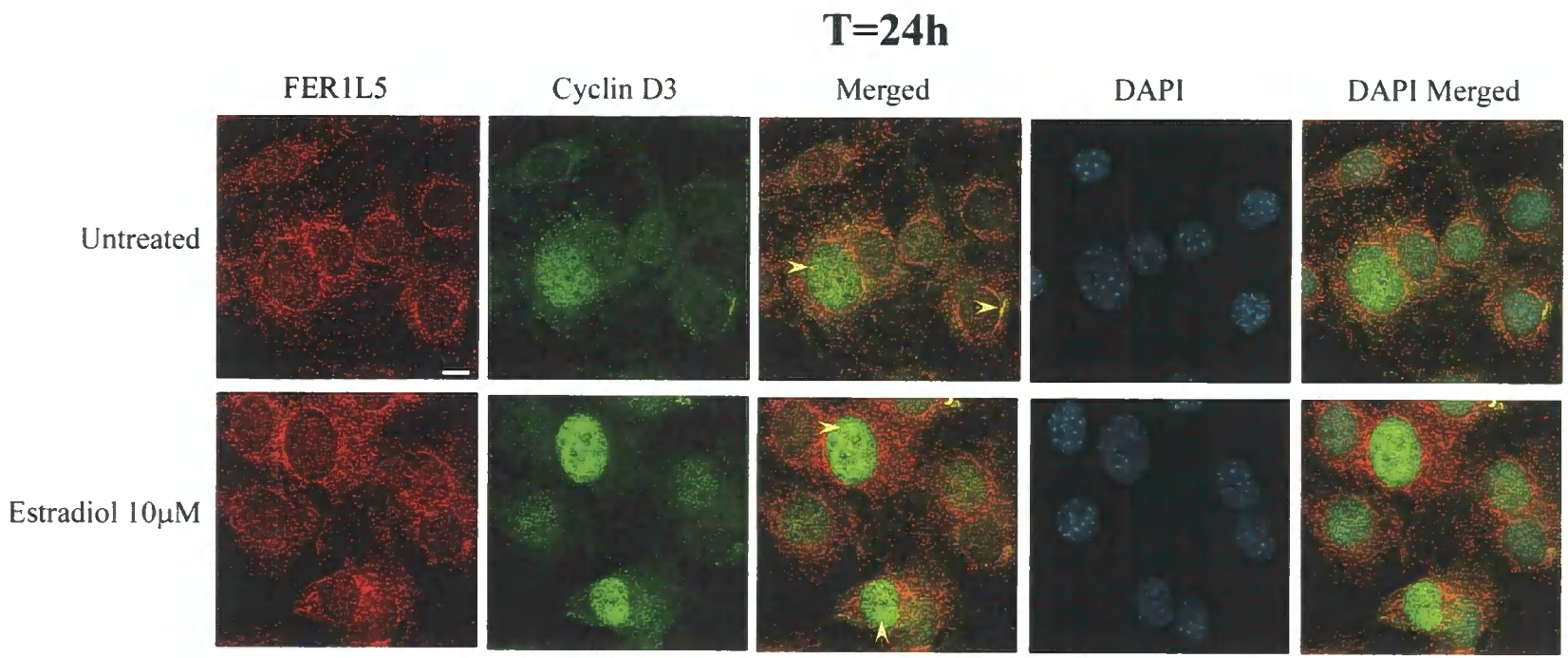
T=24h
FER1L5
Cyclin D3
Merged
DAPI
DAPI Merged
Untreated
Estradiol 10μM

Figure 4.9C. FER1L5 is expressed at all stages of C3H-ER-MyoD cell fusion, in prefusion (elongated) and fused fibroblasts (marked with asterisk). *Increased cytoplasmic expression of FER1L5 was observed in cells cultured in hormone containing differentiation media. In these cells, nuclear membrane staining of FER1L5 was also prominent. All cells showed increased nuclear staining of cyclin D3 at 48h, following serum withdrawal. Co-staining of FER1L5 and cyclin D3 was detected in cytoplasmic aggregates and also in the nucleus (indicated by arrowheads). Scale bar, 10μm.*

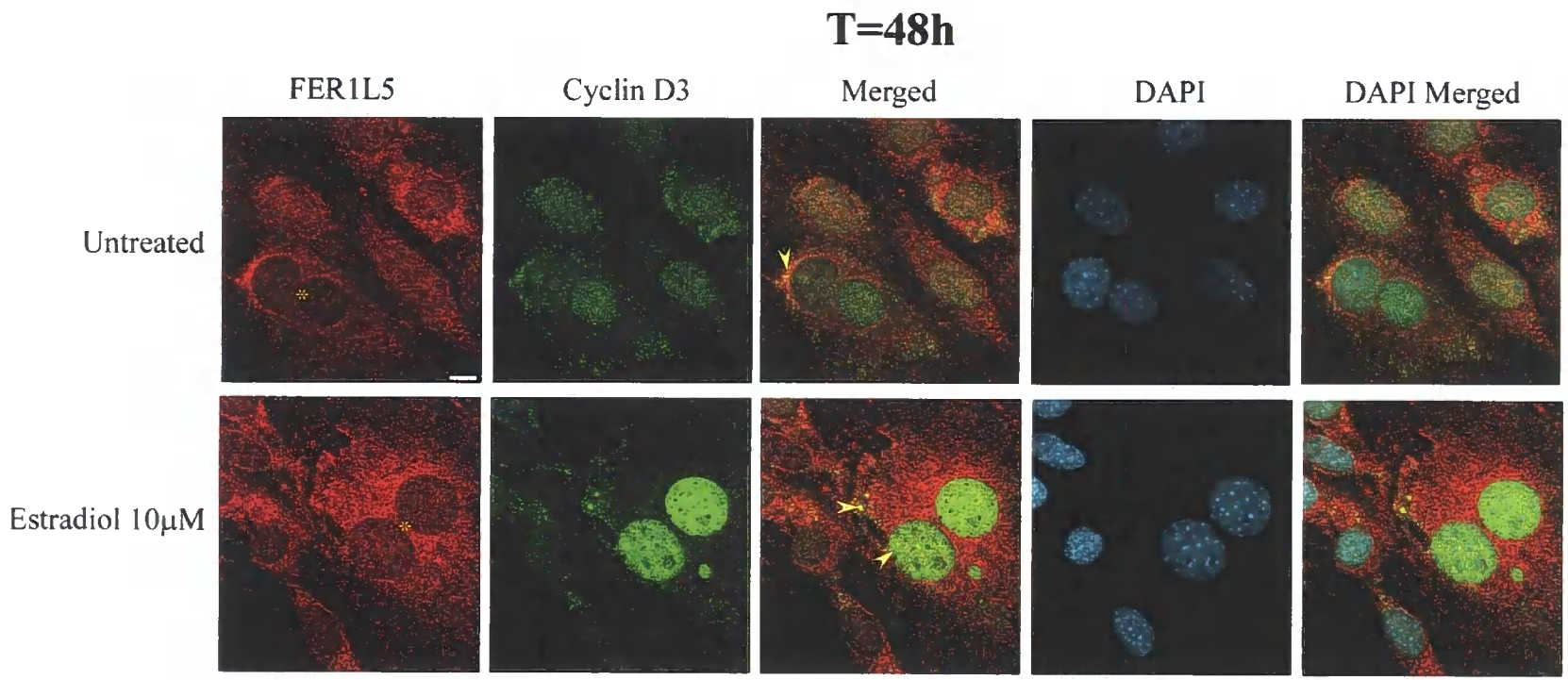
T=48h
FER1L5
Cyclin D3
Merged
DAPI
DAPI Merged
Untreated
Estradiol 10μM

observed in aggregates **(Figure 4.9B)**. In the presence of hormone there were many areas of nuclear co-staining of FER1L5 and cyclin D3 in myogenic cells. At 48h after serum withdrawal FER1L5 expression was observed at all stages of cell fusion in hormone treated and untreated cells. FER1L5 staining was observed in "prefusion", elongated cells and cells which had fused **(Figure 4.9C)**. Expression of FER1L5 was increased in media containing estradiol there was increased cytoplasmic staining and at the nuclear membrane. In cells grown in hormone free differentiation media all cells (mono and multi nucleated) showed increases in nuclear cyclin D3 expression Figure compared to earlier time points. The nuclear cyclin D3 expression was increased in estradiol treated multinucleated cells. Co-staining of FER1L5 and cyclin D3 in cytoplasmic aggregates was observed in untreated cells and there was also some nuclear co-staining. In estradiol treated cells there was extensive nuclear costaining of FER1L5 and cyclin D3. Overall the data obtained suggests that FER1L5 is not linked to MyoD activation. Collectively these studies indicate that FER1L5 is not a myogenic marker.

4.3 Discussion

The expression profile of FER1L5 during C2C12 myoblast fusion appears to be different from that of dysferlin and myoferlin. FER1L5 is expressed at all stages of myoblast fusion and no increases in FER1L5 levels were observed in myotube cultures by western blotting as has been reported for dysferlin and myoferlin respectively and confirmed for dysferlin in this study (Davis *et al.*, 2002; Foxton *et al.*, 2004). However, a slight increase (20%-30%) in the FER1L5 expression levels was observed during early stages of myoblast fusion. To gain a better understanding of FER1L5 distribution during myoblast fusion immunofluorescence studies followed by confocal microscopy was performed. In myoblasts and myotubes FER1L5 staining was detected in vesicular structures in the cytoplasm. In myotubes, there was a characteristic nuclear staining of FER1L5 in aggregate like structures. In addition to the characteristic nuclear FER1L5 staining, cytoplasmic vacuoles ranging from 2-3μm, largely free of FER1L5 staining were detected. In some C2C12 myotubes intercellular FER1L5 stained connections emerging from the vacuolar regions and linking adjacently located myotubes were detected. Increased FER1L5 expression in vesicular structures was observed at the membrane fusion sites in fusing myoblasts. No concentration of FER1L5 stained vesicles was observed at apposed myoblast/myotube membranes and apposed myotube/myotube membranes respectively as has been reported for dysferlin and myoferlin (Luna *et al.*, 2006; Doherty *et al.*, 2005). This data suggests that FER1L5 may operate differentially to dysferlin and myoferlin during C2C12 myoblast fusion. The concentration of dysferlin and myoferlin in vesicular structures at myoblast/myotube fusion sites has led to the hypothesis that dysferlin and myoferlin vesicles are involved in the merging of apposed myoblast/myotube membranes. The concentration of FER1L5 at apposed myoblasts membranes indicates that this ferlin may operate in membrane fusion events at the early stages of the myoblast fusion.

The subnuclear distribution of FER1L5 during C2C12 myoblast fusion was interesting and was confirmed by western analysis of whole nuclear extracts generated from myoblasts and myotube cultures respectively. This work was performed by Dr. Khalil Saleki and demonstrated that nuclear levels of FER1L5 were modestly elevated in myotube cultures compared to myoblasts cultures but for myoferlin and especially dysferlin, their nuclear levels was highly elevated in myotube cultures compared to

myoblasts. These findings prompted me to examine the nuclear distribution of FER1L5 by confocal microscopy by co-immunolabelling C2C12 myotubes using antibodies to protein residing at the nuclear lamina, nucleoskeleton and subnuclear bodies. FER1L5 was shown to have a subnuclear body distribution. Subnuclear bodies are present in all cells and are non-membrane structures consisting of nucleoli, Cajal bodies, promyelocytic leukemia (PML) nuclear bodies and speckles (Handwerger *et al.*, 2006). PML bodies have a diverse function ranging from DNA repair, apoptosis, gene regulation and tumour suppression (Dellaire *et al.*, 2004). Cajal bodies, nucleoli and nuclear speckles are associated with transcription and splicing (Handwerger *et al.*, 2006). The subnuclear body distribution of FER1L5 was examined further by treating myotubes with the drug actinomycin D, which disrupts the integrity of subnuclear bodies by targeting the enzymes RNA polymerase I and II (Sobell *et al.*, 1985). Following actinomycin D treatment there was a nucleoplasmic redistribution of FER1L5 from aggregates to a diffuse similar to that observed for fibrillarin, a nucleolar protein. These studies demonstrated that in C2C12 myotubes FER1L5 is localized to subnuclear bodies which are sensitive to actinomycin D. A partial co-staining of FER1L5 and fibrillarin, a nucleolar protein was observed in myotubes. Since the nucleolus is the site for RNA biogenesis FER1L5 may have a role in RNA biogenesis but further studies are required to confirm this because the co-immunolabelling studies were limited due to the unavailability of monoclonal antibodies to other subnuclear markers. The role of myoferlin and dysferlin in muscle regeneration has been described in Chapter 1 (Doherty *et al., 2005;* Luna *et al.*, 2006). It has been suggested that dysferlin may be involved in muscle regeneration through a myogenic signaling pathway since dysferlin null myoblasts show impaired formation of large myotubes and the reduction of dysferlin correlates with the reduction in myogenin expression (Luna *et al.*, 2006). To explore whether FER1L5 is a myogenic marker the C3H-ER-MyoD fibroblast cell line (Micheli *et al.*, 2004) was used and FER1L5 expression in estradiol treated and untreated cells was examined by a combination of western blotting and immunofluorescence. The western data showed that FER1L5 expression did not change in differentiating C3H-ER-MyoD cells cultured in hormone free and hormone containing media. The expression of cyclin D3, a known myogenic marker was increased following serum withdrawal in the hormone treated cells consistent with the published data (Micheli *et al.*, 2004). The western data obtained for FER1L5 suggested that FER1L5 was not a myogenic marker and this was

confirmed by co-immunolabelling of differentiating C3H-ER-MyoD cultures with cyclin D3 and FER1L5 antibodies. No significant differences were observed in the expression of FER1L5 in estradiol treated and untreated cells as compared to cyclin D3, following serum withdrawal. What was noteworthy was the partial co-staining of cyclin D3 and FER1L5 in the cytoplasm and the nuclear region of differentiating C3H-ER-MyoD. The significance of these findings is not known yet and will require further studies.

CHAPTER V: FER1L5 MEDIATES IN MYOBLAST FUSION AND MUSCLE MEMBRANE REPAIR

5.1 Introduction

In this chapter the role of FER1L5 in myoblast fusion and membrane repair are described. To examine the role of FER1L5 in myoblast fusion and membrane repair, inhibition of FER1L5 in C2C12 cells by siRNAs was initiated but was shown to be ineffective in reducing FER1L5 protein levels. Several FER1L5 siRNA targets were tested alone and as a cocktail using different transfection methods but no protein knockdown of FER1L5 was observed **(Appendix C).** Against this background I developed an alternative approach to inhibiting FER1L5 function, by loading C2C12 cells with FER1L5 antibody using the Amaxa nucleofector system. This adapted antibody loading technique is described in this chapter and then its application in C2C12 cells to examine the role of FER1L5 in myoblast fusion and membrane repair. Microinjection (Kreis *et al.*, 1979; Kreis *et al.*,1982; Rose *et al.*, 2007) and scrape loading (McNeil *et al.*, 1984; McNeil *et al.*, 1987) are two approaches that have been used to load cells with inhibitory antibodies for functional studies. Scrape loading is a simpler technique and although ensuring highly efficient delivery of antibody in large cell numbers it can often result with loss of cell viability resulting in high mortality rates (McNeil *et al.*, 2006). In our laboratory we tested an alternative method, the Amaxa nucleofector system to load large cell numbers with FER1L5 antibody.

5.2 Results

5.2.1 Loading cells with large molecules using nucleofection

Electroporation is generally used for delivery of nucleic acids into mammalian cells. The electroporation conditions for C2C12 cells using Amaxa nucleofection system are known. The optimal electroporation conditions recommended by Amaxa for delivery of nuclei acids into C2C12 cells were employed to test the delivery of a GFP plasmid and a membrane impermeant fluorescent dextran suspended in rabbit serum (replacing the nucleofactor buffer) was investigated **(Figure 5.1A).** 24 hours after transfection 50% of the cells were shown to be positive for the GFP plasmid and fluorescent dextran (10,000 kDa) respectively **(Figure 5.1A).** The electroporation conditions used for the successful entry of GFP plasmid and fluorescent dextran were then applied to C2C12 cells resuspended in FER1L5 antiserum, peptide blocked FER1L5

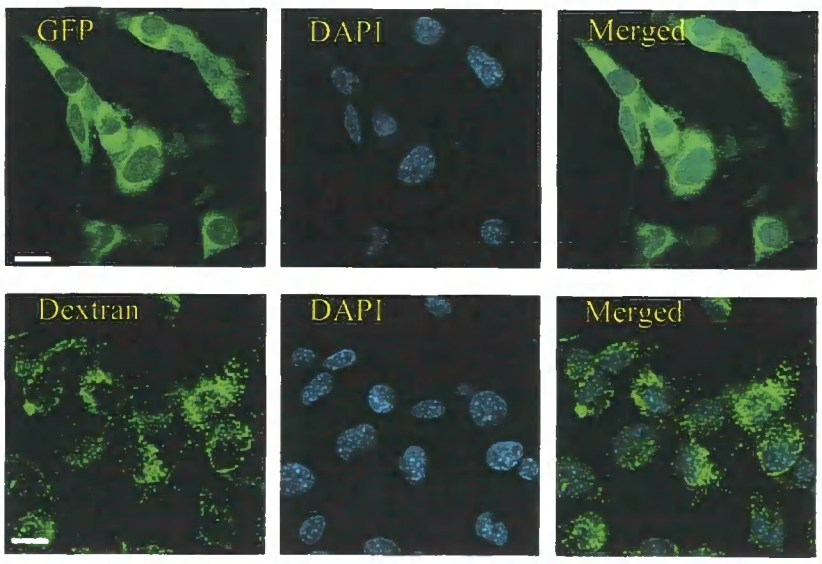

Figure 5.1. A. *Successful delivery into C2C12 myoblasts of GFP plasmid DNA and fluorescently labeled dextran (10,000 kDa) resuspended in rabbit serum, by nucleofection. Cells were analyzed 24h after transfection. Scale bar, 10μM.*

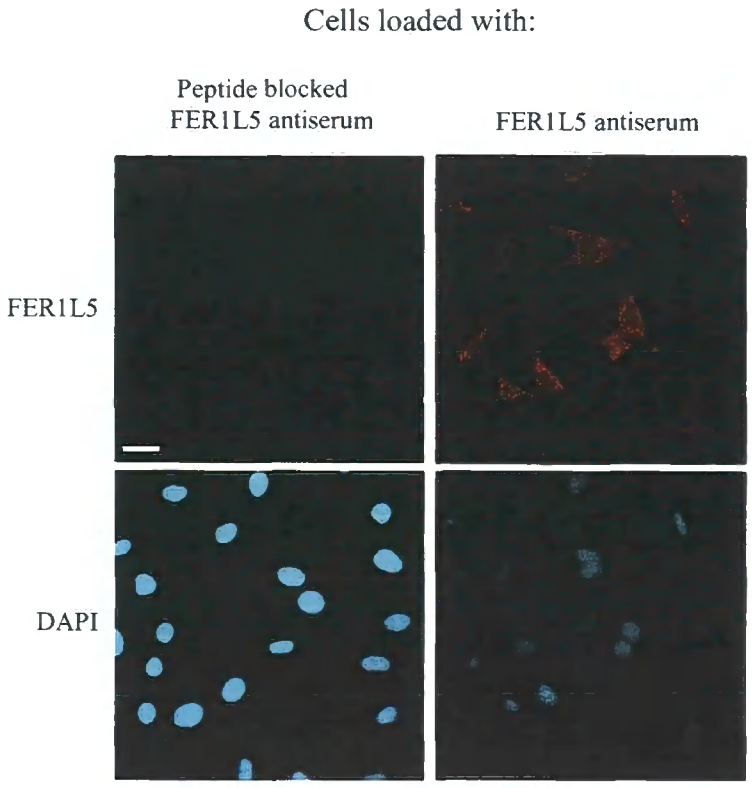

Figure 5.1. B *C2C12 cells loaded with FERIL5 anti-serum by nucleofection show 60% staining for FER1L5 similar to the staining pattern as described in previous chapters. Peptide blocked FERIL5 anti-serum showed no staining. No specific staining pattern was obtained for preimmne serum. Scale bar, 10μM.*

antiserum and preimmune serum respectively. The FER1L5 antiserum, peptide blocked FER1L5 antiserum and preimmune serum were tested for their immunoreactivity by immunoblotting prior to electroporation. This was performed by Dr. Khalil Saleki and the data was as shown in **Figure 3.1A.** The successful entry of FER1L5 inhibitory antiserum into the C2C12 cells were also analysed after electroporation by confocal microscopy. Equal cell densities of C2C12 cells loaded with FER1L5 antiserum, peptide blocked FER1L5 antiserum and preimmune serum respectively were fixed after 24 hours of electroporation. These cells were then permeabilized and stained with Alexa 546 secondary antibody and mounted in Mowiol containing DAPI. The percentage knockdown of the FER1L5 antiserum in the C2C12 cells loaded with FERIL5 inhibitory antiserum were obtained by counting the cells showing specific staining on the coverslips with respect to the total number of nuclei viewed in 20 randomly chosen areas **(Figure 5.1B)**. Mean percentage was obtained for these chosen areas and showed 60% knockdown in the FER1L5 inhibitory antiserum loaded coverslips. Cells loaded with peptide-blocked FER1L5 anti-serum showed no staining as shown in **Figure 5.1B**. No specific staining pattern was obtained for preimmune serum (data not shown). Using this approach the role of FER1L5 in myoblast fusion and membrane repair was examined in C2C12 myoblasts.

5.2.2 Inhibition of FER1L5 impairs formation of large myotubes

C2C12 cells were loaded with FER1L5 antiserum, peptide blocked FER1L5 antiserum and preimmune serum respectively. Following electroporation the three groups of cultures of equal cell densities were grown on coverslips and allowed to differentiate till day 9. During this time no differences in the proliferation rate was observed between the cultures (data not shown). At day 9 cells were fixed and stained with anti-desmin antibody and mounted in Mowiol containing DAPI. Desmin staining was used to identify myogenic myoblasts (Doherty *et al.*, 2005) and the fusion index of the three groups of cultures was determined by quantifying the number of desmin positive myoblasts, myotubes containing two or three nuclei and myotubes containing four or more nuclei. Upon examination the cultures loaded with FER1L5 anti-serum showed significantly higher number of desmin positive myoblasts and small myotubes containing 2 or 3 nuclei compared to cultures loaded with preimmune serum and

Figure 5.2A. Reduced myogenic index of C2C12 cells loaded with FER1L5 antiserum. *Equal densities of cells electroporated in the presence of preimmune serum, peptide blocked FER1L5 antiserum and FER1L5 antiserum respectively were differentiated. Desmin staining identified the myogenic cells. Fusion index was determined by quantifying the number of singly nucleated desmin-positive cells, myotubes containing two or three nuclei, and those containing four or more nuclei. The number of nuclei counted in preimmune serum, peptide blocked FER1L5 antiserum and FER1L5 antiserum loaded cultures were 2792, 2784 and 2787 respectively. Forty fields at 40x magnification on the coverslips for each of the cultures from three independent experiments were analyzed.* ***i)*** *Myotubes were immunolabelled with desmin antibody and confocal imaging shows that cultures loaded with FER1L5 antiserum displayed fewer multinucleated myotubes (=4 nuclei). Scale bar, 20μM.* ***ii)*** *Histograms representing the fusion index of equal densities of C2C12 cultures loaded with preimmune serum, peptide blocked FER1L5 antiserum and FER1L5 antiserum respectively. The fusion index of the FER1L5 antiserum loaded cultures containing multinucleated myotubes (=4 nuclei) was significantly lower (37.2%) than that obtained for preimmune serum loaded (69.6%) and peptide blocked FER1L5 antiserum loaded (67.4%) cultures respectively. Statistical analysis was performed using student T-test. P values for FER1L5 vs preimmune serum and peptide blocked FER1L5 antiserum are indicated in the histograms. In the FER1L5 antiserum loaded cultures the number of cytoplasmic ring shaped structures (quantified in the same fields as used to quantify fusion index) were also significantly lower in number (n=17) compared to preimmune serum loaded cultures (n=50; P=<0.0005) and peptide blocked FER1L5 antiserum loaded cultures respectively (n=50; P<0.005). n = number of cytoplasmic ring shaped structures.*

Ai

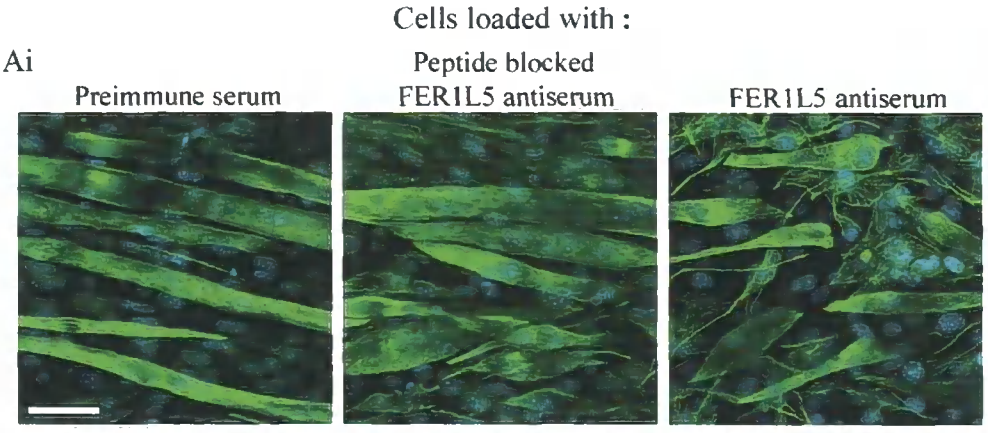
Cells loaded with :
Preimmune serum
Peptide blocked FER1L5 antiserum
FER1L5 antiserum

ii

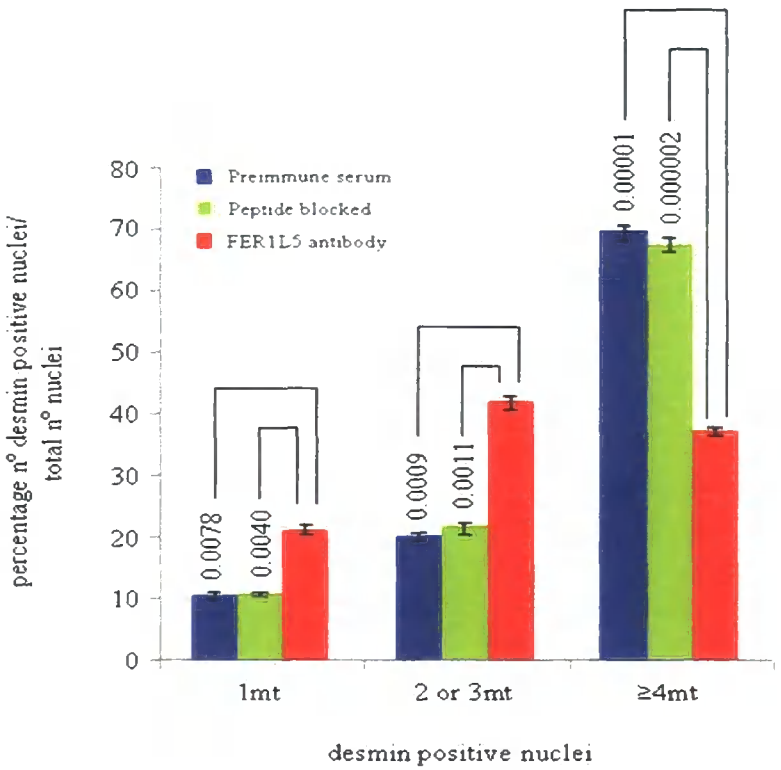
Preimmune serum
Peptide blocked
FER1L5 antibody
percentage n° desmin positive nuclei/ total n° nuclei
0
10
20
30
40
50
60
70
80
0.0078
0.0040
0.0009
0.0011
0.00001
0.000002
1mt
2 or 3mt
≥4mt
desmin positive nuclei

Figure 5.2B. Reduced myogenic index of C2C12 myoblasts loaded with myoferlin antiserum by nucleofection. *Cells were loaded with growth media and peptide blocked myoferlin antibody and myoferlin antibody and cultured as described above in Figure 5.2A. For fusion index analysis equal amount of specific myoferlin peptide (4.25μg) was used to abolish the immunoreactivity signal that obtained for myoferlin antibody (12.75μg) by peptide blocking as described for FER1L5 (data not shown). Three independent experiments were performed. Fusion index was determined as described in Figure 5.2A. The number of nuclei counted in the growth media, peptide blocked myoferlin antibody and myoferlin antibody loaded cultures were 2753, 2775 and 2730 respectively.* ***i)*** *Cells were stained with monoclonal anti-desmin antibody. Confocal imaging shows that cultures loaded with myoferlin antibody showed reduced number of multinucleated myotubes (=4 nuclei) compared to controls. Scale bar, 20μM.* ***ii)*** *Histograms were plotted and the fusion index was obtained for the three groups of cultures as described above for FER1L5 loaded cultures. The fusion index of the myoferlin antibody loaded cultures containing multinucleated myotubes (=4 nuclei) was significantly lower (39.13%) than that obtained for growth media loaded (70.93%) and peptide blocked myoferlin antibody loaded (68.16%) cultures respectively. P values of the three cultures are shown in the histograms.*

Bi

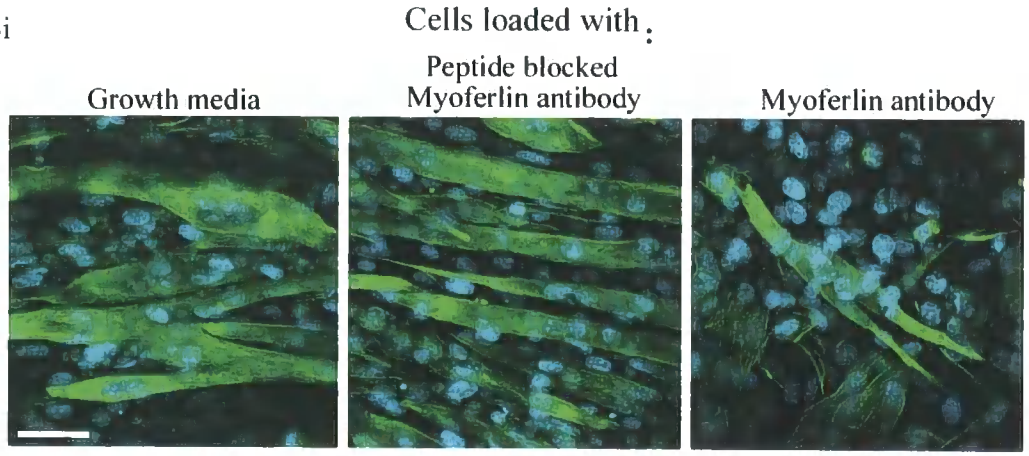
Cells loaded with:
Growth media
Peptide blocked Myoferlin antibody
Myoferlin antibody

ii

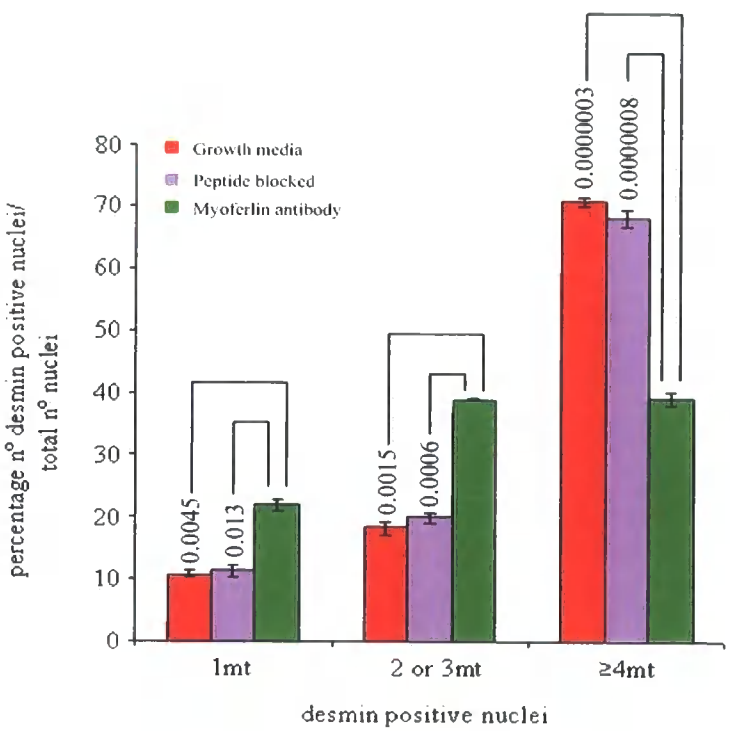
Growth media
Peptide blocked
Myoferlin antibody
percentage n° desmin positive nuclei/ total n° nuclei
0
10
20
30
40
50
60
70
80
0.0045
0.013
0.0015
0.0006
0.0000003
0.0000008
1mt
2 or 3mt
≥4mt
desmin positive nuclei

Figure 5.2C. Impaired formation of multinucleated myotube in the C2C12 cell lines stably expressing myoferlin siRNA.

C2C12 myoblasts stably expressing myoferlin siRNA and controls; scrambled siRNA and no siRNA (cells grown only in nucleofection solution) were allowed to differentiate till day 9 .To quantify the fusion index myoferlin deficient and control cell lines were treated as described above and the statistical analysis were followed as described in Figure 5.2A. Three independent experiments were performed. The number of nuclei counted in the myoferlin deficient, scrambled myoferlin siRNA and no siRNA cell lines were 2765, 2750 and 2785 respectively. ***i)*** *Cells were fixed and stained with monoclonal anti-desmin antibody. Confocal imaging shows lesser number of large multinucleated myotubes in the myoferlin deficient cell lines (=4 nuclei) compared to controls. Scale bar, 20μM.* ***ii)*** *Statistical analysis was performed for all these three cell lines as described above. The fusion index of the myoferlin deficient cell lines containing multinucleated myotubes (=4 nuclei) was significantly lower (38.1%) than that obtained for scrambled myoferlin siRNA (68.7%) and cell lines that has no siRNA (69.8%) respectively. P values for these three cell lines are shown in the histograms.*

Ci

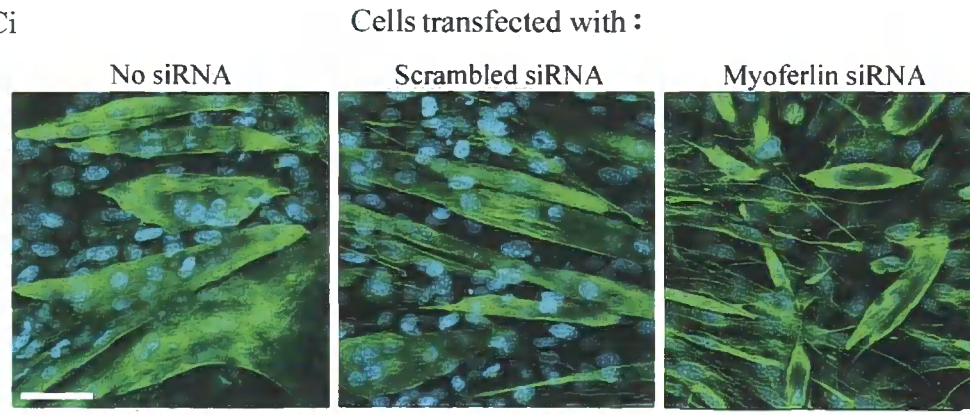
Cells transfected with :
No siRNA
Scrambled siRNA
Myoferlin siRNA

ii

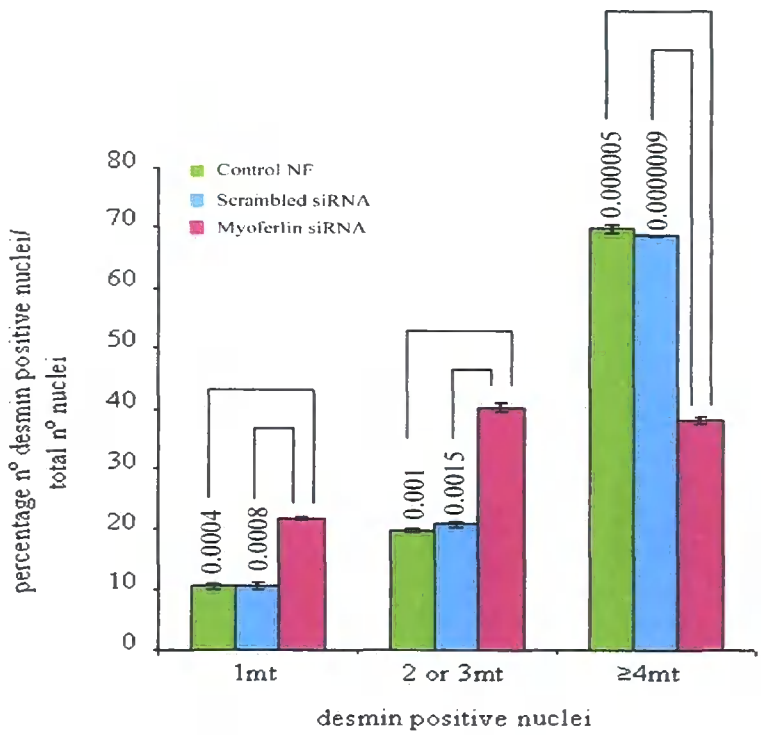
Control NF
Scrambled siRNA
Myoferlin siRNA
percentage n° desmin positive nuclei/ total n° nuclei
80
70
60
50
40
30
20
10
0
0.0004
0.0008
0.001
0.0015
0.000005
0.0000009
1mt
2 or 3mt
≥4mt
desmin positive nuclei

peptide blocked serum respectively **(Figure 5.2A)**. In contrast, cultures loaded with FER1L5 anti-serum displayed significantly fewer large multinucleated myotubes containing four or more nuclei (=4 nuclei). The fusion index of the three groups of cultures was determined by calculating the mean percentage of desmin positive nuclei in myoblasts and myotubes in respect to the total number of nuclei viewed in 40 randomly chosen areas on the coverslips. The fusion index was calculated from three independent experiments. The fusion index of FER1L5 antiserum loaded cultures (37.2%) was significantly lower than that obtained for preimmune serum loaded (69.6%; $P=1x10^{-5}$) and peptide blocked FER1L5 antiserum loaded (67.4%; $P=2x10^{-6}$) cultures respectively **(Figure 5.2B; Table 5.1A)**. The results indicated that C2C12 cells loaded with FER1L5 antibody are impaired in the formation of multinucleated myotubes.

In addition to quantifying the number of desmin positive nuclei in the 40 randomly chosen areas on the coverslips of the three groups of cultures I also quantified the number of the cytoplasmic vacuolar like structures present in myotubes on the same coverslips. In myotubes formed in cultures loaded with FER1L5 antiserum there were a significantly less number of the cytoplasmic vacuolar like structures compared to myotubes formed in the cultures loaded with preimmune serum and peptide blocked FER1L5 antiserum **(see Table 5.1B)**. These results suggested that inhibition of FER1L5 in C2C12 cells restricts the formation of the cytoplasmic vacuolar like structures in myotubes. The effectiveness of nucleofection for antibody loading of large cell numbers was confirmed by measuring the myogenic fusion index of electroporated C2C12 myoblasts loaded with characterized myoferlin monoclonal antibody (Jaiswal *et al.*, 2007) **(Figure 5.2B)** and compared the results with myoferlin deficient cells generated by stable transfection of myoferlin siRNA **(Figure 5.2C)**. Short interfering RNA (siRNA) is often used in functional gene studies and in the validation of novel drug targets. Impaired fusion of myoferlin null myoblasts generated from the myoferlin knockout mouse has previously been demonstrated (Doherty *et al.*, 2005). C2C12 myoblasts loaded with myoferlin monoclonal antibody show an impaired myogenic fusion index **(Figure 5.2Bii)** similar to that observed for myoferlin deficient cells generated by stable transfection of myoferlin siRNA **(Figure 5.2Cii)**. Morphological changes were also observed in all the antibody loaded cells.

The cells were more like spread out, thickened and flattened shape compared to the control cells.

As an extra control, C2C12 cultures were also loaded with an antibody to a non-muscle protein. The antibody used was raised to NMDAR1, which is a characterized protein found only in brain (Chazot *et al.*, 1995). Cultures were loaded with NMDAR1 antiserum, peptide blocked NMDAR1 antiserum and preimmune serum as described for FER1L5. The fusion index was determined as described for FER1L5. No differences were observed between the fusion index of anti-NMDAR1 serum loaded cultures (70.1%), preimmune serum loaded (70.0%; $P=1.8x10^{-1}$) and peptide blocked NMDAR1 antiserum loaded (70.3%; $P=4.9x10^{-1}$) cultures **(Figure 5.2D)**. These results showed that the control antibody has no effect on the formation of myotubes highlighting the specific inhibitory function of the FER1L5 antibody. The fusion index data obtained for FER1L5 antiserum and NMDAR1 antiserum loaded cultures is summarized in **Table 5.1A.**

5.2.3 Defective muscle membrane repair following inhibition of FER1L5

The most common and accurate membrane repair assay used to examine the role of dysferlin in membrane repair is the multiphoton laser wounding assay. This assay measures the fluorescence of the membrane impermeant dye FM-143 following wounding of membranes by irradiation. Identical wounds can be created using a multiphoton confocal microscope. FM1-43 fluoresces when it binds membranes and in this assay in wounded cells FM1-43 binds to membranes resulting in an increase in its fluorescence, which stops increasing once the injured membrane is repaired impeding dye entry in the presence of calcium. The rate of FM-143 fluorescence influx is a measure of membrane repair following laser wounding. Laser wounding assays were performed in collaboration with Isabelle Richard at Genethon, on wild type C2C12 cells and C2C12 cells loaded with FER1L5 antiserum, peptide blocked FER1L5 antiserum and preimmune serum respectively. The wounding assays were performed by Williams Lostal. Membrane injury was induced by multiphoton laser irradiation in the presence of the dye FM-143 and the fluorescence of this dye near the disruption site was measured at 7s intervals over a 75s time course following membrane injury. Wild type C2C12 cells injured in the presence of Ca^{2+} resealed the

Figure 5.2D. No differences were observed in the fusion index of C2C12 cells loaded with NMDAR1 antiserum, peptide blocked NMDAR1 antiserum and preimmune serum respectively. *Myotubes were labelled with desmin antibody. i) All the three groups of cultures showed multinucleated myotubes. Scale bar, 20μM. ii) The fusion index of C2C12 cultures loaded with NMDAR1 antiserum, peptide blocked NMDAR1 antiserum and preimmune serum was 70%, 70.3% and 70.1% respectively. The number of nuclei quantified was 2843 for NMDAR1 anti-serum loaded cultures, 2775 for peptide blocked NMDAR1 anti-serum loaded cultures and 2889 for preimmune serum loaded cultures. Three independent experiments were performed. P values are shown.*

Bi

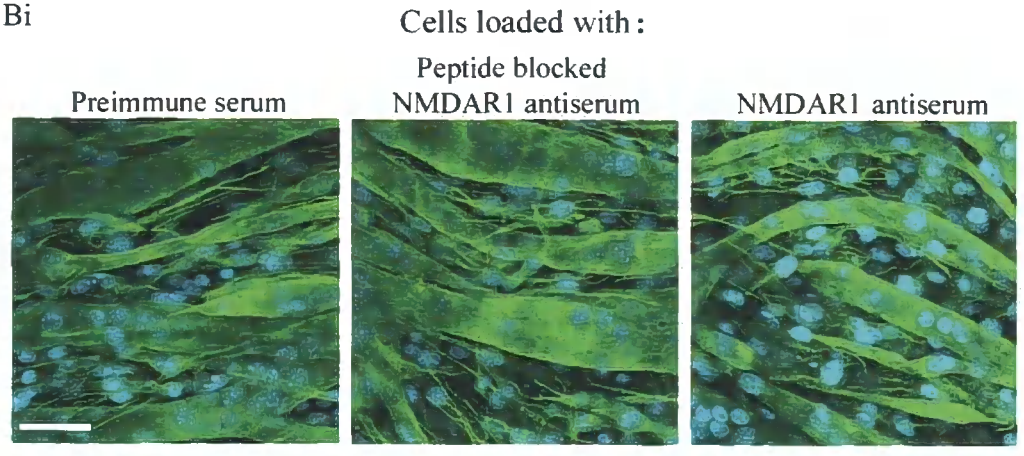
Cells loaded with :
Preimmune serum
Peptide blocked NMDAR1 antiserum
NMDAR1 antiserum

ii

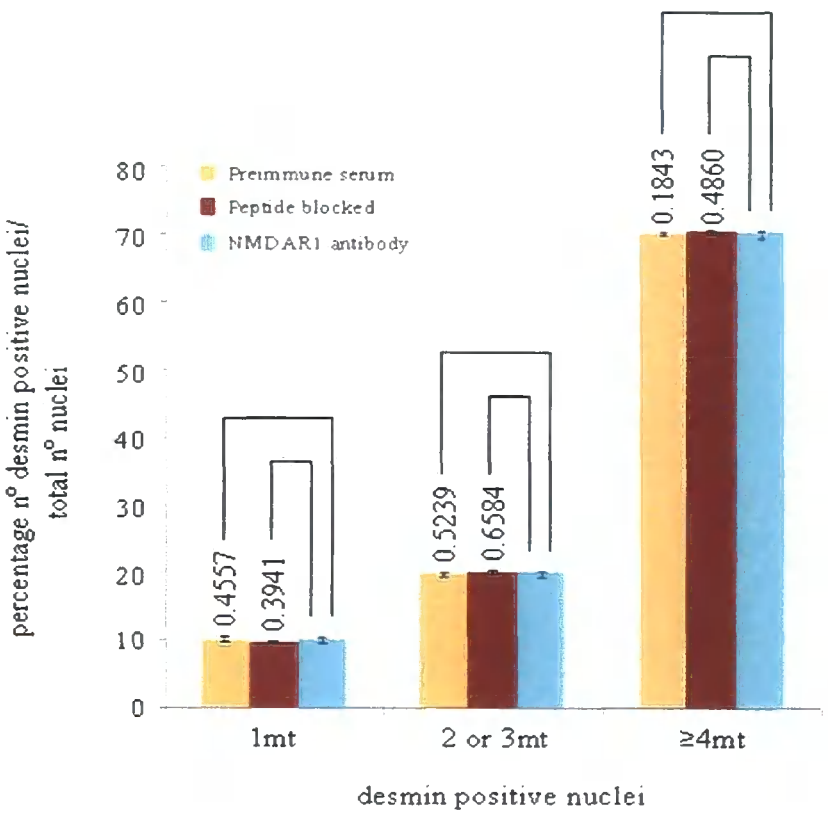
Preimmune serum
Peptide blocked
NMDAR1 antibody
percentage n° desmin positive nuclei/ total n° nuclei
80
70
60
50
40
30
20
10
0
0.4557
0.3941
0.5239
0.6584
0.1843
0.4860
1mt
2 or 3mt
≥4mt
desmin positive nuclei

Table 5.1A: Summary of fusion index data

Cultures loaded with	% of myotubes	p-values
FER1L5 antiserum	37.2%	-
Preimmune serum loaded	69.6%	$P=1x10^{-5}$
Peptide blocked FER1L5 antiserum loaded	67.4%	$P=2x10^{-6}$
NMDAR1 anti-serum loaded cultures	70.1%	-
Preimmune serum loaded	70.0%	$P=1.8x10^{-1}$
Peptide blocked NMDAR1 antiserum loaded	70.3%	$P=4.9x10^{-1}$

Table 5.1B: Quantification of cytoplasmic vacuolar structures formed in myotubes following FER1L5 inhibition

Cultures loaded with	No. of cytoplasmic vacuolar like structures detected in myotubes (n)	p-values
FER1L5 antiserum	17	-
Peptide blocked antiserum	50	P<0.005
Preimmune serum	50	P<0.0005

damaged membrane within the 75s time course because FM-143 fluorescence stopped increasing over this time course. Wild type C2C12 cells injured in the absence of Ca^{2+} were unable to impede dye entry during the same time course (75s) indicating that the torn membranes were unable to reseal in the absence of calcium **(Figure 5.4A, B).** C2C12 cells loaded with preimmune serum and peptide blocked FER1L5 antiserum respectively efficiently resealed their disrupted membranes as measured by the rate of FM-143 fluorescence influx following membrane injury. C2C12 cells loaded with FER1L5 antiserum were unable to impede FM-143 dye entry over the 75s time course indicating that their membranes had not resealed **(see Figure 5.5).** These results demonstrated that FER1L5 has a role in muscle cell membrane repair.

Figure 5.5. Impaired membrane resealing in C2C12 cell myoblasts loaded with FER1L5 antiserum. *Membrane repair assays were performed on wild type C2C12 cells with (w/) or without (w/o) calcium and then in C2C12 cells loaded with FER1L5 antiserum (FER1L5 Ab), peptide blocked FER1L5 antiserum (FER1L5 Ab and peptide) or preimmune serum respectively. Membrane repair was examined in the loaded cells in the presence of calcium.* ***A)*** *Fluorescent images of C2C12 cells following laser wounding. The white lines indicate the injury site. The time at which the images were captured following wounding is indicated in seconds. The images were analyzed using ImageJ software and the look up table was set to "Fire" (the table is depicted at the bottom of the last panel). Scale bar =100μM.* ***B)*** *Histogram representing the deduced rates of fluorescence influx (Δ [fluorescence]/ Δt) in C2C12 cells, w/ (n=3); w/o calcium (n=4); loaded with FER1L5 antiserum (n=4), peptide blocked FER1L5 antiserum (n=5) or preimmune serum (n=3). Data are means ± S.E.M. Statistical analysis was performed using Student's t-test. * indicate a P- value <0.05; ** P-value <0.01 compared to C2C12 cells injured in the presence of calcium.*

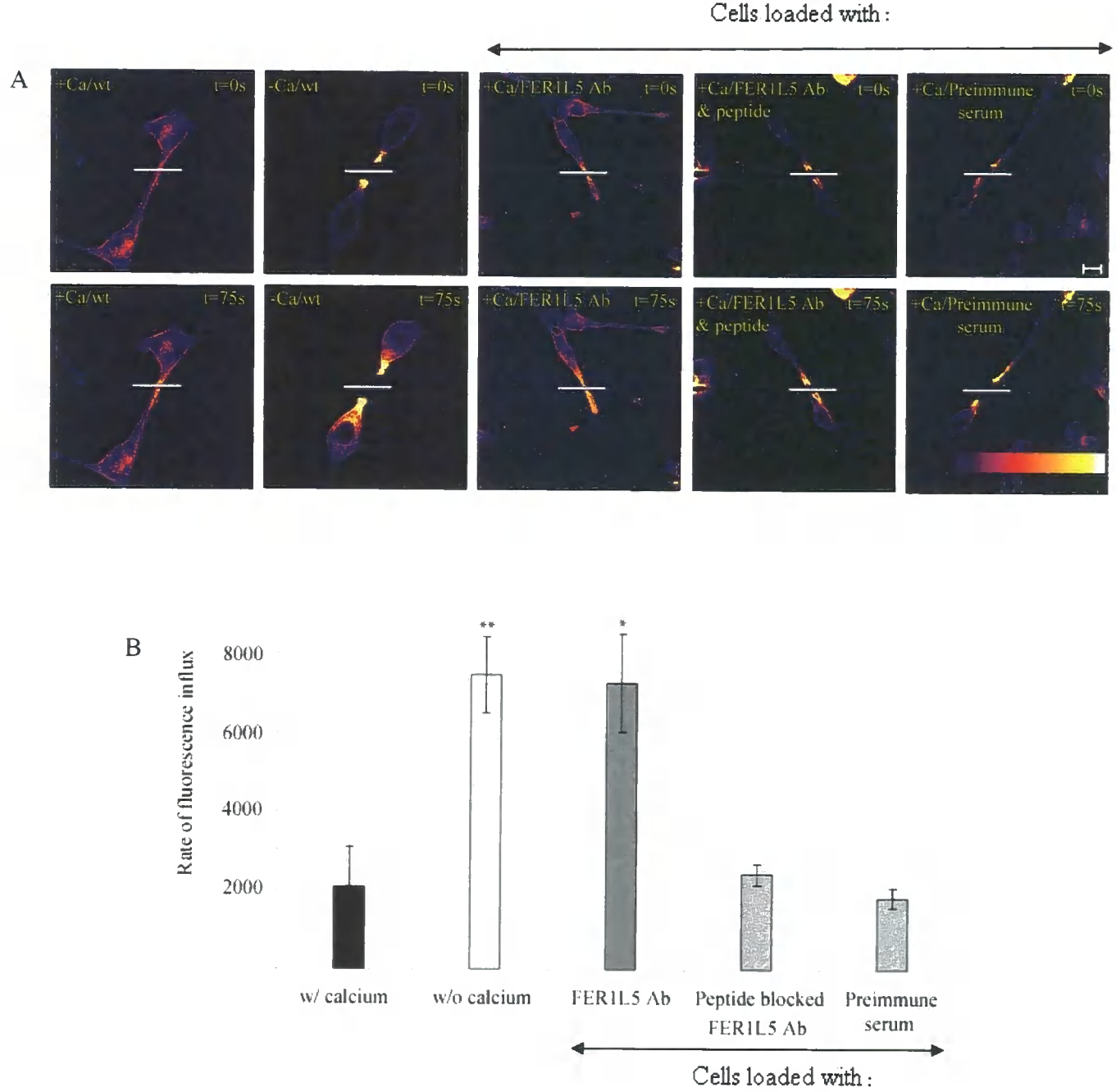
Cells loaded with :
A
+Ca/wt t=0s
-Ca/wt t=0s
+Ca/FER1L5 Ab t=0s
+Ca/FER1L5 Ab & peptide t=0s
+Ca/Preimmune serum t=0s
+Ca/wt t=75s
-Ca/wt t=75s
+Ca/FER1L5 Ab t=75s
+Ca/FER1L5 Ab & peptide t=75s
+Ca/Preimmune serum t=75s
B
Rate of fluorescence influx
8000
6000
4000
2000
**
*
w/ calcium
w/o calcium
FER1L5 Ab
Peptide blocked FER1L5 Ab
Preimmune serum
Cells loaded with :

5.3 Discussion

In muscle there are two important membrane fusion events: myoblast fusion which occurs during muscle development (myogenesis) and following the regeneration phase after injury and the repair of muscle cell membrane tears occurring during muscle contraction (Horsley and Pavlath, 2004; Taylor, 2003; Abmayr *et al.,* 2003; Bansal and Campbell, 2004; Doherty and McNally, 2003). During myoblast fusion proliferating mononucleated myoblasts irreversibly exit from the cell cycle and fuse to form multinucleated muscle fibers at sites of muscle development (Horsley and Pavlath, 2004; Taylor, 2003; Abmayr *et al.,* 2003). In mammals myogenesis occurs in two well-characterized phases termed primary and secondary myogenesis (Ontell *et al.,* 1988). In the first phase primary fibres with several nuclei (myotube) are formed by the fusion of mononucleated myoblast-myoblast till the first few days of life followed by the secondary phase when muscle is developed through hypertrophy of the existing fibres. Myoblast fusion also occurs during adulthood following muscle injury whereupon satellite cells proliferate and fuse either with existing myotubes in injured muscle or they form *de novo* myotubes (Kelly, 1996; Pena *et al.,* 1995). Many of the mechanisms involved in myoblast fusion have been delineated in *Drosophila* because of its rapidly developing and simple musculature (Taylor, 2003; Abmayr *et al.,* 2003; Chen and Olsen, 2004). In *Drosophila* myoblast fusion founder myoblasts acts as seeds to attract, adhere and fuse to fusion-competent myoblasts (fcms). Following cell alignment and adhesion the apposing plasma membranes coalesce, allowing fusion. Multinucleated myotubes are then formed by successive rounds of fusion (Taylor, 2003; Abmayr *et al.,* 2003; Chen and Olsen, 2004). Through the analysis of the *Drosophila* mutants several proteins involved in myoblast fusion have been characterised including Dumbfounded (Duf/Kin), Sticks and stones (Sns), Blownfuse (Blow), myoblast city (Mbc), rolling pebbles/antisocial (Rols7) and Loner [Taylor, 2003; Abmayr *et al.,* 2003; Chen and Olsen, 2004). Dumbfounded and rolling pebbles are involved in the attraction and adhesion steps, blownfuse and the other proteins have a role in the fusion process since mutations in the corresponding genes produces mutants with severe fusion defects producing bi- or trinucleated muscle cells. Several of the fusion relevant proteins are involved in mediating actin dynamics such as Loner, the small GTPases Drac1 and Drac2 highlighting the role of the actin cytoskeleton in *Drosophila* myoblast fusion (Taylor, 2003; Abmayr *et al.,* 2003; Chen

and Olsen, 2004). In vertebrates there is no evidence for the presence of founder and fusion competent cells and some mammalian orthologs of many of the above proteins do not have similar functions (Kestila *et al.,* 1998) whilst for others such as Myoblast city and Rac1 vertebrate homologs have been identified (Lu *et al.,* 2005; Charasse *et al.,* 2007). In vitro studies and analysis of primary myoblasts derived from mouse knockout models have identified several gene products that are essential for mammalian myoblast fusion **(Appendix D)** (Richardson *et al.,* 2008). Several membrane proteins however have been implicated in vertebrate myoblast fusion including ADAM12, NFACT2, caveolin-3, calpain 3, integrins, tetraspanins, dysferlin and myoferlin but their molecular mechanisms in myoblast fusion are not fully understood (Horsley and Pavlath, 2004; Charasse *et al.,* 2007; Luna *et al.,* 2006). Disruption of these gene products impairs or blocks myoblast-myoblast fusion process (Richardson *et al.,* 2008).

Since recent studies have demonstrated the role of dysferlin and myoferlin in the fusion of myoblasts with existing myofibers during mammalian muscle development and regeneration the role of FER1L5 was also analysed during myoblast fusion and membrane repair.

In this study, an alternative approach to inhibit FER1L5 protein function, by antibody loading was adopted because transfection of FER1L5 siRNAs was shown to be ineffective in reducing FER1L5 protein expression. Five different FER1L5 siRNAs used independently and as a cocktail were tested and despite the optimization of the electroporation protocol for C2C12 myoblasts using G3PDH siRNAs no FER1L5 protein knockdown was observed. Therefore the nucleofection protocol was modified and used to inhibit FER1L5 protein in C2C12 myoblasts. Using this approach the role of FER1L5 in myoblast fusion and membrane repair was demonstrated. The data obtained from the fusion index assays and the laser wounding membrane repair assay suggests that FER1L5 has a role in muscle membrane fusion. My results demonstrate that inhibition of FER1L5 results in a significantly reduced myogenic index. Inhibition of FER1L5 was shown to impair the formation of multinucleated myotubes similar to what has been reported for dysferlin null and myoferlin null myoblasts (Luna *et al.,* 2006; Doherty *et al.,* 2005). The effectiveness of nucleofection was also demonstrated by showing that C2C12 myoblasts loaded with myoferlin monoclonal antibody show an impaired myogenic fusion index similar to that observed for

myoferlin deficient cells generated by stable transfection of myoferlin siRNA. These results are consistent with those reported for myoferlin null myoblasts generated from the myoferlin knockout mouse highlighting the effectiveness of nucleofection for inhibiting FER1L5 protein function by antibody loading. These results strengthen our functional data on FER1L5 and show that FER1L5 is involved in myoblast fusion and the inhibition of FER1L5 function leads to defective myoblast fusion thereby reduced myogenic index was observed. In the cultures loaded with FER1L5 antiserum, in which the formation of multinucleated myotubes was disrupted there were a significantly higher number of desmin positive myoblasts (myogenic myoblasts). Changes in the cell morphology were also seen in the antibody transfected cells than control cells. The cells appear to be more thickened, flattened and tapering at both ends suggesting that this could be due to a disruption in the cytoskeletal architecture possibly reorganization of the desmin cytoskeleton. In the previous chapter FER1L5 was shown to concentrate at apposed myoblast/myoblast membrane fusion sites but not at apposed myotube/myoblast fusion sites, like dysferlin and myoferlin (Luna *et al.,* 2006; Doherty *et al.,* 2005). The fusion index data and these observations suggest that FER1L5 may function differentially to dysferlin and myoferlin in the merging of myoblast/myoblast membranes and not myoblast/myotube membranes as proposed for dysferlin and myoferlin (Doherty *et al.,* 2005; Klinge *et al.,* 2007).

In chapter IV, I have shown that in C2C12 myotubes cytoplasmic vacuoles not stained for FER1L5 were present and from some of these vacuoles intercellular connections linking neighbouring myotubes and staining for FER1L5 were observed. Following inhibition of FER1L5 the number of the cytoplasmic vacuoles detected in the myotubes from the cultures loaded with FER1L5 antiserum was reduced. The significance of these findings are not clear at present but the vacuolar regions represent sites of membrane remodeling (see next chapter) and their reduced formation following inhibition of FER1L5 may reflect a disruption of their process.
Inhibition of FER1L5 also leads to defective membrane resealing as shown using laser wounding assays. Membrane repair in mammalian cells is proposed to occur by 'patch' hypothesis, which involves Ca^{2+} entry into the cell through the wound site. Entry of calcium is thought to result in accumulation of a large population of vesicles underneath the membrane injury site, which undergo vesicle-vesicle fusion. This eventually creates the formation of a new 'patch' membrane, which is added to the

wound site by exocytosis (McNeil *et al.*, 2003; McNeil *et al.*, 2005). Although lysosomes have been considered to be the primary endomembrane source of membrane repair vesicles in some mammalian cells (Reddy *et al.*, 2001; McNeil *et al.*, 2005) dysferlin vesicles are thought to be the sarcolemmal repair vesicles. The origin and the identity of dysferlin vesicles is not known but dysferlin is considered to be the emergency fusogen involved in the formation of the patch membrane (Han *et al.*, 2007; McNeil *et al.*, 2005) because ultrastructural studies show accumulation of vesicles at disrupted membrane sites in dysferlin deficient muscle and dysferlin null muscle fibres fail to reseal their damaged membranes resulting in a dystrophic phenotype (Bansal *et al.*, 2003; Selcen *et al.*, 2001; Cenacchi *et al.*, 2005). Several studies have begun to identify other proteins involved with dysferlin in membrane repair, which include AHNAK (Benaud *et al.*, 2004), caveolin-3 (Hernandez *et al.*, 2007), annexin (A1 and A2) (McNeil *et al.*, 2005; Lennon *et al.*, 2003), affixin (Matsuda *et al.*, 2005), calpain 3 (Huang *et al.*, 2005) and the recently discovered MG53 (Cai *et al.*, 2009[a]). A recent study has highlighted the functional interaction between MG53 and caveolin 3 to regulate the trafficking of dysferlin to the injury sites of muscle membranes (Cai *et al.*, 2009[c]). MG53-/- mice showed impaired membrane resealing following membrane damage and the mice also develop a mild muscular dystrophy (Cai *et al.*, 2009[c]). Our results indicate that in C2C12 myoblasts, FER1L5 may also have a role in the emergency membrane repair response given the molecular similarities of dysferlin and FER1L5, the similar properties of their vesicles and their role in membrane repair. Based on these results FER1L5 may compensate for the loss of dysferlin in muscular dystrophy. Further studies are required to demonstrate if FER1L5 is a component of the muscle membrane repair machinery. Currently the expression of FER1L5 in dysferlin deficient muscle is being examined to determine if FER1L5 expression is upregulated in the absence of dysferlin.

CHAPTER VI: C2C12 MYOTUBES ARE ACTIVE IN MEMBRANE SHEDDING

6.1 Introduction

Many signalling molecules and proteins are known to undergo extracellular release from cells and this occurs through different mechanisms including regulated vesicular exocytosis membrane shedding, transcytosis and ectocytosis (Moss and Lambert, 2002). Many cell types have been shown to display membrane shedding, transcytosis and ectocytosis, which involve the release of vesicles termed ectosomes or exosomes. Exosomes are vesicles of 50-90nm in diameter contained in multivesicular bodies (MVBs), which are intracellular organelles (200nm in size) derived from the endosomal system. Exosomes are released extracellularly by exocytosis following fusion of the MVB with the plasma membrane (Piper and Katzmann, 2007; Fevrier and Raposo, 2004; Thery *et al.,* 2002). Exosomes have been extensively studied in immune cells where they function in stimulatory responses but they are thought to have a wider physiological role in intercellular signaling and communication (Piper and Katzmann, 2007; Fevrier and Raposo, 2004; Thery *et al.,* 2002; Greco *et al.,* 2003). The shed vesicles are thought to play a role in coagulation, inflammation and tumor progression (Piper and Katzmann, 2007; Cocucci *et al.,* 2009). Besides exosomes many cells can release vesicles by direct outward budding of the plasma membrane by a process known as ectocytosis (reviewed in Pilzer *et al.,* 2005; Gasser and Schifferli, 2008; Moskovich and Fishelson, 2007). Vesicles from platelets and monocytes shed by this process have been designated ectosomes or microparticles (Pilzer *et al.,* 2005).

In chapter 5 following immunostaining of C2C12 myotubes with affinity purified FER1L5 antibody, cytoplasmic vacuolar regions largely devoid of FER1L5 staining were detected. **(see Figure 4.3 in Chapter IV)**. The size of the vacuoles detected ranged from 2-3 μm and were present as single or multiple units. From some of the vacuolar regions intracellular connections were observed linking adjacently located myotubes. These connections were stained for FER1L5. In this chapter further details are given on how these vacuolar regions are formed.

6.2 Results

6.2.1 The FER1L5 free vacuolar regions detected in C2C12 myotubes are sites of membrane shedding

C2C12 myotubes were stained with FER1L5 antibody and confocal imaging was performed. By performing extensive confocal Z-series imaging to examine FER1L5 stained myotubes I observed the shedding of FER1L5 stained ball shaped structures, which were released extracellularly from C2C12 myotubes (as shown in Figure 6.1A). The Z-series images as shown in **Figure 6.1Ai** show that the site in the C2C12 myotubes from which the ball shaped structure begins to appear vacuolar and displaying less FER1L5 staining **(Figure 6.1A, see middle row of complete Z-series)**. Punctate FER1L5 staining was observed in the shed ball shaped structure and through the shedding of the structure a connection was formed with the neighboring myotube leading to a closer alignment of the myotubes **(Figure 6.1A, Top row of Z-series; Figure 6.1Aii).** Shedding process can be viewed in **Movie 6.1.** Further confocal imaging of FER1L5 labelled C2C12 myotubes was performed and this demonstrated that the ball shaped structures containing FER1L5 were shed by outward budding of the myotube membrane **(Figure 6.1B)**. The punctate staining of FER1L5 in the shed ball shaped structures suggested that FER1L5 was present in vesicles. To determine whether FER1L5 was released extracellularly in vesicular structures differentiation media was collected at different time points during C2C12 myoblast differentiation (D0 to D11) and the media from several culture dishes (representing the same time point) was pooled and subjected to ultracentrifugation. The 'precipitated' material was tested for FER1L5 immunoreactivity by western blotting **(Figure 6.2)**. Western analysis displayed no immunoreactivity for FER1L5 in the precipitated material from supernatants collected at different stages of myoblast differentiation even at day 11 post serum withdrawal when the culture dishes were abundant in myotubes **(Figure 6.2)**. This suggested that FER1L5 vesicles were not released directly in the culture medium.

6.2.2 Concentration of cytoskeletal and membrane proteins at sites of membrane shedding in C2C12 myotubes

The confocal data described above suggested that the vacuolar regions detected in myotubes represented sites of membrane shedding from C2C12 myotubes. Since such

Figure 6.1. Formation of the vacuolar regions during C2C12 myoblast fusion by membrane shedding. A[i] *Confocal Z-series of adjacently located C2C12 myotubes immunolabeled with affinity purified FER1L5 antibody. The images show the extracellular release from a myotube of a ball shaped structure showing punctate FER1L5 staining (highlighted by arrows in Ai). The region in the myotube from which the ball shaped structure is shed is beginning to appear vacuolar (top regions of the myotube) with less FER1L5 staining (indicated by asterisk in Ai). The shed structure connects with a neighbouring myotube (bottom regions of the myotube).* ***[ii]*** *Insets of the second last and first Z-stack are presented. Scale bar, 8μm.* ***B)*** *Confocal images taken from a Z-series showing the formation of the ball shaped structure from a myotube by outward budding. Scale bar, 8μm.*

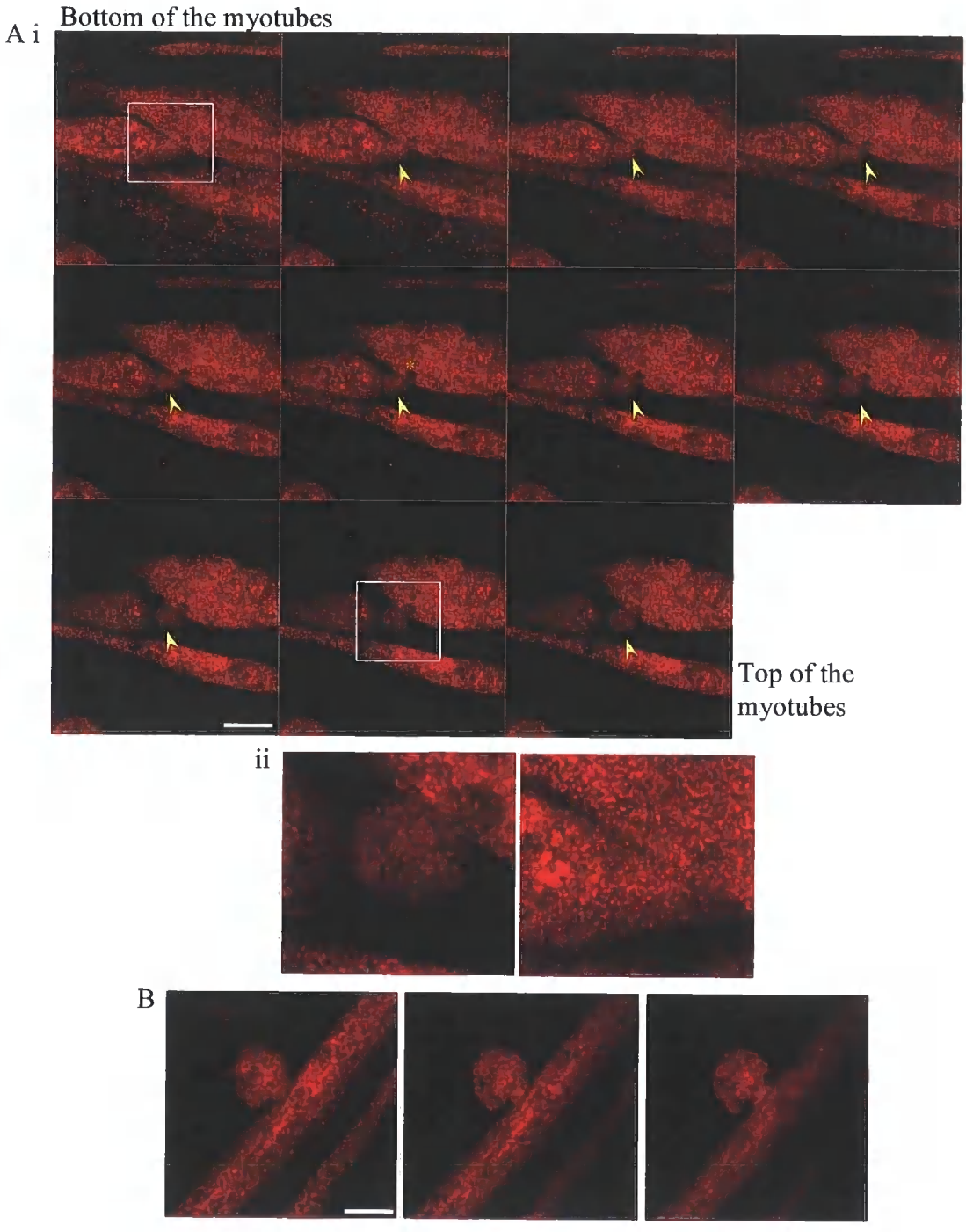
A i
Bottom of the myotubes
Top of the myotubes
ii
B

regions had not been described previously C2C12 myotubes were immunolabelled with characterized antibodies to cytoskeletal proteins (actin, ß-tubulin) and membrane associated proteins (ß-dystroglycan, caveolin-3, dysferlin and myoferlin) to determine if the vacuolar regions could be detected with these antibodies. Before labelling the myotubes the staining specificity of all of the antibodies was ascertained by immunolabeling of C2C12 myoblasts (except for dysferlin, which does not display high expression in C2C12 myoblasts) **(Figure 6.3A)**. For dysferlin the staining pattern obtained in myotubes was consistent with published data (Doherty *et al.,* 2005). Following immunolabeling of myotubes with the different antibodies confocal imaging was used to show that vacuolar regions could be detected in C2C12 myotubes as described following staining of myotubes with the FER1L5 antibody. Staining of actin (detected both by anti-actin antibody and phalloidin stain), ß-tubulin, ß-dystroglycan, dysferlin and caveolin-3 respectively was concentrated at the rim of the vacuolar regions **(Figure 6.3B).** For myoferlin a strong punctate staining was observed at regions surrounding the vacuolar regions **(Figure 6.3B)**. Like FER1L5, all of the proteins examined were largely absent from the centre of the vacuolar regions. This data confirmed that vacuolar regions are formed in C2C12 myotubes.

6.2.3 Enhanced membrane shedding from C2C12 myotubes by cholesterol depletion

Since the cytoplasmic vacuolar regions were thought to represent sites of membrane shedding in C2C12 myotubes it was hypothesized that the formation of the vacuolar regions could be enhanced by cholesterol depletion using the drug methyl-ß-cyclodextrin (MCD). Several publications have reported enhanced vesicle shedding in mammalian cells following cholesterol depletion using the drug MCD. MCD is known to stimulate the extracellular release of vesicles from immune and cancer cells (Gutwein *et al.,* 2003; von Tresckow *et al.,* 2004). C2C12 myotubes treated with MCD (2mM) for 30, 45 and 75 minutes respectively were fixed and then immunolabelled with FER1L5 antibody. Following MCD treatment FER1L5 showed less punctate and more aggregate like staining that was uniformly distributed throughout the cytoplasm of myotubes. Multiple ring shaped and irregular shaped cytoplasmic vacuolar regions were detected in the MCD treated myotubes and these regions appeared closely dispersed **(Figure 6.4i-ii).** FER1L5 stained ball shaped

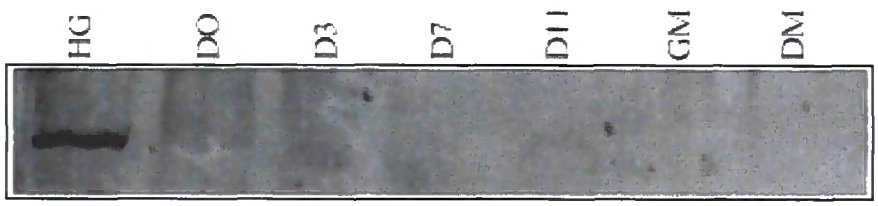

Figure 6.2. *Western blot showing no immunoreactivity for FER1L5 in the precipitates from supernatants collected at different time points during myoblast differentiation even at day 11 following serum withdrawal, when the dishes were full of myotubes. 'D' refers to time in days following serum withdrawal. As a positive control homogenate (HG) obtained from C2C12 myoblast lysate was used and showed strong FER1L5 immunoreactivity. Growth (GM) and differentiation media (DM) were used as negative controls and displayed no immunoreactivity to FER1L5.*

Figure 6.3. Detection of vacuolar regions in C2C12 myotubes. ***A)*** *Immunolabelling of myoblasts with antibodies to actin, ß-tubulin, ß-dystroglycan, myoferlin and caveolin-3 to show their specific staining pattern respectively. Rhodamine phalloidin stain was also used to label actin filaments. Scale bar, 10µm.* ***B)*** *C2C12 myotubes were stained with rhodamine phalloidin or labelled with antibodies to actin, ß-tubulin, ß-dystroglycan, dysferlin, myoferlin and caveolin-3 respectively. Confocal analysis revealed the presence of cytoplasmic vacuolar regions, which were shown not to be nuclei by imaging the DAPI staining. In the images the DAPI staining has been merged. In myotubes, filamentous actin, ß-tubulin, ß –dystroglycan, caveolin-3 and dysferlin were concentrated at the rim of the vacuolar regions and myoferlin was concentrated at the regions surrounding the vacuole. The center of the vacuolar region was free of staining for all of the proteins examined.*

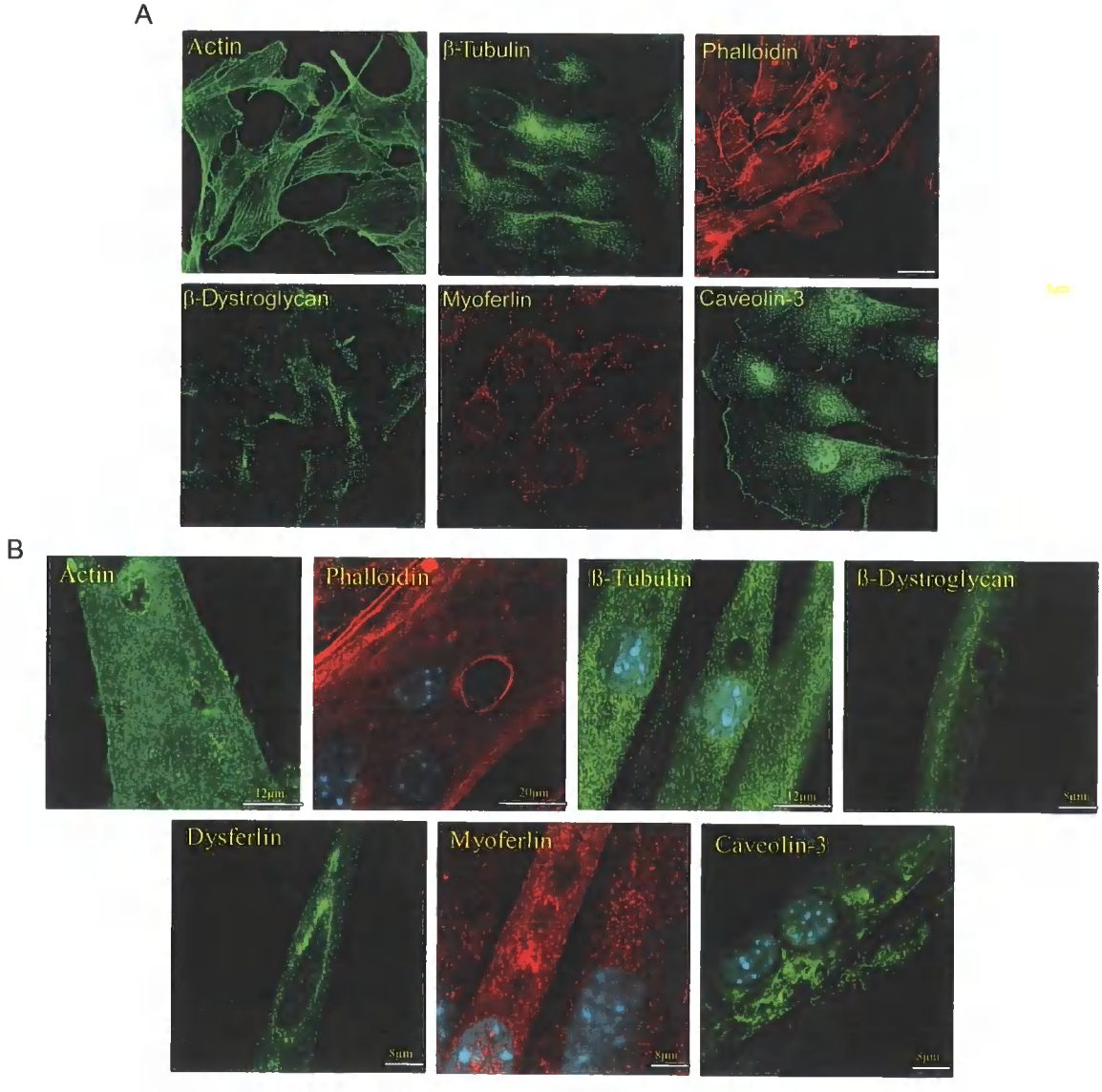
A
Actin
β-Tubulin
Phalloidin
β-Dystroglycan
Myoferlin
Caveolin-3
B
Actin
Phalloidin
ß-Tubulin
ß-Dystroglycan
Dysferlin
Myoferlin
Caveolin-3

structures were detected on the coverslips containing MCD treated C2C12 myotubes. The FER1L5 staining was less punctate in the shed structure following MCD treatment **(Figure 6.4iii)**.

6.2.4 Ball shaped structures resembling MVB are shed from C2C12 myotubes

Complimenting the above studies time lapse video microscopy of living C2C12 myotubes was performed to further investigate membrane shedding from C2C12 myotubes. Living C2C12 myotubes were incubated with 2mM MCD for varying times up to 45 minutes and cells were imaged at 5 second intervals. The captured images show many ball shaped structures being shed from C2C12 myotubes **(see Movie 6.2).** The formation of ball shaped structures by outward budding from MCD treated myotube membranes was observed **(Figure 6.5B)**. In the MCD treated myotubes multiple vacuolar regions were present **(Figure 6.5B, 6.5C).**

To examine the membrane shedding further living C2C12 myotubes were first labelled with the lipid raft stain Vybrant Alexa 488 labelled cholera toxin B subunit and then treated with MCD. Live cell imaging was performed on the MCD treated fluorescently labelled myotubes. **Figure 6.6A** shows the shedding of a ball shaped structure and the vacuolar region formed at the site in the myotube from which the ball shaped structure is shed. For visualization of the membrane shedding events stimulated by MCD treatment see **Movie 6.3.** The ball shaped structure released extracellularly appears membrane bound and containing vesicular like structures **(Figure 6.6A,** frames taken at 257s and 264s), resembling a multivesicular body (Piper and Katzmann *et al.,* 2007). Time lapse images taken at 513s and 536s show that the shed ball shaped structure are connected to the myotube from which it is shed **(Figure 6.6A).** To confirm the presence of FER1L5 vesicles in in the membrane structures that were shed from myotubes co-immunolabelling of fixed MCD treated C2C12 myotubes was performed with affinity purified FER1L5 antibody and the fluorescently labelled lipid raft stain. Following confocal imaging many areas on the coverslips showed myotubes engaged in membrane shedding as highlighted in **Figure 6.6B,** which shows FER1L5 stained vesicles in a ball shaped structure, which is in the process of being shed. This structure is also stained for the lipid raft dye. No co-labelling of FER1L5 and the lipid raft stain was observed in the outward budding

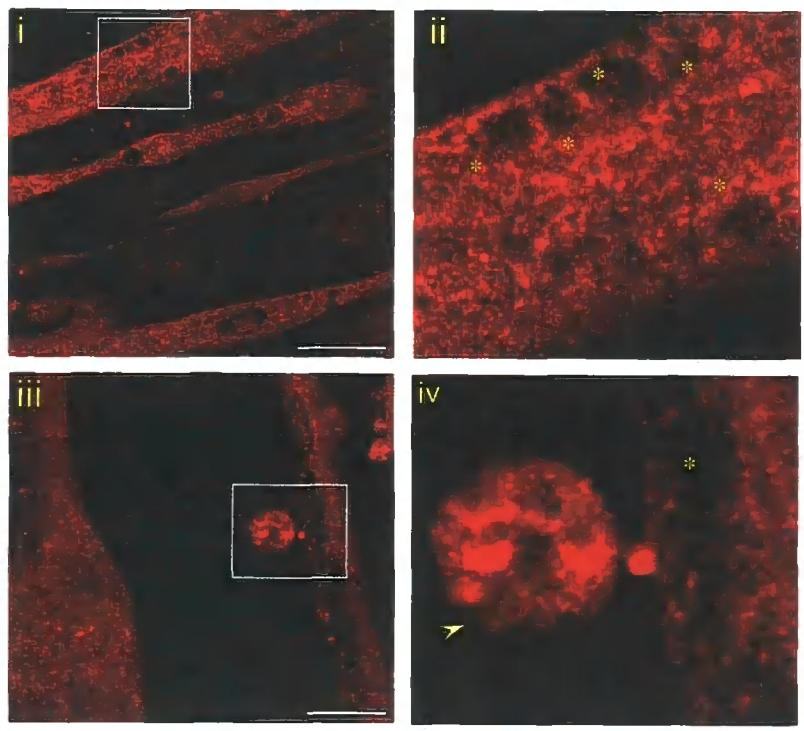

Figure 6.4. Depletion of cholesterol from myotube membranes by MCD treatment enhances the formation of the cytoplasmic vacuolar regions detected following FER1L5 staining. *Confocal images show that C2C12 myotubes incubated with MCD for 75 minutes display multiple ring shaped and irregular vacuolar regions dispersed closely and throughout the cytoplasm (highlighted by asterisk in* ***[i]*** *and* ***[ii]****). Scale bar, 20μm. The cytoplasmic staining pattern of FER1L5 is less punctate and aggregate like in appearance following MCD treatment as shown in [ii], which is an inset of [i].* ***[iii]*** *Evidence of membrane shedding from a myotube treated with MCD. Note that the ball shaped structure stains intensely for FER1L5 and is located close to the vacuolar region in the myotube, which is the site of membrane shedding (marked by asterisks in* ***[iv]****, which is an inset of [iii]. Scale bar, 12μm.*

Figure 6.5. Membrane shedding from C2C12 myotubes following MCD treatment. *Living C2C12 myotubes were incubated with 2mM MCD (Images shown in B) respectively for 45 minutes and imaged using Zeiss AxioVision microscopy. A) Images represent the untreated living C2C12 myotubes. Images were acquired every 5 seconds over a period of 60 minutes using a 20x objective. Phase contrast images were processed using AxioVision software version 4.5. B) The sequence of time lapse frames of growing myotubes treated with MCD demonstrate shedding of ball shaped structures from myotubes following MCD treatment. The data is representative of two independent experiments. Myotubes treated with MCD contain multiple vacuolar regions as seen in all the frames as dark circles. Regions highlighted in white line circles show myotube membranes undergoing membrane shedding. C) (i) Insets of these areas from frames taken at 7, 45 and 80s show membrane budding. (ii) Insets of the square areas from frames taken at 70s, 80s and 86s showing the vacuolar regions.*

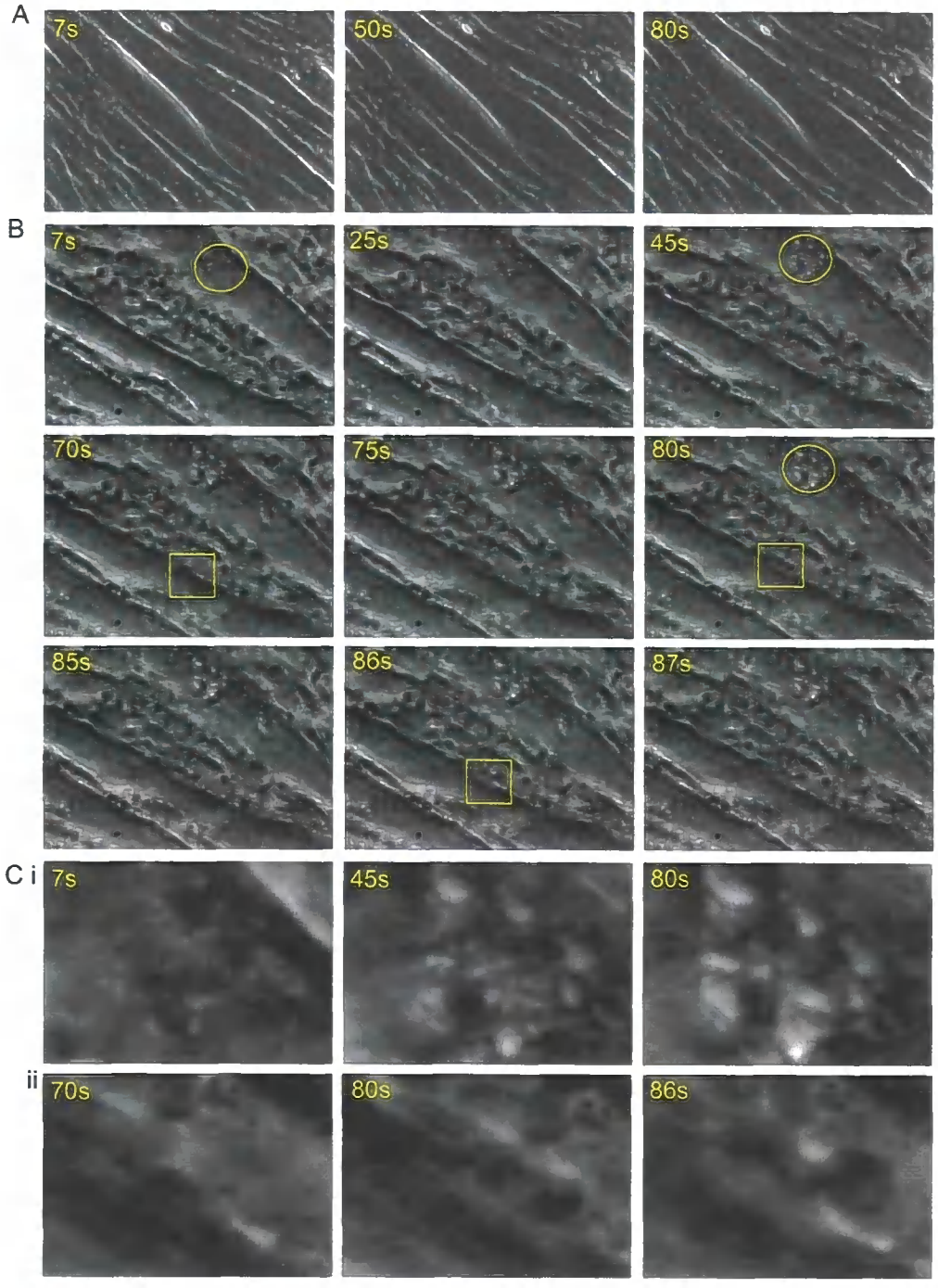
A
7s
50s
80s
B
7s
25s
45s
70s
75s
80s
85s
86s
87s
C i
7s
45s
80s
ii
70s
80s
86s

Figure 6.6. MVB like structures are shed from C2C12 myotubes following cholesterol depletion. ***A)*** *Living C2C12 myotubes stained with Alexa 488 tagged cholera toxin to label the lipid raft microdomains were incubated with 2mM MCD and imaged as described in the foregoing section. The sequence of time lapse frames demonstrate the expulsion of a ball shaped structure following MCD treatment. Note* ***1)*** *the presence of green fluorescence corresponding to the lipid raft stain in the shed ball shaped structure indicating that lipid raft microdomains may be involved in the membrane shedding* ***2)*** *the vacuole formed in the myotube membrane from which the ball shaped structure is released (indicated by arrow in frames taken at 160s and 187s). The expelled ball shaped structure appears to be membrane bound containing vesicles as depicted in frames taken at 257s and 264s, resembling a MVB.* ***B)*** *Co-immunolabeling of fixed MCD treated C2C12 myotubes with Alexa 488 tagged cholera toxin subunit and FER1L5 affinity purified antibody. Z-series stacks showing a membrane budding intermediate in the process of being released from C2C12 myotube. The structure is stained with the lipid 'raft' stain and also shows FER1L5 staining in vesicular structures. Scale bar, 12μm.* ***C)*** *MCD treated C2C12 myotubes fixed on coverslips were independently immunolabeled using antibodies to the muscle membrane proteins ß-dystroglycan and caveolin-3 and imaged by confocal microscopy. Both proteins are present at the surface and in the lumen of the ball shaped structures budding from the myotube membrane.* ***[ii]*** *and* ***[iii]*** *are insets of* ***[i].*** *Scale bar, 12μm.*

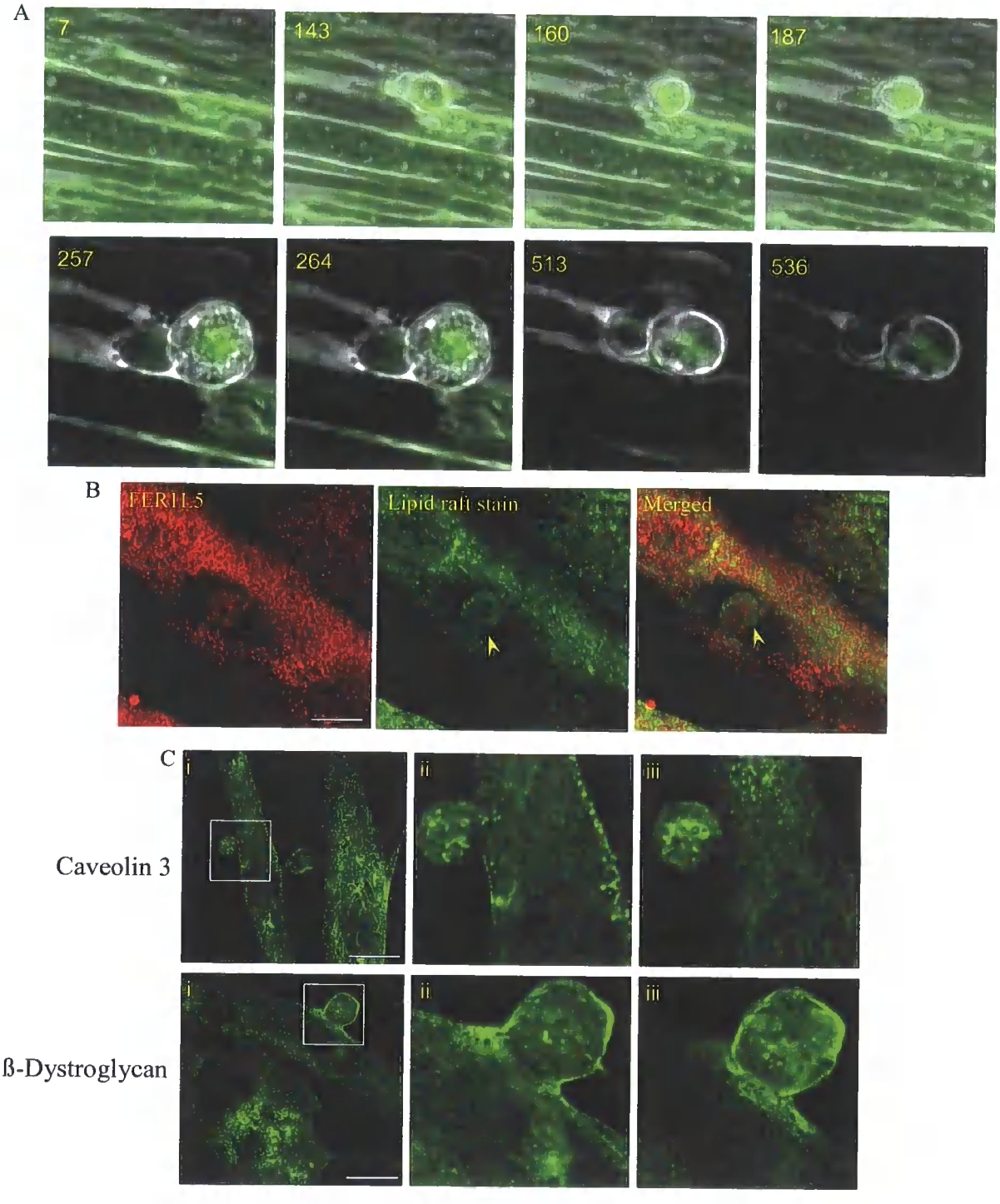
A
7
143
160
187
257
264
513
536
B
FER1L5
Lipid raft stain
Merged
C
Caveolin 3
ß-Dystroglycan
i
ii
iii

structure. Fixed MCD treated myotubes were also stained for caveolin 3 and ß-dystroglycan to show that the ball shaped structures shedding from C2C12 myotubes were membrane bound **(Figure 6.6C).** Caveolin-3 staining was detected at the surface as well as in the lumen of the outward budding ball shaped structure preparing for expulsion **(Figure 6.6Cii and iii).** ß-dystroglycan staining was detected predominantly at the surface of the budding structures **(Figure 6.6Cii and iii).** Taken together the data provided evidence that ball shaped structures are shed from C2C12 myotube membranes and that the shed structure resembles MVB and contain FER1L5 possibly in vesicular structures. Fixed MCD treated myotubes were also immunolabelled with dysferlin and myoferlin antibodies to determine if these proteins were also present in shed ball shaped structures. **Figure 6.7A** shows images taken following confocal imaging of fixed MCD treated C2C12 myotubes stained for dysferlin and myoferlin respectively. Both dysferlin and myoferlin were shown to be present in the ball shaped structures, which were either at the budding stage or released extracellularly. Punctate staining was detected for both dysferlin and myoferlin indicating that these proteins were most likely present in vesicles. **Figure 6.7B** describes further images showing budding structures formed in C2C12 myotube, which stain for dysferlin and myoferlin respectively.

Membrane shedding from C2C12 myotubes was confirmed by ultrastructural studies, which were performed by Daniella Emokpare, a student in the laboratory under my supervision. Control and MCD treated myotubes were analyzed by Scanning Electron Microscope (SEM) and Transmission Electron Microscope (TEM) and some of the images are shown in **Figure 6.8**. The images show ball shaped structures formed on the surface of control and MCD treated myotubes. The images also highlight different stages of the membrane shedding, some structures are being expelled from myotubes whilst other stuctures are still attached to the myotube as budding intermediates **(Figure 6.8A).** Additionally, the images also highlight the differences of the membrane surface of MCD treated and control myotubes. In untreated myotubes many finger like membrane extensions are visible projecting outwardly from the myotube surface **(Figure 6.8A)**. EM images of control myotubes show ball shaped structures ready for extracellular release but attached to the myotube membrane via filamentous membrane like connections **(Figure 6.8A)**. Following cholesterol

Figure 6.7. Dysferlin and myoferlin are also present in the ball shaped structures shed from C2C12 myotubes. *MCD treated fixed C2C12 myotubes were independently labelled for dysferlin and myoferlin and imaged by confocal analysis. Both dysferlin and myoferlin are present in ball shaped structures being released from C2C12 myotube. The staining is in vesicular structures. The images show shed structures and budding intermediates, which are stained for dysferlin and myoferlin* ***(A and B).*** *In (A) images* ***[ii]*** *and* ***[iii]*** *are insets of* ***[i]****. Scale bar, 20μm for (A) and 12μm for (B).*

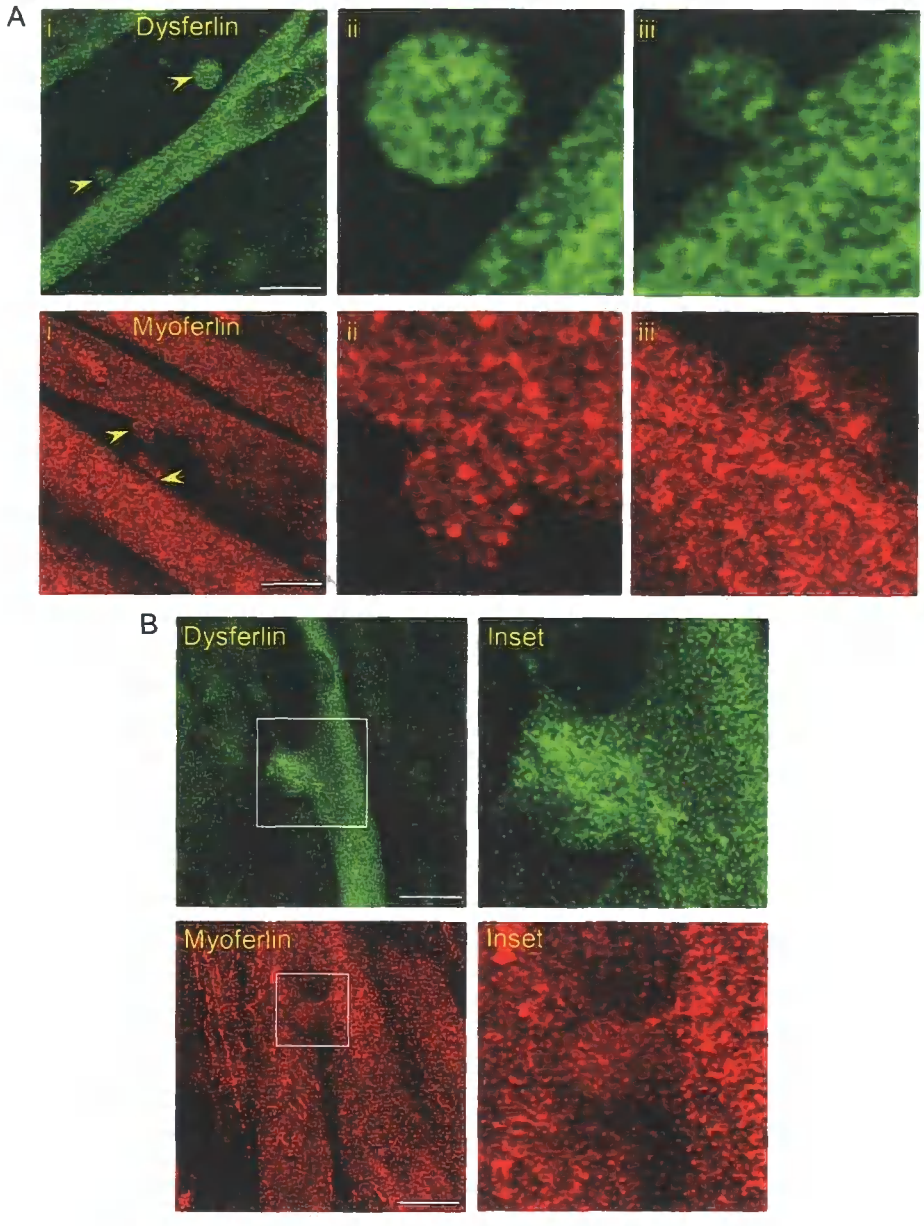
A
i
Dysferlin
ii
iii
i
Myoferlin
ii
iii
B
Dysferlin
Inset
Myoferlin
Inset

Figure 6.8. Ultrastructural analysis of C2C12 myotubes. *A) SEM analysis was performed on control and MCD (2mM) treated C2C12 myotubes. The MCD treated myotube surface shows many ball shaped structures undergoing membrane shedding compared to untreated myotubes. Images showing the different stages of the shedding process are presented. Note the finger like protrusions present on the surface of the control myotubes but in the MCD treated myotubes these protrusions are absent and the myotube surface appears smoother. The ball shaped structures are shed by outward budding.* ***B)*** *TEM analysis of control and MCD treated.*

A

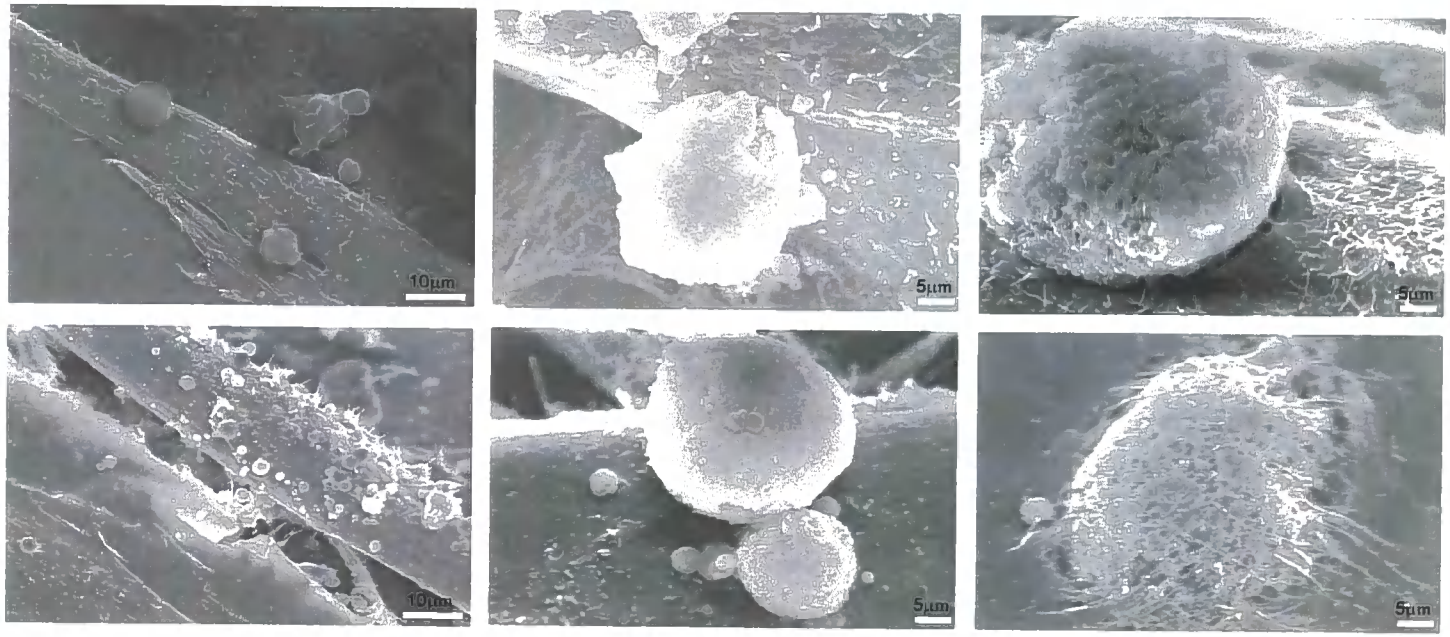
Control
MCD treated
10μm
5μm
5μm
10μm
5μm
5μm

B

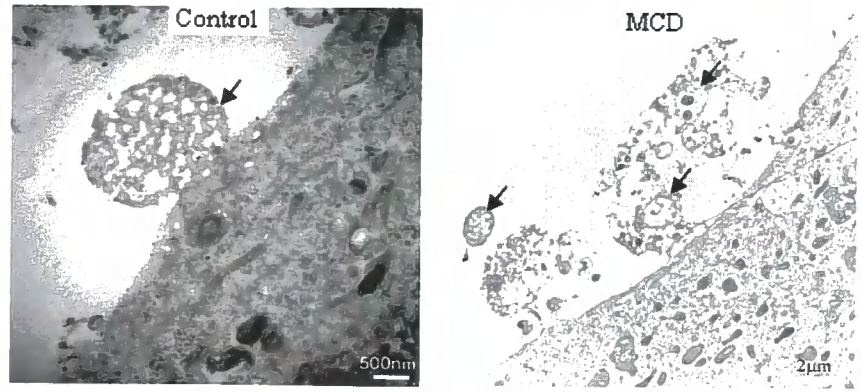
Control
MCD
500nm
2μm

depletion, the surface of the myotube appears modified. The surface of MCD treated myotubes is smoother compared to untreated myotubes. Interestingly, secondary budding structures formed from primary buds were detected in MCD treated myotubes. Following MCD exposure no finger like projections were detected on myotubes, which had a smooth surface appearance **(Figure 6.8A)**. TEM analysis of MCD treated myotubes revealed that the ball shaped structures contain small vesicles (indicated by arrows) **(Figure 6.8B).** The size of these structures range from 500nm to 2 microns and the structures appear to contain small vesicles (**Figure 6.8B**). The size of these structures and the vesicles present in these structures are similar to those that reported for MVBs containing small vesicles, exosomes in other systems. MVBs of 150-200nm to 2μm and the consequent release of 40–90nm vesicles (exosomes), have been described for various cell types, including reticulocytes (Johnstone *et al.,* 1987; Vidal and Stahl, 1993; Rieu *et al.,* 2000), B- and T-lymphocytes (Raposo *et al.,* 1996; Escola *et al.,* 1998; Peters *et al.,* 1989), dendritic cells (Zitvogel *et al.,* 1998; Kleijmeer *et al.,* 1998), mast cells (Raposo *et al.,* 1997), platelets (Heijnen *et al.,* 1999), macrophages and alveolar lung cells (Denzer *et al.,* 2000). Exosome-Like Vesicles found in epididymal Fluid and the seminal plasma are between 25- and 75-nm diameter (Gatti *et al.,* 2005).

In Yeast, (*Saccharomyces cerevisiae*) ~200-nm diameter of MVBs were shown to contain ~25nm diameter intraluminal vesicles (Hurley, 2008). Giant multivesicular bodies (MVBs) with diameters up to 4.5μm were shown in the rat hippocampal pyramidal cells after chronic alcohol consumption compared to normal cells (0.2 – 0.5 μm) and 2μm diameter in vaginal epithelium and rat satellate cells (Paula-Barbosa *et al.,* 1986). Recent studies have well documented the structure and size of MVBs in nerve rootlet and axons and the structure was shown to be relatively spherical or oval, but not tubular (Amy, *et al.,* 2009). They are briefly categorized into five different types; Type 1, 50–200-nm diameter, single limiting membrane, small (~30-nm diameter) internal vesicles; type 2, 70–200 nm diameter, single limiting membrane enclosing small internal vesicles, central empty space; type 3, classic MVB, generally >250 nm in diameter, single limiting membrane, multiple internal vesicles (~50–80 nm diameter); type 4,: similar to type 3, but noticeably more electron dense; and type 5, generally >250-nm diameter, outer limiting membrane less distinct, very electron dense, internal vesicles less distinct (Amy, *et al.*, 2009). Amy, *et al.,* (2009) also

reported that the quantity of the types 1 and 2 MVB-like organelles increased by 2-fold, whereas type 5 MVBs increased by 7-fold in dystrophic conditions.

In muscle cells, the mechanism of exocytosis is well established for glucose transporter protein GLUT4 (Costin *et al.,* 2009). GLUT4 is a member of the SLC2 (solute carrier 2) transporter family of facilitated hexose transporters and is selectively expressed in muscle and fat cells (He *et al.,* 2000). Extensive study for nearly 30 years of the traffic of GLUT4 in these two cell types has revealed that the transporter is a constitutively recycling membrane protein, and defects in its cycling are associated with insulin resistance (Thong *et al.,* 2005; Zaid *et al.,* 2008). Such cycling consists of exocytic movement of the transporter within postbiosynthetic vesicles of endosomal origin towards the plasma membrane, and of endocytic movement from the membrane back to the sorting endosomal system. Glucose uptake into skeletal muscle fibres occurs primarily through the glucose transporter GLUT4 in response to insulin stimulation (Zisman *et al.,* 2000). In muscle cells, glucose is readily used to produce energy and is also stored as glycogen, a secondary short term energy source. Investigations of many signaling molecules have implicated a range of different signaling pathways involved in regulating GLUT4 translocation to PM in response to insulin and non-insulin factors (Costin *et al.,* 2009; He *et al.,* 2000). Different types of cells perform similar signaling steps in response to changes in the environment. GLUT4 is enriched in the storage vesicles that continuously recycling from the cell membrane to an inactive location of the cytosol. GLUT4 is a protein that facilitates the movement of glucose into the cell (Costin *et al.,* 2009; He *et al.,* 2000). GLUT4 storage vesicles (GSVs) are held in a recycling state near the cell membrane. The vesicles are most held in this region because Rab proteins (small GTP binding proteins) that interact with the motor proteins necessary to move the vesicles to the membrane are in inactive state (He *et al.,* 2000). Evidence is emerging that supports the hypothesis that both the actin and microtubule-based cytoskeleton play a key role in the translocation of GLUT4 to the plasma membrane in response to insulin (Costin *et al.,* 2009). Furthermore cytoskeletal reorganization may connect the GLUT4 translocation with regulating molecules of distal insulin signaling pathway. The final step in this signaling pathway involves the phosphorylation of protein that prevents the Rab from interacting with the vesicles. When the Rab proteins are no longer inhibited the storage vesicles can freely merge with the cell membrane. Once the

vesicles have merged many GLUT4 proteins are embedded in the membrane and large quantities of glucose released into the cell by exocytosis (He *et al.*, 2000; Costin *et al.*, 2009).

Movie 6.1: *Wild type C2C12 myotubes fixed on coverslips and stained with FER1L5 antibody (affinity purified) shows the formation of cytoplasmic vacuolar structures through the expulsion of ball shaped structures containing FER1L5 from the myotube.*

Movie 6.2: *Living C2C12 myotubes were incubated with and without 2mM MCD and imaged using Zeiss AxioVision microscopy. Images were acquired at 5 second intervals over a period of 60 minutes using a 20x objective and demonstrate the expulsion of ball shaped structures from myotubes following cholesterol depletion.*

Movie 6.3: *Living C2C12 myotubes stained with Alexa 488 tagged cholera toxin were incubated with 2mM MCD and imaged as described for control myotubes and revealed the expulsion of a ball shaped structure resembling a MVB following cholesterol depletion by MCD treatment.*

6.3 Discussion

In this chapter evidence is provided that differentiating C2C12 myoblast are active in membrane shedding. Using confocal analysis I demonstrated that the vacuolar regions detected in FER1L5 stained myotubes represent sites of membrane shedding. The vacuolar regions were detected following staining with different antibodies to membrane and cytoskeletal proteins and therefore they were not an artifact. By performing Z-series imaging of FER1L5 stained C2C12 myotubes ball shaped structures were shown to be released extracellularly and showing punctate stain for FER1L5 suggesting that these structures contain FER1L5 vesicles. Further studies demonstrated that dysferlin and myoferlin was also present in the shed structures and also in vesicular structures.

The formation of the vacuolar regions in myotubes could be enhanced following cholesterol depletion and by actinomycin D induced genomic stress. Following cholesterol depletion multiple vacuolar regions could be detected, irregular shaped and closely dispersed. The shedding of the ball shaped structure was shown to occur by outward budding of the myotube membrane. Live cell imaging was performed to confirm these findings and to obtain further information on the shed structures. Living myotubes stained with a lipid raft stain were imaged following cholesterol depletion and this demonstrated that the shed structure appeared to be membrane bound containing vesicular structures and also staining for the lipid raft stain. The data indicated that the structures resemble MVB like structures and that their formation may require membrane regions, which are rich in lipid rafts. To confirm that the shed structures were membrane bound MCD treated myotubes were stained for the proteins ß-dystroglycan and caveolin 3 and staining was detected at the periphery of the shed structure. Ultrastructural studies were also performed on control and MCD treated myotubes to examine membrane shedding from C2C12 myotubes. These experiments confirmed that ball shaped structures are released extracellularly by outward budding and that the structures contain vesicles. Evidence was also obtained that outward budding intermediates ready for expulsion appear to be attached to the myotube via membrane like protrusions. In MCD treated myotubes secondary buds emerging from the shed structure were observed. Membrane budding has recently been reported in C2C12 myotubes overexpressing the protein MG53, a muscle specific TRIM protein mediating in muscle membrane repair (Cai *et al.*, 2009[c]). MG53 was shown to be

involved in membrane budding and exocytosis through an interaction with caveolin 3 (Cai *et al.*, 2009[b]). Apart from these studies there are very few reports of membrane shedding in C2C12 myotubes. In one study, a lectin has been reported to be released extracellularly from C2C12 myotubes (Harrison and Wilson, 1992), in ball shaped structures resembling those that have been described in this chapter. Moreover the study of Harrison and Wilson (1992) showed that the lectin could not be released by trypsinization and could not be eluted by lactose from the surface of myotubes indicating that the lectin is held within stable structures. This lectin has been identified as galectin 1 (Gal-1) (Barondes *et al.*, 1994). Galectin-1 is a 14 kDa carbohydrate binding protein family protein with an affinity for ß-galactosides (Harrison and Wilson, 1992; Camby *et al.*, 2006). Gal-1 is differentially expressed by various normal and pathological tissues (Camby *et al.*, 2006). Galectin-1 has been implicated in multiples functions including signaling, growth regulation, immune response and cell homeostasis etc (Camby *et al.*, 2006; Gabriel *et al.*, 2002). Galectin-1 has intracellular and extracellular muscle functions (Camby *et al.*, 2006). Galectin-1 is secreted extracellularly in muscle tissue but the mechanisms are not known (Camby *et al.*, 2006). The extracellular secretion of Gal-1 is thought to occur by an unconventional secretory pathway similar to that proposed for FGF2 and IL1ß (Nickel, 2007) since these proteins do not contain leader sequences and by pass the secretory pathway. Galectin-1 knock out mice shows defects in muscle regeneration (Cerri *et al.*, 2008) and galectin-1 has been shown to be secreted at high levels into the extracellular space from dystrophin deficient and exercised muscle (Cerri *et al.*, 2008). Furthermore, these studies showed that there was significant increase in extracellular Gal-1 levels (240% in relation to control) after $BaCl_2$ induced muscle injury in wild-type C57BL/6 mice suggested that a potential role for Gal-1 in muscle homeostasis and repair (Cerri *et al.*, 2008). This increased extracellular expression of Gal-1 following muscle injury was thought to regulate immune responses required for muscle healing. Consistent with this possibility Cerri *et al.*, (2008) have shown increased Gal-1 levels, which appear to localize both inside and outside the sarcolemma where significant extracellular Gal-1 was shown to colocalize with infiltrating $CD45^+$ leukocytes as highlighted by a previous study by Baum *et al* (1995), where Gal-1 expression was thought to increase following inflammatory stimuli induced by TNFa. In the study by Cerri *et al* (2008) Gal-1 was considered to be important for leukocyte homeostasis and turnover. Gal-1 has been shown to induce

phosphatidylserine exposure, a membrane phospholipid responsible for signaling the phagocytic removal of neutrophils during inflammatory resolution (Dias-Baruffi *et al.*, 2003; Karmakar *et al.*, 2005; Stowell *et al.*, 2007). It is not known yet the link between Gal-1 and neutrophil activation during muscle repair and regeneration but it is possible to suggest that the continued degeneration may result in sustained levels of proinflammatory cytokines that retain elevated Gal-1 levels or regenerating tissue may signal tissue to resume normal Gal-1 expression. I have performed some preliminary experiments which show that galectin-1 is present in the ball shaped structures that are released extracellularly from C2C12 myotubes (data not shown). Since Gal-1 is found in the extracellular space in dystrophic and exercised muscle, the ball shaped structures detected in myotubes may also be responsible for the extracellular secretion of galectin-1 from muscle fibres. Since the ferlin proteins are involved in membrane remodelling they may be involved in the extracellular transport of galectin-1.

GENERAL DISCUSSION

7.1. Implications of current work

Skeletal muscle cells are highly organized multinucleated cells, which are composed of the contractile apparatus, the sarcomere, surrounded by specialized membrane structures, which include the muscle cell membrane, the sarcolemma, which connects to T-tubule membranes and a specialized endoplasmic reticulum, the sarcoplasmic reticulum (Towler *et al.*, 2004; Rossi *et al.*, 2008). These specialized membrane structures undergo extensive remodeling to function in many physiological process, including Ca^{2+} signaling and membrane trafficking such as GLUT4 trafficking, muscle membrane repair and the merging of apposed membranes during muscle development and regeneration (Towler *et al.*, 2004; Antonescu *et al.*, 2009 Dowling *et al.*, 2008). Disruption of muscle cell membrane remodeling leads to defective membrane repair and impairs muscle regeneration and is observed in several muscle pathologies (Doherty *et al.*, 2005; Han and Campbell, 2007; Glover and Brown, 2007). The proteins involved in the remodeling of muscle membranes are beginning to be identified and include dysferlin and myoferlin, which belong to the ferlin protein family (Bansal *et al.*, 2003; Doherty *et al.*, 2003; Doherty *et al.*, 2005; Doherty *et al.*, 2008; Han and Campbell, 2007; Glover and Brown, 2007). Dysferlin has been shown to be linked with many types of muscular dystrophies and cardiomyopathy, which are characterized by defective muscle membrane repair (Bansal *et al.*, 2003: Han *et al.*, 2007). Myoferlin has a role in myogenesis and is required for the development of mature muscle fibres. Myoferlin null mice are impaired in the formation of mature myofibers. Myoferlin has been implicated in the merging of membranes at muscle cell fusion sites and also in membrane recycling (Doherty *et al.*, 2005; Bernatchez *et al.*, 2007).

In this thesis I have shown that FER1L5, a novel ferlin most similar to dysferlin and myoferlin, has a role in muscle membrane fusion. My findings are summarized below.

7.1.1 FER1L5 is found in distinct vesicles in C2C12 cells

This was shown by biochemical fractionation and immunolabelling. Although present in distinct vesicles, FER1L5 vesicles are similar to dysferlin and myoferlin vesicles. The identity of the FER1L5 vesicles is not known but FER1L5 is not localized to conventional organelles nor other vesicles involved in muscle membrane fusion. No

colocalization of FER1L5 with the T-tubule marker Bin 1 was observed in C2C12 cells. Dysferlin is proposed to be present in vesicles, which are derived from T-tubules (Klinge *et al.*, 2007). The distribution of FER1L5 in adult human muscle is being examined and the preliminary data indicate that FER1L5 and myoferlin are localized to the sarcoplasmic reticulum. This underlined data suggests that the origin of the vesicles involved in muscle membrane fusion vesicles are derived from the specialized membranes.

7.1.2 FER1L5 is required for C2C12 myoblast fusion

Following inhibition of FER1L5 the formation of large myotubes is impaired. I also observed strong FER1L5 staining at membrane fusion sites of myoblasts. My data suggest that FER1L5 has a role in membrane merging of apposed myoblast-myoblast membranes. FER1L5 is predicted to operate upstream from dysferlin and myoferlin in membrane merging. A model depicting the proposed role of FER1L5 in myoblast fusion is shown in **Figure 7.1.**

7.1.3 FER1L5 mediates in muscle membrane repair

This is the first dysferlin related protein that has been implicated in membrane repair. It was not possible during my study to examine the trafficking of FER1L5 following membrane injury. It is not known whether FER1L5 concentrates at membrane wound site as shown for dysferlin. At present we don't know whether FER1L5 operates in the dysferlin repair pathway. The distribution and expression of FER1L5 in dysferlin deficient muscle is currently being examined. C2C12 cell lines deficient for dysferlin are being characterized in the laboratory. In future studies stable cell lines expressing FER1L5 shRNA plasmids will be generated and through these studies the precise role of FER1L5 in membrane repair and its relationship with dysferlin will be examined. Through these studies we will be able to determine whether FER1L5 is a therapeutic target for the dysferlinopathies.

7.1.4 Evidence of membrane shedding in differentiating C2C12 cells

Another interesting finding from my study is that muscle cells are active in membrane shedding. I have provided evidence that C2C12 myotubes release MVB like structures extracellularly and that these structures contain dysferlin, myoferlin and FER1L5

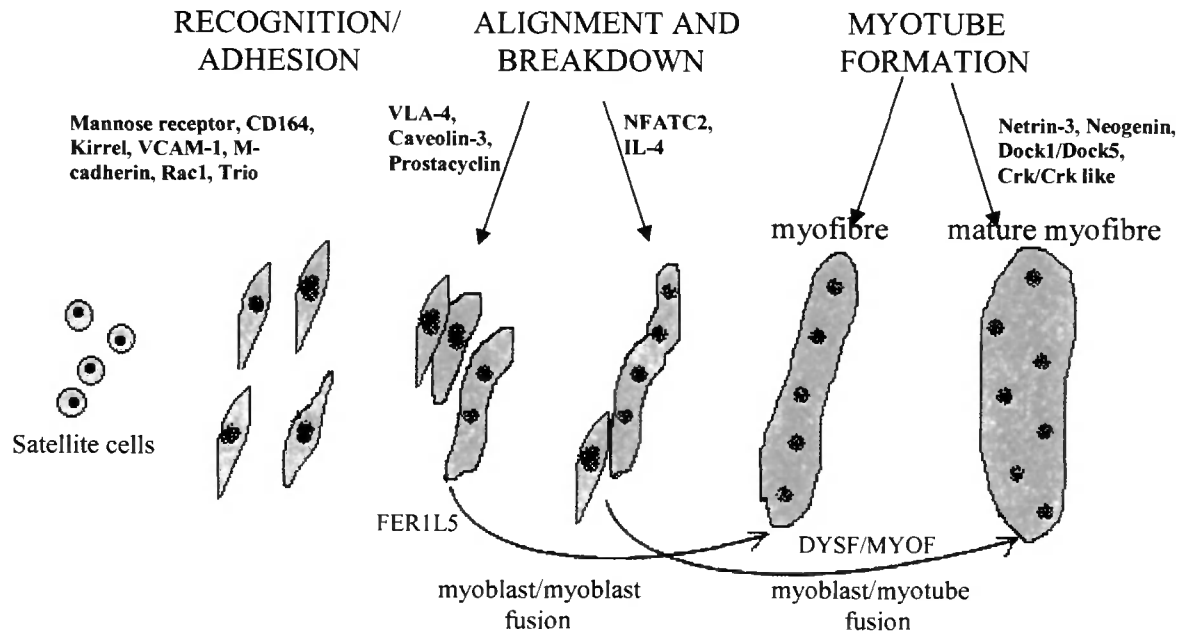

Figure 7.1. The basic events in mammalian myoblast fusion. *Muscle is formed of bundles of myofibres. Myofibres are formed by fusion of myoblasts to form multinucleated myotube. These increase in size by additional myoblast fusion. There are two phases, first phase is formation of myofibres by myoblast/myoblast fusion and the second phase is the maturation of myofibres, which occurs by myoblast/myotube fusion. Both phases are essential for muscle regeneration and repair. The proteins, which are involved in the different stages during muscle development, are shown in bold letters (Richardson et al., 2008). The data obtained for FER1L5 during C2C12 fusion suggests that this ferlin is involved in the first phase of myotube formation. Since dysferlin and myoferlin concentrate at sites of myoblast/myotube membrane fusion these ferlins are predicted to function in the second phase of myotube development.*

vesicles. Ultrastructural studies have confirmed that MVB like structures are released extracellularly and further structural information has been obtained. My work suggests that these structures may be involved in the secretion of cytokines. I am proposing that these structures are required for the extracellular secretion of cytokines that bypass the secretory pathway, for example Gal 1 and IL1ß. These cytokines were shown to be present in the MVB like structures by immunolabelling. There is evidence that extracellular secretion of the cytokines from muscle is important for muscle regeneration and repair (De Rossi *et al.*, 2000; Hirata *et al.*, 2003; Pelosi *et al.*, 2007; Chiu *et al.*, 2009). Currently, this is an exciting area of research. The group led by Gillian Butler-Brown have shown that differentiating human myoblasts are active in extracellular protein secretion (Institute of Myology Newsletter, July 2009, "Are secreted microvesicles a novel mechanism of communication for skeletal muscle?", Columbia University, New York). Proteomics analysis of conditioned media identified 965 non-redundant proteins, which were secreted. 27% of these were proteins, were secreted extracellularly via the ER/Golgi secretion pathway, 85 of which were extracellular matrix components. Several other proteins that bypass the secretory pathway were also identified, including Gal-1. The work suggests that proteins secreted through microvesicles are required for communication in skeletal muscle. This work supports my data and opens up an exciting new area of further research which will be discussed below.

7.2 Future research on FER1L5

In vitro studies

1) Generating stable cell lines deficient for FER1L5 to mediate the mechanism by which FER1L5 operates in myoblast fusion and membrane repair.
2) Investigating the nuclear distribution of ferlins during myoblast fusion.
    - Do they colocalize with myogenin?
    - Is myogenic signaling disrupted in the absence of these ferlins?
3) Examining FER1L5 expression in dysferlin deficient C2C12 muscle cells.
4) Characterization of the FER1L5 promoter.
5) Identification of interacting proteins.

In vivo studies

1) Generation of a FER1L5 knock out mice to determine whether the mice develop a muscle phenotype and whether it is linked with muscular dystrophy or myogenesis or another phenotype.
2) Generation of transgenic mice overexpressing FER1L5. This model will allow us to study whether FER1L5 is a therapeutic target in muscular dystrophy.

7.3 Future research on extracellular secretion of galectin-1 and IL1ß from muscle cells

1) Determine if muscle fibres release MVB like structures.
2) Examine the expression and distribution of Gal 1 and IL1ß
   - During myoblast fusion
   - During muscle membrane repair.
   - In regenerating muscle eg SJL/J and myoferlin null mice.
   - In dystrophic muscle and in muscle subjected to eccentric exercise.

APPENDIX

A. The amino acid sequence of the FER1L5 long isoform (AY461813.1:1-6297). Amino acid sequences highlighted in bold were used for generate the FER1L5 polyclonal antibody.

mlrlvvqsak idpp**laplpr pcmsidfrdi** kkrtrvvegn dpvwnetliw hlwnrplend
sflqvtlqdm gsqkkerfig latvllkpll kqpsevlfvk dltllnhsmk ptdctvtlqv
ahmsnqdiek tgaedhlgit areaasqklm vpgstahral sskpqhfqvr vkvfearqlm
gnnikpvvkv siagqqhqtr ikmgnnpffn evgiffqnfh evpakffdet iliqtdigfi
yhspghtllr kwlglcqpnn pgsgvtgylk vtiyalgvgd qalvdqklly gtddtdiqif
ksavvpinma ylqlfiycae dlhlefiekh qsvnpqleve ligeklrthm qtqtdnpiwn
qiltfriqlp clssyikfrv ldcrkkdcpd eigtaslsln qisstgeeie evysgflpcf
gpsfltlhgg kkapfriqee gacipdsvrd glayrgrvfl elitqiksyq dstikdlshe
vtriekhqnr qkyglcvifl sctmmpnfke lihfevsigh ygnkmdlnyk plvsstpysp
viydgniyhy vpwyntkpvv avtsnwedvs frmnclnllh itrdrlkanl dtlkstrnpk
dpallyqwek llrelaedck rplpcmtyqp katsldrkrw qlrslllqel aqkakqakpk
dmvataedwl yrlntvlpep qmglpdvmiw lvakeqrvay aqvpahsvlf spagalhsgr
lcgkiqypeg egqkdvlpah lrvcmwlgnv tdskdlqllr qgdtavyaem vsyenqakyr
dqwgqqglyh cpnfsdvmgn ktlpmtdfqp plgwhwqdsw tvepqrrlll didinksqvl
eevyenqgrd trgawgpaai pntdvngqpm earenvkcpq gwhfkkdwvv elnhavdskg
weygvgipps glpqvwspve ktyhscrrrr warvrfrnhg elshelsheq etlsflqlgl
akgeeegwey dtfgskfhln pqpqsrfrrr cwrrrlapnk dkgiapifll egslamdlky
hagkeqqtwp wgldrqsgnp qrqdtrppnl pfiyctfnkp hyyqlfcyiy qarnlvsnqi
ltfqgpfirv vflnhsqctq tlrssagptw aqtlifqhll lyenpqdtke spplvvlelw
qrdfwgkesl wgrsvwppmv wldlqdrilp pmrwhplvke lgkeegeila scelilqtek
lgekqlpils vpwkngaytl pksiqptikr maievlamwd gdgggqdrrgw sgvrcslllv
lpdywiqssh pekdylgggg rqerneevlv ilawglrnmk kssspqllve fgeeslrtep
irdfqtnpnf prsesvlvlt vlmpteeaya lplvvkvvdn wafgqqtvtg qanidflqpy
fcdpwaqdym hpklptlsek khqdflgyly rkfwfksska edeyehevdw wsklfwatde
hkslkykykd yhtlkvyece leavpsfqgl qdfcqtfkly qeqpkldspv vgefkglfri
ypfpenpeap kpplqflvwp eredfpqpcl vrvymvrain lqpqdynglc dpyvilklgk
telgnrdmyq pntldpifgm feltcniple kdleiqlydf dlfspddkig ttvidlenrl
lsgfgahcgl sksycqsgpf rwrdqmppsy lleryakrkg lppplfspee davfyngkkf
klqsfepktp tvhglgpkke rlalyllhtq glvpehvetr tlyshsqpgi dqgkvqmwvd
ifpkklgppg pqvninprkp kryelrciiw ktanvdlvdd nlsrektsdi yikgwlygle
kdmqktdlhy hsltgeadfn wrfiftmdyl aaertcvqsq kdyiwsldat smkfparlii
qvwdndifsp ddflgvlelg lsdmplparh akqcsirmmd adpkwpyfiq ykhfslfkkk
tvtgwwpcqv ldggkwrlsg kvkmsleils ekealikpag rgqsepnqyp tlhpplrtnt
sftwlrspvq nfcyifwkry rfkliafmvi siialmlfnf iysapdylam swikpqlqly
ppikifniin lntsnasssi lptqdpnlkp tidhewklhp gptnhlsdif pelpapgd

B. The following primers were designed from the 3' UTR region of the mouse ferlin genes. G3pdh (glyco aldehyde 3 phosphate dehydrogenase) gene is a house keeping gene used to normalise the RT-PCR analysis.

1	G3PDH_FOR	5' – AAG GTC ATC CCA GAG CTG AAC GG – 3'
	_REV	5' – ACA ACC TGG TCC TCA GTG TAG CC – 3'
2	DYSFERLIN_FOR	5' – CTG GAG AAG GGG GTG CAG – 3'
	_REV	5' – TGA AAA TAA CGT GAT TCC CAA G – 3'
3	MYOFERLIN_FOR	5' – CAA AGC CAT GGA CCC TCT TA – 3'
	_REV	5' – GTC AAG CTT GGG GTT CAT GT– 3'
4	OTOFERLIN_FOR	5' – TCT GGT TCC TGA ACC CAC TC – 3'
	_REV	5' – AGG CAA AAT ACG CAG CAG – 3'
5	FER1L5_FOR	5' – AAC AGG CTG CTG TCC AAG TT – 3'
	_REV	5' – GCC TTG TTG CTG AG GAC AT – 3'

C.

(i) siRNA transfection in C2C12 cells using Silencer® GAPDH siRNA and Ambion Silencer® Negative Control siRNA. For GAPDH efficient reduction of GAPDH protein levels was obtained at 24 hours, 48 hours and 72 hours after transfection, 1=wild type (no transfection), 2= Mock (no target), 3= Negative control siRNA, 4=GAPDH siRNA. The data shown is for time point 48h following transfection.

(ii) FER1L5 siRNA studies in C2C12 cells. FER1L5 siRNAs were designed using the Ambion-Cenix Biosciences siRNA Design Algorithm (for targets 1-3) and BLOCK-iT ™ RNAi Designer Algorithm (for targets 4 and 5). The five siRNA targets synthesized were as follows: Target 1, sense, 5' CUACUACCAGCUCUUCUGC-3',

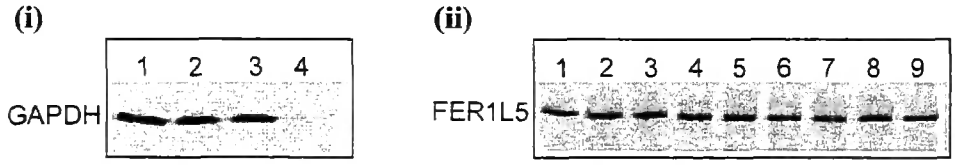

antisense, 5' –GCAGAAGAGCUGGUAGUAG-3' , Target 2, sense 5'-CCCUUAUGUGAUCCUGAAA-3', antisense, 5'-UUUCAGGAUCACAUAAGGG-3' , Target 3, sense 5'- CCAUUAUGUGCCCUGGUAC-3', antisense 5'-GUACCAGGGCACAUAAUGG-3', Target 4, sense 5'-UGUGGUUGUAGUU CAAGGACUUGUC-3', antisense, 5' GACAAGUCCUUGAACUACAACCACA-3', Target 5, sense 5'-UAAAGAUGAACCUCCAGUUGA AGGU-3', antisense, 5'-ACCUUCAACUGGAGGUUCAUCUUUA-3'. Nucleofection was performed using optimized conditions obtained with GAPDH siRNA. No reduction of FER1L5 protein was observed. The data shown is for 72 hours after transfection. Similar data was obtained at 48 hours and 96 hours after transfection. 1=wild type (no transfection), 2=Mock (no target), 3=Negative control siRNA, 4=target 1, 5=target 2, 6=target 3, 7=target 1 and target 2, 8=target 1 and 3, 9=target 2 and 3. 100pmol of each target was used and chemical transfection also produced the same result. Targets 4 and 5 were also used at similar concentrations and produced no reduction in FER1L5 protein. Data provided by Dr. Khalil Saleki.

(iii) Myoferlin siRNA studies in C2C12 cells.

Western blot showing the different levels of myoferlin expression in the C2C12 cells transfected with myoferlin siRNA plasmids from Human and mouse (C) and Human (D) constructs respectively **(See section 2.9.1)**. Seven independent single cell colonies (C1-4; D1-3) were selected for western analysis. Reduction or no signal was observed in the myoferlin expression levels in some of these clones. Clone D1 was further propagated for fusion index analysis **(Chapter V)**. Controls; scrambled siRNA and wild type (no siRNA) showed immunoreactivity to myoferlin antibody. Actin was used to show the equal loading.

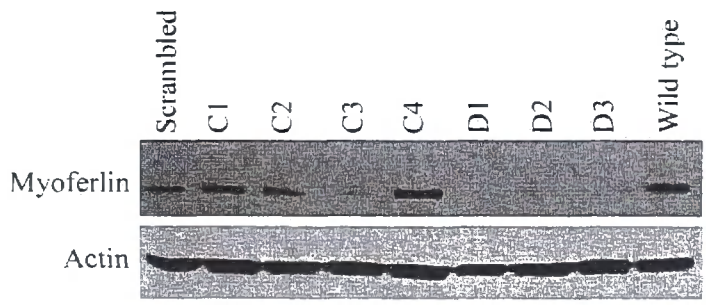

D. Some of the gene products identified as critical for myoblast fusion in mammals and vertebrates. Taken from Richardson *et al.*, (2008).

Protein	Proposed function	Localization	References
Caveolin-3	Required for myoblast–myoblast fusion	Membrane	Galbiati *et al.*, (1999)
VLA-4	Myoblast alignment	Membrane	Rosen *et al.*, (1992)
VCAM-1	Cell adhesion	Membrane	Rosen *et al.*, (1992)
NFATC2	Regulation of myotube growth	Cytoplasm/nucleus	Horsley *et al.*, (2001)
PGF_{2a}	Activation of NFATC2	Extracellular matrix	Horsley and Pavlath (2003)
IL-4	Promotion of fusion of myoblasts with growing myotube	Extracellular matrix	Horsley *et al.*, (2003)
Netrin-3	Promote myotube formation	Membrane	Kang *et al.*, (2004)
Neogenin	Netrin receptor and promotion of myotube formation	Membrane	Kang *et al.*, (2004)
Myoferlin	Promote membrane fusion	Membrane	Doherty *et al.*, (2005)
DGK-ζ	Regulation of actin reorganization	Membrane	Abramovici and Gee (2007)
Prostacyclin	Regulation of myoblast motility/promotion of fusion	Secreted	Bondesen *et al.*, (2007)
PGI_2	Prostacyclin receptor	Membrane	Bondesen *et al.*, (2007)
CD9	Cell surface protein interaction	Membrane	Tachibana and Hemler (1999)
$ß_1$ integrin	CD9 cell surface expression	Membrane	Schwander *et al.*, (2003)
Mannose receptor	Myoblast migration	Membrane	Jansen and Pavlath (2006)
CD164	Myoblast migration	Membrane	Bae *et al.*, (2008)
Trio	Rac1 regulation	Cytoplasm	Charrasse *et*

Protein	Proposed function	Localization	References
			al., (2007)
M-cadherin	Cell adhesion and Rac1 regulation	Membrane	Charrasse *et al.*, (2007)
Dock1/Dock5	Required for fast-twitch fiber fusion	Cytoplasm (zebrafish fast-twitch fibers)	Moore *et al.*, (2007)
Crk/Crk like	Dock1/Dock5 adaptor proteins, required for fast-twitch fiber fusion	Cytoplasm (zebrafish fast-twitch fibers)	Moore *et al.*, (2007)
Kirrel	Cell recognition/adhesion	Membrane (zebrafish fast muscle precursors)	Srinivas *et al.*, (2007)
Rac	Regulation of number and polarity of fusion events	Ubiquitous	Srinivas *et al.*, (2007)

REFERENCES

Abmayr, S.M., Balagopalan, L., Galletta, B.J., Hong, S.J. (2003) Cell and molecular biology of myoblast fusion. *Int. rev. Cytol.* **225:** 33-89.

Abramovici, H. and Gee, S.H. (2007) Morphological changes and spatial regulation of diacylglycerol kinase-ζ, syntrophins and Rac1 during myoblast fusion. *Cell Motil. Cytoskeleton,* **64:** 549-67.

Amy, L. A., Larisa, M. B., Tania, Q. Vu., Christopher, S.V.B. (2009). Quantitative Analysis of Multivesicular Bodies (MVBs) in the Hypoglossal Nerve: Evidence That Neurotrophic Factors Do Not Use MVBs for Retrograde Axonal transport. *The Journal of Comparative Neurology,* **514:** 641–657.

Arnold, L., Henry, A., Poron, F., Baba-Amer, Y., van Rooijen, N., Plonquet, A., Gherardi, R.K., Chazaud, B. (2007) Inflammatory monocytes recruited after skeletal muscle injury switch into antiinflammatory macrophages to support myogenesis. *J Exp Med,* **204:** 1057-69.

Achanzar, W. E. and Ward, S. (1997). A nematode gene required for sperm vesicle fusion. *J. Cell Sci,* **110:** 1073-1081.

Ampong, B.N., Imamura, M., Matsumiya, T., Yoshida, M., Takeda, S. (2005) Intracellular localization of dysferlin and its association with the dihydropyridine receptor. *Acta Myol,* **2:** 134-44.

Anderson, L.V.B., Davison, K., Moss, J.A., Young, C., Cullen, MJ., Walsh, J., Johnson, M.A., Bashir R. et al. (1998) Dysferlin is a plasma membrane protein and is expressed early in human embryonic development. *Hum Mol Genet,* **8:** 855-862.

Anderson, L. V., Davison, K., Moss, J. A., Young, C., Cullen, M. J., Walsh, J., Johnson, M. A., Bashir, R., Britton, S., Keers, S. et al. (1999). Dysferlin is a plasma membrane protein and is expressed early in human development. *Hum. Mol. Genet,* **8:** 855-861.

Aoki, M., Liu, J., Richard, I., Bashir, R., Britton, S., Keers, S. M., Oeltjen, J., Brown, H. E., Marchand, S., Bourg, N. et al. (2001). Genomic organization of the dysferlin gene and novel mutations in Miyoshi myopathy. *Neurology,* **57:** 271-278.

Babiychuk, E. B., and Draeger, A. (2000) Annexins in Cell Membrane Dynamics: Ca2+-regulated Association of Lipid Microdomains. *J. Cell Biol,* **150:** 1113–1124.

Bansal, D. and Campbell, K. P. (2004). Dysferlin and the plasma membrane repair in muscular dystrophy. *Trends Cell Biol,* **14:** 206-213.

Bansal, D., Miyake, K., Vogel, S. S., Groh, S., Chen, C. C., Williamson, R., McNeil, P. L. and Campbell, K. P. (2003). Defective membrane repair in dysferlin-deficient muscular dystrophy. *Nature,* **423:** 168-172.

Bashir. R., Britton, S., Strachan, T., Keers, S., Vafiadaki, E., Lako, M., Richard, I., Marchand, S., Bourg, N., Argov, Z., Sadeh, M., Mahjneh, I., Bushby, K. (1998) A gene related to Caenorhabditis elegans spermatogenesis factor fer-1 is mutated in limb-girdle muscular dystrophy type 2B. *Nat Genet,* **20:**37-42.

Barondes SH, Castronovo V, Cooper DN, Cummings RD, Drickamer K, Feizi T, Gitt MA, Hirabayashi J, Hughes C, Kasai K, et al. (1994) Galectins: a family of animal beta-galactoside-binding lectins. *Cell*, **76:** 597-8.

Baum, L.G., Seilhamer, J.J., Pang, M., Levine, W.B., Beynon, D., Berliner, J.A. (1995) Synthesis of an endogeneous lectin, galectin-1, by human endothelial cells is up-regulated by endothelial cell activation. *Glycoconj J*, **12:** 63-8.

Benaud, C., Gentil, B.J., Assard, N., Court, M., Garin, J., Delphin, C., Baudier, J., (2004) AHNAK interaction with the annexin 2/S100A10 complex regulates cell membrane cytoarchitecture. *J Cell Biol,* **164:**133-44.

Bernatchez, P.N., Acevedo, L., Fernandez-Hernando, C., Murata, T., Chalouni, C., Kim, J., Erdjument-Bromage, H., Shah, V., Gratton, J.P., McNally, E.M., Tempst, P., Sessa, W.C. (2007) Myoferlin regulates vascular endothelial growth factor receptor-2 stability and function. *J Biol Chem,* **282:** 30745-53.

Bernatchez, P., Sharma, A., Kodaman, P., Sessa, W.C. (2009) Myoferlin is critical for endocytosis in endothelial cells. *Am J Physiol Cell Physiol,* doi:10.1152/ajpcell.00498.

Beurg, M., Safieddine, S., Roux, I., Bouleau, Y., Petit, C., Dulon, D. (2008) Calcium- and otoferlin-dependent exocytosis by immature outer hair cells. *J Neurosci,* 28: 1798-803.

Bittner RE, Anderson LV, Burkhardt E, Bashir R, Vafiadaki E, Ivanova S, Raffelsberger T, Maerk I, Hoger H, Jung M, Karbasiyan M, Storch M, Lassmann H, Moss JA, Davison K, Harrison R, Bushby KM, Reis A. (1999) Dysferlin deletion in SJL mice (SJL-Dysf) defines a natural model for limb girdle muscular dystrophy 2B. *Nat Genet* **23:** 141-142.

Borgonovo, B., Cocucci, E., Racchetti, G., Podini, P., Bachi, A. and Meldolesi, J. (2002). Regulated exocytosis: a novel, widely expressed system. *Nat. Cell Biol,* **4:** 955-962.

Britton, S., Freeman, T., Vafiadaki, E., Keers, S., Harrison, R., Bushby, K.M.D., Bashir, R. (2000) The third human FER-1-like protein is highly similar to dysferlin. *Genomics,* **68:** 313-321.

Butte, A. J., Tamayo, P., Slonim, D., Golub, T. R., and Kohane, I. S. (2000). Discovering functional relationships between RNA expression and chemotherapeutic susceptibility using relevance networks. *Proc. Natl. Acad. Sci. U. S. A.,* **97:** 12182–12186.

Cagliani, R., Fortunato, F., Giorda, R., Rodolico, C., Bonaglia, MC., Sironi, M., D'Angelo, M.G., Prelle, A., Locatelli, F., Toscano, A., Bresolin, N., Comi, G.P.,

(2003) Molecular analysis of LGMD-2B and MM patients: identification of novel DYSF mutations and possible founder effect in the Italian population. *Neuromuscul Disord,* **13:** 788-95.

Cagliani, R., Magri, F., Toscano, A., Merlini, L., Fortunato, F., Lamperti, C., Rodolico C., Prelle, A., Sironi, M., Aguennouz, M., Ciscato, P., Uncini, A., Moggio, M., Bresolin, N., Comi, G.P. (2005) Mutation finding in patients with dysferlin deficiency and role of the dysferlin interacting proteins annexin A1 and A2 in muscular dystrophies. *Hum Muta,.* **26:** 283.

Cai, C[a]., Masumiya, H., Weisleder, N., Matsuda, N., Nishi, M., Hwang, M., Ko, J.K., Lin, P., Thornton, A., Zhao, X., Pan, Z., Komazaki, S., Brotto, M., Takeshima, H., Ma, J. (2009) MG53 nucleates assembly of cell membrane repair machinery. *Nat Cell Biol,* **11:** 56-64.

Cai, C[b]., Masumiya, H., Weisleder, N., Pan, Z., Nishi, M., Komazaki, S., Takeshima, H., Ma, J. (2009) MG53 regulates membrane budding and exocytosis in muscle cells. *J Biol Chem,* **284:** 3314-22.

Cai, C[c]., Weisleder, N., Ko, J.K., Komazaki, S., Sunada, Y., Nishi, M., Takeshima, H., Ma, J. (2009) Membrane repair defects in muscular dystrophy are linked to altered interaction between MG53 caveolin-3 and dysferlin. *J Biol Chem,* **284:** 15894-902.

Camby, I., Le Mercier, M., Lefranc, F., Kiss, R. (2006) Galectin-1: a small protein with major functions. *Glycobiology,* **16:** 137R-157R.

Campanaro, S., Romualdi, C., Fanin, M., Celegato, B., Pacchioni, B., Trevisan, S., Laveder, P., De Pitta, C., Pegoraro, E., Hayashi, Y. K., Valle, G., Angelini, C., and Lanfranchi, G. (2002) Gene expression profiling in dysferlinopathies using a dedicated muscle microarray. *Hum. Mol. Genet,* **11:** 3283–3298.

Carozzi, A.J., Ikonen, E., Lindsay, M.R., Parton, R.G. (2000) Role of cholesterol in developing T-tubules: analogous mechanisms for t-tubule and caveolae biogenesis. *Traffic,* **1:** 326-341.

Costin, N. A., Michelangelo F., Nathalie, S., Amira K. (2009) Ready, set, internalize: mechanisms and regulation of GLUT4 endocytosis. Review. *Biosci. Rep,* **29:** 1–11.

Cenacchi, G., Fanin, M., De Giorgi, L.B., Angelini, C. (2005) Ultrastructural changes in dysferlinopathy support defective membrane repair mechanism. *J Clin Pathol,* **58:** 190-195.

Cenciarelli, C., Santa, D.F., Puri, P.L., Mattei, E., Ricci, L., Bucci, F., Felsani, A and Caruso.,M. (1999) Critical role played by cyclin D3 in the MyoD-mediated arrest of cell cycle during myoblast differentiation. *Mol. Cell Biol,* **19:** 5203-5217.

Cerri, D.G., Rodrigues, L.C., Stowell, S.R., Araujo, D.D., Coelho, M.C., Oliveira, S.R., Bizario, J.C., Cummings, R.D., Dias-Baruffi, M., Costa, M.C. (2008) Degeneration of dystrophic or injured skeletal muscles induces high expression of Galectin-1. *Glycobiology,* **18:** 842-50.

Chapman, E.R. (2002) Synaptotagmin: a Ca^{2+} sensor that triggers exocytosis?. *Nat. Rev. Mol. Cell Biol,* **3:** 498-508.

Chazot, P.L., Cik, M., Stephenson, F.A. (1995) An investigation into the role of N-glycosylation in the functional expression of a recombinant heteromeric NMDA receptor. *Mol Membr Biol*, **12:** 331-7.

Charasse, S., Comunale, F., Fortier, M., Portales-Casamar, E., Debant, A., Gauthier-Rouviere, C. (2007) M-cadherin activates Rac1 GTPase through the Rho-GEF Trio during myoblast fusion. *Mol. Biol. Cell,* **18:** 1734-43.

Chen, E.H. and Olsen, E.N. (2004) Towards a molecular pathway for myoblast fusion in Drosophila. *Trends Cell Biol.* **14:** 452-460.

Chiu, Y.H., Hornsey, M.A., Klinge, L., Jørgensen. L.H., Laval, S.H., Charlton,R., Barresi, R., Straub, V., Lochmüller, H. and Bushby, K. (2009). Attenuated muscle regeneration is a key factor in dysferlin-deficient muscular dystrophy. *Hum. Mol. Genet,* **18:** 1976-1989.

Cho, W. and Stahelin, R.V. (2006) Membrane Binding and Subcellular Localization of C2 Domains. *Biochim. Biophys. Acta,* **1761:** 838-49.

Cocucci, E., Racchetti, G., Podini, P., Rupnik, M., Meldolesi, J. (2004) Enlargeosome, an exocytotic vesicle resistant to nonionic detergents undergoes endocytosis via a nonacidic route. *Mol. Biol.Cell,* **15:** 5356-5368.

Cocucci, E., Racchetti, G., Meldolesi, J. (2009) Shedding microvesicles: artefacts no more. *Trends Cell Biol,* **19:** 43-51.

Confalonieri, P., Oliva, L., Andreetta, F., Lorenzoni, R., Dassi, P., Mariani, E., Morandi, L., Mora, M., Cornelio, F., Mantegazza, R. (2003) Muscle inflammation and MHC class I up-regulation in muscular dystrophy with lack of dysferlin: an immunopathological study. *J Neuroimmunol,* **142:** 130-136.

Cooper, D.N. and Barondes, S.H. (1990) Evidence for export of a muscle lectin from cytosol to extracellular matrix and for a novel secretory mechanism. *J. Cell Biol,* **110:** 1681 - 1691.

Davis, D. B., Delmonte, A. J., Ly, C. T. and McNally, E. M. (2000). Myoferlin, a candidate gene and potential modifier of muscular dystrophy. *Hum. Mol. Genet,* **9**: 217-226.

Davis, D. B., Doherty, K. R., Delmonte, A. J. and McNally, E. M. (2002). Calcium-sensitive phospholipid binding properties of normal and mutant ferlin C2 domains. *J. Biol. Chem,* **277:** 22883-22888.

Davletov, B. A. and Sudhof, T.C. (1993) A single C2 domain from synaptotagmin I is sufficient for high affinity Ca2+/phospholipid binding. *J. Biol. Chem,* **268:** 26386-26390.

Dellaire, G. and Bazett-Jones, D.P. (2004) PML nuclear bodies: dynamic sensors of DNA damage and cellular stress. *Bioessays,* **26:** 963-977.

Denzer, K., Kleijmeer, M.J., Heijnen, H.F., Stoorvogel, W., Geuze, H.J. (2000). Exosome: from internal vesicle of the multivesicular body to intercellular signaling device. *J. Cell Sci.* **113:** 3365-3374.

Dias-Baruffi, M., Zhu, H., Cho, M., Karmakar, S., McEver, R.P., Cummings, R.D. (2003) Dimeric galectin-1 induces surface exposure of phosphatidylserine and phagocytic recognition of leukocytes without inducing apoptosis. *J Biol Chem,* **278:** 41282-93.

Doherty, K.R., McNally, E.M. (2003) Repairing the tears: dysferlin in muscle membrane repair. *Trends Mol Med,* **9:**.327-30.

Doherty, K.R., Cave, A., Davis, D.B., Delmonte, A.J., Posey, A., Earley, J.U., Hadhazy, M., McNally, EM. (2005) Normal myoblast fusion requires myoferlin, *Development,* **132:** 5565-5575.

Doherty, K.R., Demonbreun, A.R., Wallace, G.Q., Cave, A., Posey, A.D., Heretis, K., Pytel, P., McNally, E.M. (2008) The endocytic recycling protein EHD2 interacts with myoferlin to regulate myoblast fusion. *J Biol Chem,* **283:** 20252-60.

Emery, A.E. (2002) The muscular dystrophies. *Lancet,* **359:** 687-95.

Escola, J. M., Kleijmeer, M. J., Stoorvogel, W., Griffith, J. M., Yoshie, O. Geuze, H. J. (1998). Selective enrichment of tetraspan proteins on the internal vesicles of multivesicular endosomes and on exosomes secreted by human B-lymphocytes. *J. Biol. Chem.* **273:** 20121-20127.

Fanin, M., Angelini, C. Muscle pathology in dysferlin deficiency. *Neuropathol Appl Neurobiol,* **28:** 461-70.

Fernández-Chacón, R., Königstorfer, A., Gerber, S.H., García, J., Matos, M.F., Stevens, C.F., Brose, N., Rizo, J., Rosenmund, C., Südhof, T.C. (2001). Synaptotagmin I functions as a calcium regulator of release probability. *Nature,* **410:** 41-9.

Festing, (1979). M.F.W. Festing, Inbred Strains in Biomedical Research. *In:* , *MacMillan*, London, p.483.

Fevrier, B. and Raposo, G. (2004) Exosomes:endosomal derived vesicles shipping extracellular messages. *Curr. Opin. Cell Biol,* **16:** 415-421.

Foxton, R.M., Laval, S.H., Bushby, K.M.D. (2004) Characterisation of the dysferlin skeletal muscle promoter. *European Journal of Human Genetics,* **12:** 127–131.

Gallardo, E., Rojas-Garcia, R., de Luna, N., Pou, A., Brown, R.H., Jr., Illa, I. (2001) Inflammation in dysferlin myopathy: immunohistochemical characterization of 13 patients. *Neurology,* **57:** 2136-2138.

Galvin, J.E., Palamand, D., Strider, J., Milone, M., Pestronk, A. The muscle protein dysferlin accumulates in the Alzheimer brain. *Acta Neuropathol*, 2006 **112:** 665-71.

Gatti, J.L., Me'tayer, S., Belghazi, M., Dacheux, F., Dacheux, J.L. (2005). Identification, Proteomic Profiling, and Origin of Ram Epididymal Fluid Exosome-Like Vesicles. *Biology of reproduction,* **72:** 1452–1465.

Gentil, B.J., Delphin, C., Benaud, C., Baudier, J. (2003) Expression of the giant protein AHNAK (desmoyokin) in muscle and lining epithelial cells. *J Histochem Cytochem*, **51:** 339-48.

Georgiadis, V., Stewart, H.J., Pollard, H.J., Tavsanoglu, Y., Prasad, R., Horwood, J., Deltour, L., Goldring, K., Poirier, F., Lawrence-Watt, D.J. (2007) Lack of galectin-1 results in defects in myoblast fusion and muscle regeneration. *Dev Dyn.* **236:** 1014-24.

Gerke, V., and Moss, S. E. (2002) Annexins: From Structure to Function. *Physiol. Rev,* **82:** 331–371.

Gerona, R.R., Larsen, E.C., Kowalchyk, J.A., Martin, T.F. (2000) The C terminus of SNAP25 is essential for Ca(2+)-dependent binding of synaptotagmin to SNARE complexes. *J Biol Chem,* **275:** 6328-36.

Glover, L. and Brown, R.H. Jr. (2007) Dysferlin in membrane trafficking and patch membrane repair. *Traffic,* **8:** 785-794.

Greco, V., Hannus, M., Eaton, S. Argosomes: a potential vehicle for the spread of morphogens through epithelia. *Cell,* **106:** 633-45.

Gutwein, P., Mechtersheimer, S., Riedle, S., Stoeck, A., Gast, D., Joumaa, S., Zentgraf, H., Fogel, M., Altevogt, D.P. (2003) ADAM10-mediated cleavage of L1 adhesion molecule at the cell surface and in released membrane vesicles. *FASEB J*, **2:** 292-4.

Han, R., Bansal, D., Miyake, K., Muniz, V.P., Weiss, R.M., McNeil, P.L., Campbell, KP. (2007) Dysferlin-mediated membrane repair protects the heart from stress-induced left ventricular injury. *J Clin Invest,* **117:** 1805-13.

Handwerger, K.E., Gall, J.G. (2006) Subnuclear organelles: new insights into form and function. *TRENDS Cell Biol,* **16:** 19-26.

Harrison, F.L., Wilson, T.J. (1992) The 14 kDa beta-galactoside binding lectin in myoblast and myotube cultures: localization by confocal microscopy. *J Cell Sci,* **101:** 635-46.

Harris, J.B., Johnson, M.A., Karlsson, E. (1974) Proceedings: histological and histochemical aspects of the effect of notexin on rat skeletal muscle. *Br. J. Pharmacol,* **52:** 152P.

Haslett, J.N., Sanoudou, D., Kho, A.T., Bennett, R.R., Greenberg, S.A., Kohane, I.S., Beggs, A.H., Kunkel, L.M. Gene expression comparison of biopsies from Duchenne muscular dystrophy (DMD) and normal skeletal muscle. *Proc Natl Acad Sci,* **99:** 15000-15005.

He, A., Liu X., Liu L., Chang Y., Fang F. (2000). How many signals impinge on GLUT4 activation by insulin? Review. *Cellular Signalling*, **19:** 1–7.

Heijnen, H. F. G., Schiel, A. E., Fijnheer, R., Geuze, H. J., Sixma, J. J. (1999). Activated platelets release two types of membrane vesicles: microvesicles by surface shedding and exosomes derived from exocytosis of multivesicular bodies and alpha-granules. *Blood,* **94:** 3791-3799.

Hernández-Deviez, D.J., Martin, S., Laval, S.H., Lo, H.P., Cooper, S.T., North, K.N., Bushby, K., Parton, R.G. (2006) Aberrant dysferlin trafficking in cells lacking caveolin or expressing dystrophy mutants of caveolin-3. *Hum Mol Genet,* **15:**129-42.

Hernández-Deviez D.J., Howes M.T., Laval S.H., Bushby K., Hancock J.F., Parton R.G. (2008) Caveolin regulates endocytosis of the muscle repair protein, dysferlin. J. *Biol. Chem,* **283:** 6476–6488.

Ho, M., Post, C. M., Donahue, L. R., Lidov, H. G., Bronson, R. T., Goolsby, H., Watkins, S. C., Cox, G. A. and Brown, R. H., Jr (2004). Disruption of muscle membrane and phenotype divergence in two novel mouse models of dysferlin deficiency. *Hum. Mol. Genet,* **13:** 1999-2010.

Hochmeister, S., Grundtner, R., Bauer, J., Engelhardt, B., Lyck, R., Gordon, G., Korosec, T., Kutzelnigg, A., Berger, J.J., Bradl, M., Bittner, R.E., Lassmann, H. (2008). Dysferlin is a new marker for leaky brain blood vessels in multiple sclerosis. *J Neuropathol Exp Neurol*, **65:** 855-65.

Horsley, V. and Pavlath, G.K. (2004) Forming os multinucleated cell: molecules that regulate myoblast fusion, Cells Tissues Organs, **176:** 67-78.

Huang, Y.C., Verheesen, P., Roussis, A., Frankhuizen, W., Ginjaar, I., Haldane, F., Laval, S., Anderson, L.V.B., Verrips, T., Frants, R.R. et al. (2005) Protein studies in dysferlinopathy patients using llama-derived antibody fragments selected by phage display. *Eur. J. Hum. Genet,* **13:** 721–730.

Huang, Y., Laval, S.H., Remoortere, A., Baudier, J., Benaud, C., Anderson, L.V.B., Straub, V., Deelder, A., Frants, R.R., den Dunnen, J.T., Bushby, K., van der Maarel, S. (2007) AHNAK, a novel component of the dysferlin protein complex redistributes to the cytoplasm with dysferlin during skeletal muscle regeneration. *FASEB J,* **21:** 732-742.

Hurley, J.H. (2008). ESCRT complexes and the biogenesis of multivesicular bodies *Current Opinion in Cell Biology,* **20:** 4–11.

Illa I., Serrano-Munuera C., Gallardo E., Lasa A., Rojas-Garcia R., Palmer J., Gallano

P., Baiget M., Matsuda C., Brown R.H. (2001) Distal anterior compartment myopathy: a dysferlin mutation causing a new muscular dystrophy phenotype. *Ann. Neurol,* **49:** 130–134.

Inoue, M., Wakayama, Y., Kojima, H., Shibuya, S., Jimi, T., Oniki, H., Nishino, I., Nonaka, I. (2006) Expression of myoferlin in skeletal muscles of patients with dysferlinopathy. *Tohoku J Exp Med,* **209:** 109-16.

Hassane I, Brocheriou I, Eymard B, Le Charpentier M, Romero NB, Lenaour G, Bourry E, Deray G. Loss of podocyte dysferlin expression is associated with minimal change nephropathy. Am J Kidney Dis. 2006 Jul;48(1):143-50.

Jaiswal, J., Marlow, G., Summerill, G., Mahjneh, I., Mueller, S., Hill, M., Haase, H., Anderson, L.V.B., Richard, I., Kiuru-Enari, S., Simon, S., Bashir, R. (2007) Defect in a novel membrane repair pathway in patients with a non-dysferlin Miyoshi myopathy. *Traffic,* **8:** 77-88.

Jasmer, D.P. and Kwak, D. (2006) Fusion and differentiation of murine C2C12 skeletal muscle cells that express Trichinella spiralis p43 protein. *Exp Parasitol,* **112:** 67-75.

Jimenez, J., Bashir, R. (2007) In silico functional and structural characterization of ferlin proteins by mapping disease-causing mutations and evolutionary information onto three-dimensional models of their C2 domains. *J. Neurol. Sci,* **260:** 114-123.

Johnstone, R. M., Adam, M., Hammond, J. R., Orr, L. and Turbide, C. (1987). Vesicle formation during reticulocyte maturation. Association of plasma membrane activities with released vesicles (exosomes). *J. Biol. Chem.* **262:** 9412-9420.

Karmakar, S., Cummings, R. D., and McEver, R. P. (2005). Contributions of Ca^{2+} to galectin-1–induced exposure of phosphatidylserine on activated neutrophils. *J. Biol. Chem,* **280:** 28623–28631.

Kee, Y., Scheller, R.H. (1996) Localization of synaptotagmin-binding domains on syntaxin. *J Neurosci,* **16:** 1975-81.

Kelly, G. Mechanical overload and skeletal muscle fibre hyperplasia: a meta-analysis. *J. App. Physiol.* **81:** 1584-1588.

Kesari, A., Fukuda, M., Knoblach, S., Bashir, R., Nader, G.A., Rao, D., Nagaraju, K., Hoffman, E.P. (2008) Dysferlin deficiency shows compensatory induction of Rab27A/Slp2a that may contribute to inflammatory onset. *Am J Pathol.* **173:** 1476-87.

Kestila, M., Lenkkeri, U., Mannikko, M., Lamerdin, J., McCready, P., Putaala, H., Ruotsalainen, V., Morita, T., Nissinen, M., Herva, R., Peltonen, C.E., Holmberg, C., Olsen, A., Tryggvason, K. (1998). Positionally cloned gene for a novel glomerular protein nephrin is mutated in congenital nephrotic syndrome. *Mol. Cell.* **1:** 575-582.

Klinge L., Laval S., Keers S., Haldane F., Straub V., Barresi R., Bushby K. (2007)

From T-tubule to sarcolemma: damage-induced dysferlin translocation in early myogenesis. *FASEB J,* **21:** 1768–1776.

Kleijmeer, M. J., Escola, J.-M., Griffith, J., Geuze, H. J. (1998). MHC class I molecules are present in MHC class II compartments from dendritic cells and B lymphocytes. In *Keystone Symposium: Cellular and MolecularBiology of Dendritic Cells*. Santa Fe, NM, Abstract no. **220.**

Kreis, T. E., K . H . Winterhalter, and W. Birchmeier. (1979). In vivo distribution and Lamond AI, Spector DL. Nuclear speckles: a model for nuclear organelles. *Int Rev Mol Cell Biol,* **4:** 605-612.

Kreis, T. E. and Birchmeier, W. (1982). Microinjection of fluorescently labeled proteins into living cells with emphasis on cytoskeletal proteins. *Int. Rev. Cytol,* **75:** 209-227.

Komuro, A., Masuda, Y., Kobayashi, K., Babbitt, R., Gunel, M., Flavell, R.A., Marchesi, V.T. (2004) The AHNAKs are a class of giant propeller-like proteins that associate with calcium channel proteins of cardiomyocytes and other cells. *Proc Natl Acad Sci U S A.,* 101: 4053-8.

Korie, E. H. and Joseph, G. Gall. (2006) Subnuclear organelles: new insights into form and function. *Trends Cell Biol,* 16:19-26.

Kostek, C.A., Dominov, J.A., Miller, J.B. (2002) Up-regulation of MHC class I expression accompanies but is not required for spontaneous myopathy in dysferlin-deficient SJL/J mice. *Am J Pathol,* **160:** 833-9.

Lambert, O., Gerke, V., Bader, M. F., Porte, F., and Brisson, A. (1997) Structural analysis of junctions formed between lipid membranes and several annexins by cryo-electron microscopy. *J. Mol. Biol,* **272:** 42–55.

Lennon, N.J., Kho, A., Bacskai, B.J., Perlmutter, S.L., Hyman, B.T., Brown, R.H., Jr: (2003) Dysferlin interacts with annexins A1 and A2 and mediates sarcolemmal wound-healing. *J Biol Chem,* **278:** 50466-50473.

Lee, T.L., Lin, Y.C., Mochitate, K., Grinnell, F. (1993) Stress relaxation of fibroblasts in collagen matrix triggers ectocytosis of plasma membrane vesicles containing actin, annexins II and VI, and β1 integrin receptors. *J. Cell Sci,* **105:** 167-177.

Lee, E., Marcucci, M., Daniell, L., Pypaert, M., Weisz, O.A., Ochoa, G.C., Farsad, K., Wenk, M.R., De Camilli, P. (2002) Amphiphysin 2 (Bin1) and t-tubule biogenesis in muscle. *Science,* **297:** 1193-1196.

Li, C., Ullrich, B., Zhang, J.Z., Anderson, R.G., Brose, N., Südhof, T.C. (1995) Ca(2+)-dependent and -independent activities of neural and non-neural synaptotagmin. *Nature,* **375(6532):** 594-9.

Liu, J., Aoki, M., Illa, I., Wu, C., Fardeau, M., Angelini, C., Serrano, C., Urtizberea, J.A., Hentati, F., Hamida, M.B., Bohlega, S., Culper, E.J., Amato, A.A. et al. (1998)

Dysferlin, a novel skeletal muscle gene, is mutated in Miyoshi myopathy and limb girdle muscular dystrophy. *Nat Genet* **20:** 31-6.

Lo, H.P., Cooper, S.T., Evesson, F.J., Seto, J.T., Chiotis, M., Tay, V., Compton, A.G., Cairns, A.G., Corbett, A., MacArthur, D.G., Yang, N., Reardon, K., North, K.N. (2008) Limb-girdle muscular dystrophy: diagnostic evaluation, frequency and clues to pathogenesis. *Neuromuscul Disord,* **18:** 34-44.

Longo-Guess, C., Gagnon, L.H., Bergstrom, D.E., Johnson, K.R. (2007) A missense mutation in the conserved C2B domain of otoferlin causes deafness in a new mouse model of DFNB9. *Hear Res,* **234(1-2):** 21-8.

Lu, M., Kinchen, J.M., Rossman, K.L., Grimsley, C., Hall, M., Sondek, J., Hengartner, M.O., Yajnik, V., Ravichandran, K.S. (2005) A steric-inhibtion model for regulation of nucleotide exchange via the Dock180 family of GEFs. *Curr. Biol.* **15:** 371-377.

Luna, N., Gallardo, E., Illa, I. (2004) In vivo and in vitro dysferlin expression in human muscle satellite cells. *J Neuropathol Exp Neurol,* **63:** 1104-13.

Luna, N., Gallardo, E., Soriano, M., Dominguez-Perles, R., de la Torre, C., Rojas-García, R., García-Verdugo, J.M., Illa, I. (2006) Absence of dysferlin alters myogenin expression and delays human muscle differentiation "in vitro". *J Biol Chem,* **281:** 17092-8.

Mahjneh, I., Marconi, G., Bushby, K., Anderson, L.V., Tolvanen-Mahjneh, H., Somer H. (2001) Dysferlinopathy (LGMD2B): a 23-year follow-up study of 10 patients homozygous for the same frameshifting dysferlin mutations. *Neuromuscul Disord,* **11:** 20-6.

Markiewicz, E., Ledran, M,, Hutchison, C.J. (2005) Remodelling of the nuclear lamina and nucleoskeleton is required for skeletal muscle differentiation in vitro. *J. Cell Sci,* **118:** 409-420.

Masumiya, H., Asaumi, Y., Nishi, M., Minamisawa, S., Adachi-Akahane, S., Yoshida, M, Kangawa, K., Ito, K., Kagaya, Y., Yanagisawa, T., Yamazaki, T., Ma, J., Takeshima, H. (2009) Mitsugumin 53-mediated maintenance of K+ currents in cardiac myocytes. *Channels (Austin),* **3:** 6-11.

Matsuda, C., Aoki, M., Hayashi, Y.K., Ho, M.F., Arahata, K., Brown, R.H. Jr. (1999) Dysferlin is a surface membrane-associated protein that is absent in Miyoshi myopathy. *Neurology,* **53:** 1119-22.

Matsuda, C., Hayashi, Y.K., Ogawa, M., Aoki, M., Murayama, K., Nishino, I., Nonaka, I., Arahata, K., Brown, R.H. Jr. (2001) The sarcolemmal proteins dysferlin and caveolin-3 interact in skeletal muscle. *Hum Mol Genet,* **10:** 1761-6.

Matsuda, C., Kameyama, K., Tagawa, K., Ogawa, M., Suzuki, A., Yamaji, S., Okamoto, H., Nishino, I., Hayashi, Y.K. (2005) Dysferlin interacts with affixin (beta-parvin) at the sarcolemma. *J Neuropathol Exp Neurol,* **64:** 334-40.

McNally, E.M., Ly, C.T., Rosenmann, H., Mitrani Rosenbaum, S., Jiang, W., Anderson, L.V., Soffer. D., Argov, Z. (2000) Splicing mutation in dysferlin produces limb-girdle muscular dystrophy with inflammation. *Am. J. Med. Genet,* **91:** 305–312.

McNeil, P.L., Murphy, R. F., Lanni, F and Taylor, D. L. (1984) A method for incorporating macromolecules into adherent cells. *J. Cell Biol,* 98: 1556 – 1564.

McNeil, P.L. and Warder, E. (1987) Glass beads load macromolecules into living cells. *J Cell Sci,* **88:** 669-78.

McNeil, P.L. and Steinhardt, R.A. (2003) Plasma membrane disruption: repair, prevention, adaption. *Annu Rev Cell Dev Biol,* **19:** 697-731.

McNeil, P.L. and Kirchhausen, T. (2005) An emergency response team for membrane repair. *Nat Rev Mol Cell Bio,* **6:** 499-505.

McNeil, A.K., Rescher, U., Gerke, V., McNeil, P.L. (2006) Requirement for annexin A1 in plasma membrane repair. *J Biol Chem,* **281:** 35202-7.

McNeil, P. (2009) Membrane repair redux: redox of MG53. *Nat Cell Biol* **11:** 7-9.

Moskovich, O. and Fishelson, Z. (2007) Live Cell Imaging of Outward and Inward Vesiculation Induced by the Complement C5b-9 Complex. *J. Biol. Chem,* **282:** 29977-29986.

Moss, S.E. and Morgan, R.O. (2004) The annexins. *Genome Biol,* **5:** 219.

Murphy, E.D. and Roths, J.B. (1979) A Y chromosome associated factor in strain BXSB producing accelerated autoimmunity and lymphoproliferation. *Arthritis Rheum,* **22:** 1188-94.

Nagaraju, K., Rawat, R., Veszelovszky, E., Thapliyal, R., Kesari, A., Sparks, S., Raben, N., Plotz, P., Hoffman, E.P. (2008) Dysferlin deficiency enhances monocyte phagocytosis: a model for the inflammatory onset of limb-girdle muscular dystrophy 2B. *Am J Pathol,* **172:** 774-85.

Nalefski, E. A. and Falke, J. J. (1996). The C2 domain calcium-binding motif: structural and functional diversity. *Protein Sci,* **5:** 2375-2390.

Nguyen, K., Bassez, G., Bernard, R., Krahn, M., Labelle, V., Figarella-Branger, D., Pouget, J., Hammoudael, H., Béroud, C., Urtizberea, A., Eymard, B., Leturcq, F., Lévy, N. (2005) Dysferlin mutations in LGMD2B, Miyoshi myopathy, and atypical dysferlinopathies. *Hum Mutat,* **26:** 165.

Nguyen, K., Bassez, G., Krahn, M., Bernard, R., Laforêt, P., Labelle, V., Urtizberea, J.A., Figarella-Branger, D., Romero, N., Attarian, S., Leturcq, F., Pouget, J., Lévy, N., Eymard, B. (2007) Phenotypic study in 40 patients with dysferlin gene mutations: high frequency of atypical phenotypes. *Arch Neurol,* **64:** 1176-82.

Nickel W. (2007) Unconventional secretion: an extracellular trap for export of fibroblast growth factor 2. *J Cell Sci,* **120(Pt 14):** 2295-9.

Nickel, W. and Rabouille, C. (2009) Mechanisms of regulated unconventional protein secretion. *Nat Rev Mol Cell Biol*, **10:**148-55.

Ontell, M., Hughes, D., Bourke, D. (1998) Morphometric analysis of the developing mouse soleus muscle. *Am. J. Anat.* **181:** 279-288.

Patel, P., Harris, R., Geddes, S.M., Strehle, E.M., Watson, J.D., Bashir, R., Bushby, K., Driscoll, P.C., Keep, N.H. (2008) Solution Structure of the Inner DysF Domain of Myoferlin and Implications for Limb Girdle Muscular Dystrophy Type 2B. *J Mol Biol,* **379:** 981-90.

Paula-Barbosa, M.M., Borges, M.M., Cadete-leite., Tavares, M.A. (1986). Giant multivesicular bodies in the rat hippocampal pyramidal cells after chronic alcohol consumption. *Neuroscienee Letters,* **64:** 345-349.

Pena, J., Jimena, I., Luque, E., Vaamonde, R. (1995) New fiber formation in rat soleus muscle following administration of denervated muscle extract. *J. Neurol. Sci.* **128:** 14-21.

Peters, P. J., Geuze, H. J., van der Donk, H. A., Slot, J. W., Griffith, J. M., Stam, N. J., Clevers, H. C., Borst, J. (1989). Molecules relevant for T cell-target cell interaction are present in cytolytic granules of human T lymphocytes. *Eur. J. Immunol.* **19:** 1469-1475.

Piccolo, F., Moore, S. A., Ford, G. C., Campbell, K. P. (2000). Intracellular accumulation and reduced sarcolemmal expression of dysferlin in limb-girdle muscular dystrophies. *Ann. Neurol,* **48:** 902-912.

Pilzer, D., Gasser, O., Moskovich, O., Schifferli, J.A., Fishelson, Z. (2005) Emission of membrane vesicles: roles in complement resistance, immunity and cancer. *Springer Semin Immunopathol,* **27:** 375-87.

Piper, R.C. and Katzmann, D. J. (2007) Biogenesis and function of multivesicular bodies. *Ann. Rev. Cell Dev. Biol,* **23:** 519-547.

Ponting, C. P., Mott, R., Bork, P., Copley, R. R. (2001) Novel protein domains and repeats in Drosophila melanogaster: insights into structure, function, and evolution. *Genome Res,* **11:**1996–2008.

Pramono, Z.A., Lai, P.S., Tan, C.L., Takeda, S., Yee, W.C. (2006) Identification and characterization of a novel human dysferlin transcript: dysferlin_v1. *Hum Genet,* **120:** 410-9.

Rabinovich, G.A., Baum, L.G., Tinari, N., Paganelli, R., Natoli, C., Liu, F.T., Iacobelli, S. (2002) Galectins and their ligands: amplifiers, silencers or tuners of the inflammatory response? *Trends Immunol,* **23:** 313-20.

Ramakrishnan, N.A., Drescher, M.J., Drescher, D.G. (2009) Direct interaction of otoferlin with syntaxin 1A, SNAP-25, and the L-type voltage-gated calcium channel Cav1.3. *J Biol Chem,* **284:** 1364-72.

Raposo, G., Nijman, H. W., Stoorvogel, W., Leijendekker, R., Harding, C. V., Melief, C. J., Geuze, H. J. (1996). B lymphocytes secrete antigenpresenting vesicles. *J. Exp. Med.* **183:** 1161-1172.

Raposo, G., Tenza, D., Mecheri, S., Peronet, R., Bonnerot, C., Desaymard, C. (1997). Accumulation of Major Histocompatibility Complex Class II molecules in mast cell secretory granules and their release upon degranulation. *Mol. Biol. Cell,* **8:** 2631-2645.

Reddy, A., Caler, E. V. and Andrews, N. W. (2001). Plasma membrane repair is mediated by Ca(2+)-regulated exocytosis of lysosomes. *Cell,* **106:** 157-169.

Richardson, B. E., Nowak, S., Baylies, M. K. (2008) Myoblast Fusion in Fly and Vertebrates: New Genes, New Processes and New Perspectives. *Traffic,* **9:** 1050-1059.

Rieu, S., Geminard, C., Rabesandratana, H., Sainte-Marie, J. and Vidal, M. (2000). Exosomes released during reticulocyte maturation bind to fibronectin via integrin a4b1. *Eur. J. Biochem.* **267:** 583-590.

Riquelme, C., Barthel, K.K., Qin, X.F., Liu, X. (2006) Ubc9 expression is essential for myotube formation in C2C12. *Exp Cell Res,* **312:** 2132-41.

Rizo, J. and Sudhof, T. C. (1998). C2-domains, structure and function of a universal Ca^{2+}-binding domain. *J. Biol. Chem* **273:** 15879-15882.

Robinson, J.M., Ackerman, W.E.4^{th}., Behrendt, N.J., Vandre, D.D. (2009) While dysferlin and myoferlin are coexpressed in the human placenta, only dysferlin expression is responsive to trophoblast fusion in model systems. *Biol Reprod,* **81:** 33-9.

Rose, and David, W. (2007) Genetic Manipulation of Mammalian Cells by Microinjection. *Cold Spring Harbor Protocols:* pdb.prot4754.

Rossi AG, Hallett JM, Sawatzky DA, Teixeira MM, Haslett C. (2007) Modulation of granulocyte apoptosis can influence the resolution of inflammation. *Biochem Soc Trans,* **35:** 288-91.

Roux, I,, Safieddine, S., Nouvian, R., Grati, M., Simmler, M., Bahloul, A,. Perfettini, I., Le Gall, M,, Rostaing, P., Hamard, G., Triller, A., Avan, P., Moser, T., Petit, C. (2006) Otoferlin, defective in a human deafness form is essential for exocytosis at the auditory ribbon synapse. ***Cell*** **27:** 277-289.

Sardiello, M., Cairo, S., Fontanella, B., Ballabio, A., Meroni, G. (2008) Genomic analysis of the TRIM family reveals two groups of genes with distinct evolutionary properties. *BMC Evol Biol,* **8:** 225.

Seal, R.P., Akil, O., Yi, E., Weber, C.M., Grant, L., Yoo, J., Clause, A., Kandler, K., Noebels, J.L., Glowatzki, E., Lustig, L.R., Edwards, R.H. (2008) Sensorineural deafness and seizures in mice lacking vesicular glutamate transporter 3. *Neuron*, **57:** 263-75.

Selcen, D., Stilling, G., Engel, A. G. (2001). The earliest pathologic alterations in dysferlinopathy. *Neurology,* **56:** 1472-1481.

Shtivelman, E., Bishop, J.M. (1993) The human gene AHNAK encodes a large phosphoprotein located primarily in the nucleus. *J Cell Biol,* **120:** 625-630.

Sobell, H.M. Actinomycin D and DNA transcription. (1985) *Proc Natl Acad Sci U S A,* **82:** 5328-5331.

Song, K.S., Scherer, P.E., Tang, Z., Okamoto, T., Li, S., Chafel, M., Chu, C., Kohtz, D.S., Lisanti, M.P. (1996) Expression of caveolin-3 in skeletal, cardiac, and smooth muscle cells. Caveolin-3 is a component of the sarcolemma and co-fractionates with dystrophin and dystrophin-associated glycoproteins. *J Biol Chem,* **271:** 15160-5.

Stowell, S. R., Karmakar, S., Stowell, C. J., Dias-Baruffi, M., McEver, R. P., and Cummings, R. D. (2007). Human galectin-1, -2, and -4 induce surface exposure of phosphatidylserine in activated human neutrophils but not in activated T cells. *Blood,* **109:** 219–227.

Stowell, S.R., Karmakar, S., Arthur, C.M., Ju, T., Rodrigues, L.C., Riul, T.B., Dias-Baruffi, M., Miner, J., McEver, R.P., Cummings, R.D. (2009) Galectin-1 induces reversible phosphatidylserine exposure at the plasma membrane. *Mol Biol Cell*, **20:** 1408-18.

Sudhof, T.C. (2004). The synaptic vesicle cycle. *Annu. Rev. Neurosci,.* **27:** 509-547.

Taylor, M.V. (2003) Muscle differentiation: signalling cell fusion. *Curr. Biol.* **13:** R964-966.

Teixeira, C.F., Zamunér, S.R., Zuliani, J.P., Fernandes, C.M., Cruz-Hofling, M.A., Fernandes, I., Chaves, F., Gutiérrez, J.M. (2003) Neutrophils do not contribute to local tissue damage, but play a key role in skeletal muscle regeneration, in mice injected with Bothrops asper snake venom. *Muscle Nerve,* **28:** 449-59.

Terasaki, M., Miyake, K., McNeil, P.L. (1997) Large plasma membrane disruptions are Rapidly resealed by Ca2+-dependent vesicle-vesicle fusion events. *J Cell Biol*, **139:** 63-74.

Therrien, C., Fulvio, S.D., Pickles, S., Sinnreich, M.M. (2009) Characterization of Lipid Binding Specificities of Dysferlin C2 Domians Reveals Novel Interactions with Phosphoinositides. *Biochemistry* **48:** 2377-2384.

Thery, C., Zitvogel, L., Amigorena, S. (2002) Exosomes: Composition, biogenesis and function. *Nat. Rev. Immunol,* **2:** 569–579.

Thong, F. S., Dugani, C. B., Klip, A. (2005) Turning signals on and off: GLUT4 traffic in the insulin-signaling highway. *Physiology,* **20:** 271–284.

Urtizberea, J.A., Bassez, G., Leturcq, F., Nguyen, K., Krahn, M., Levy, N. (2008). Dysferlinopathies. *Neurol India,* **56:** 289-97.

Vafiadaki, E., Reis, A., Keers, S., Harrison, R., Anderson, L.V., Raffelsberger, T., Ivanova, S., Hoger, H., Bittner, R.E., Bushby, K., Bashir, R. (2001) Cloning of the mouse dysferlin gene and genomic characterization of the SJL-Dysf mutation. *Neuroreport* **12:** 625-9.

Vainzof, M., Anderson, L.V., McNally, E.M., Davis, D.B., Faulkner, G., Valle, G., Moreira, E.S., Pavanello, R.C., Passos-Bueno, M.R., Zatz, M. (2001) Dysferlin protein analysis in limb-girdle muscular dystrophies. *J Mol Neurosci*, **17:** 71-80.

Vandré, D.D., Ackerman, W.E.4th., Kniss, D.A., Tewari, A.K., Mori, M., Takizawa, T., Robinson, J.M. (2007) Dysferlin is expressed in human placenta but does not associate with caveolin. *Biol Reprod,* **77:** 533-42.

Vilchez, J.J., Gallano, P., Gallardo, E., Lasa, A., Rojas-García, R., Freixas, A., De Luna, N., Calafell, F., Sevilla, T., Mayordomo, F., Baiget, M., Illa, I. (2005) Identification of a novel founder mutation in the DYSF gene causing clinical variability in the Spanish population. *Arch Neurol,* **62:** 1256-9.

van Deurs, B., Roepstorff,.K., Hommelgaard, A.M., Sandvig, K.(2003) Caveolae: anchored, multifunctional platforms in the lipid ocean. *Trends Cell Biol,* **13:** 92-100.

van Koningsbruggen, S., Dirks, K.W., Mommaas, A.M., Onderwater, J.J., Deidda, G., Padberg, G.W., Frants, R.R., van der Maarel, S.M. (2004) FRG1P is localized in the nucleolus, Cajal bodies and speckles, *J Med Genet,* **41:** 46-54.

Vidal, M. J. and Stahl, P. D. (1993). The small GTP-binding proteins Rab4 and ARF are associated with released exosomes during reticulocyte maturation. *Eur. J. Cell Biol.* **60:** 261-267.

von der Hagen, M., Laval, S.H., Cree, L.M., Haldane, F., Pocock, M., Wappler, I., Peters, H., Reitsamer, H.A., Hoger, H., Wiedner, M., Oberndorfer, F., Anderson, L.V., Straub, V., Bittner, R.E., Bushby, K.M. (2005) The differential gene expression profiles of proximal and distal muscle groups are altered in pre-pathological dysferlin-deficient mice. *Neuromuscul Disord,* **15:** 863-77.

von Tresckow, B., Kallen, K.J., von Strandmann, E.P., Borchmann, P., Lange, H., Engert, A., Hansen, H.P. (2004) Depletion of cellular cholesterol and lipid rafts increases shedding of CD30. *J Immunol,* **7:** 4324-31.

Washington, N.L. and Ward, S. (2006) FER-1 regulates Ca2+-mediated membrane fusion during C-elegans spermatogenesis. *J. Cell Sci,* **119:** 2552-2562.

Weisleder, N., Takeshima, H., Ma, J. (2009) Mitsugumin 53 (MG53) facilitates vesicle trafficking in striated muscle to contribute to cell membrane repair. *Commun Integr Biol,* **2:** 225-6.

Yaffe, D. and Saxel, O. (1977). Serial passaging and differentiation of myogenic cells isolated from dystrophic mouse muscle. *Nature,* **270:**725 -727.

Yamaji, S., Suzuki, A., Sugiyama, Y., Koide, Y., Yoshida, M., Kanamori, H., Mohri, H., Ohno, S., Ishigatsubo, Y. (2001) A Novel Integrin-linked Kinase–binding Protein, Affixin, Is Involved in the Early Stage of Cell–Substrate Interaction. *J. Cell Biol*, **153:** 1251 - 1264.

Yamaji, S., Suzuki, A., Kanamori, H., Mishima, W., Yoshimi, R., Takasaki, H., Takabayashi, M., Fujimaki, K., Fujisawa, S., Ohno, S., Ishigatsubo, Y. (2004) Affixin interacts with alpha-actinin and mediates integrin signaling for reorganization of F-actin induced by initial cell-substrate interaction. *J Cell Biol* **165:** 39-51.

Yasunaga, S., Grati, M., Cohen-Salmon, M., El-Amraoui, A., Mustapha, M., Salem, N., El-Zir, E., Loiselet, J. Petit, C. (1999). A mutation in OTOF, encoding otoferlin, a FER-1-like protein, causes DFNB9, a nonsyndromic form of deafness. *Nat. Genet,* **21:** 363-369.

Yasunaga, S., Grati, M., Chardenoux, S., Smith, T. N., Friedman, T. B., Lalwani, A. K., Wilcox, E. R. and Petit, C. (2000). OTOF encodes multiple long and short isoforms: genetic evidence that the long ones underlie recessive deafness DFNB9. *Am. J. Hum. Genet,* **67:** 591-600.

Zaid, H., Antonescu, C. N., Randhawa, V. K., Klip, A. (2008). Insulin action on glucose transporters through molecular switches, tracks and tethers. *Biochem. J,* **413:** 201–215.

Zisman, A., Peroni, O. D., Abel, E. D., Michael, M. D., Mauvais-Jarvis, F., Lowell, B. B., Wojtaszewski, J. F., Hirshman, M. F., Virkamaki, A., Goodyear, L. J. (2000). Targeted disruption of the glucose transporter 4 selectively in muscle causes insulin resistance and glucose intolerance. *Nat. Med.* **6:** 924–928.

Zitvogel, L., Regnault, A., Lozier, A., Wolfers, J., Flament, C., Tenza, D., Ricciardi-Castagnoli, P., Raposo, G., Amigorena, S. (1998). Eradication of established murine tumors using a novel cell-free vaccine: dendritic cell-derived exosomes. *Nature Med.* **4:** 594-600.